Report Documentation Page

Form Approved
OMB No. 0704-0188

1. REPORT DATE	2. REPORT TYPE	3. DATES COVERED
1999		**00-00-1999 to 00-00-1999**

4. TITLE AND SUBTITLE	5a. CONTRACT NUMBER
Control of Complex Behavior in Cardiac Muscle	5b. GRANT NUMBER
	5c. PROGRAM ELEMENT NUMBER
6. AUTHOR(S)	5d. PROJECT NUMBER
	5e. TASK NUMBER
	5f. WORK UNIT NUMBER
7. PERFORMING ORGANIZATION NAME(S) AND ADDRESS(ES) **Duke University,Department of Physics,Durham,NC,27708**	8. PERFORMING ORGANIZATION REPORT NUMBER
9. SPONSORING/MONITORING AGENCY NAME(S) AND ADDRESS(ES)	10. SPONSOR/MONITOR'S ACRONYM(S)
	11. SPONSOR/MONITOR'S REPORT NUMBER(S)

12. DISTRIBUTION/AVAILABILITY STATEMENT
Approved for public release; distribution unlimited

13. SUPPLEMENTARY NOTES

14. ABSTRACT

15. SUBJECT TERMS

16. SECURITY CLASSIFICATION OF:			17. LIMITATION OF ABSTRACT	18. NUMBER OF PAGES	19a. NAME OF RESPONSIBLE PERSON
a. REPORT **unclassified**	b. ABSTRACT **unclassified**	c. THIS PAGE **unclassified**	**Same as Report (SAR)**	**242**	

CONTROL OF COMPLEX BEHAVIOR IN CARDIAC MUSCLE

by

George Martin Hall

Department of Physics
Duke University

Date: _____

Approved:

_____
Dr. Daniel J. Gauthier, Supervisor

_____
Dr. Robert P. Behringer

_____
Dr. Wanda Krassowska

_____
Dr. Joshua E. S. Socolar

_____
Dr. Roxanne P. Springer

Dissertation submitted in partial fulfillment of the
requirements for the degree of Doctor of Philosophy
in the Department of Physics
in the Graduate School of
Duke University

1999

ABSTRACT

(Physics)

CONTROL OF COMPLEX BEHAVIOR IN CARDIAC MUSCLE

by

George Martin Hall

Department of Physics
Duke University

Date: _____

Approved:

_____
Dr. Daniel J. Gauthier, Supervisor

_____
Dr. Robert P. Behringer

_____
Dr. Wanda Krassowska

_____
Dr. Joshua E. S. Socolar

_____
Dr. Roxanne P. Springer

An abstract of a dissertation submitted in partial fulfillment of the requirements for the degree of Doctor of Philosophy in the Department of Physics in the Graduate School of Duke University

1999

Abstract

The goal of this research program is to develop experimental methods for suppressing complex behavior in small pieces of cardiac muscle and attempt to generalize these methods to spatio-temporal disorganization in hearts during fibrillation. The general approach is to investigate methods developed by the nonlinear dynamics community for controlling complex behavior using small perturbations. This problem is of broad interest to physicists because the heart is a physical realization of a nonlinear system displaying complex spatio-temporal dynamics.

I explore the dynamics of cardiac muscle using an animal model testbed consisting of small pieces of periodically paced bullfrog. Understanding the behavior of small pieces of tissue is important for developing methods for controlling the observed behaviors as well as complex spatio-temporal dynamics observed in whole hearts. In this testbed I find alternans and bistability are common.

Using this testbed, I demonstrate experimentally feedback control of alternans, a behavior that is believed to be responsible for the genesis of fibrillation in whole hearts. To suppress alternans I use Time Delay Auto-Synchronization, a feedback scheme that compares the current behavior of the system to a previous one and adjusts a parameter to minimize the difference. I also demonstrate control with a restricted version of this protocol that only allows shortening of the pacing intervals.

I also use this simple testbed to demonstrate experimentally that it is possible to induce transitions between bistable dynamical states by injecting a single stimulus between paces. These transitions can be elicited by stimuli applied over a range of timing intervals. I observe both 1:1→2:1 transitions as well as two types of 2:1→1:1 transitions.

In an effort to understand how feedback control methods effect spatio-temporal

disorganization, I apply feedback control to a fibrillating sheep atria *in vivo*. The controller observes the dynamics of the atria from a single location and occasionally stimulates the tissue at a nearby location. In preliminary experiments, I generally find that at each location on the atria the probability of any inter-activation interval is seemingly unaffected by application of control. However, in one case, I observe that control lengthens the average inter-activation interval.

Acknowledgments

There is of course no way to thank all the people who deserve credit for helping me in my studies. There have been many people whose example I have sought to emulate and there have been people who have given me an example to avoid. I would like to thank the first set of people, the second set have their own reward.

Because no work of research is undertaken in isolation, there is a long list of people with whom I collaborated. In Biomedical Engineering at Duke I worked most closely with Robert Oliver followed by Dr. Wanda Krassowska, Dr. Patrick Wolf, Ellen Dixon-Tulloch, and was supported in my software efforts by Ned Danielly. I also benefited from theoretical discussions and calculations done by Dr. David Schaeffer of the Mathematics Department and Dr. Josh Socolar of the Physics Department. Drs. Schaeffer and Socolar have both cleared up innumerable theoretic misunderstandings on my part.

In physics, two people most directly affected my educational experience. My advisor Dr. Daniel Gauthier at first buried me with research option and then helped me stay focused on one long enough to finish. I appreciate his efforts to make me a better scientist and writer. In addition, I had the pleasure to work closely with Sonya Bahar. I have benefited from her help, enthusiasm, and experience. I hope she finds a faculty position in a hip section of town.

I would also like to thank all of the sources that financed this hobby. The Whitaker Foundation, the Army Research Office, National Science Foundation and Duke University all provided financial support.

Others played an invaluable role in my physics education and education in general with whom I never worked on a project. I have had the good fortune to have great lab mates, Hope Concannon, David Sukow, Jon Blakely, Michael Stenner and

Seth Boyd. They helped me with all the little physics problems that every experimentalist encounters, and with companionship. I would like to thank David for sharing his wisdom and coffee time, Jon and Michael for engaging me in a favored past time: arguing. In addition, there were three post-docs, Jeff Gardner, Olivier Pfister, and John Schwartz, in the lab who never failed to help if I asked.

A special and separate thanks is required for the three friends I had lunch with almost every day for four years. Bill Brown, Mark Steen, and Adam Wax did not laugh too hard when I said stupid or arrogant things, and they did not remind me about 'graduating in three years' more than once or twice. Que? In each phase of my life I seem to find one close friend, except now I found three.

I would like to acknowledge God for allowing me to discover and wonder at some small part of His creation. I would also like to acknowledge my family. My parents George and Roxie who support everything I do with patience and love. Michon, who, while she may have suggested that I drop out of school and work for a year, always provided a kind ear and sympathy. George, Hunter and Lucy allowed me, and in some cases forced me, to relax and recover my sanity every time I visited.

I would like to dedicate this work to my wife Cynthia V. Hall. She graciously consented to suffer with me and help me.

Contents

List of Figures

List of Tables

Chapter 1

Introduction

The heart is a complex and nonlinear system, designed to pump blood. Its mechanical contractions are mediated by waves of electro-chemical excitation that sweep through specialized conduction systems and the muscle of the heart. Under normal and healthy conditions, these waves of excitation cause a coordinated contraction of the muscle. In some situations, this orderly procession of waves can evolve into a spatially complex dynamical state known as fibrillation [1], in which the waves of excitation and consequent contractions of the heart are not coordinated, causing a loss of blood pressure and death [2]. It is important to understand the mechanisms that trigger fibrillation in order to identify methods to prevent or terminate fibrillation.

While research on complex cardiac dynamics was conducted by Mines at the beginning of the 20th century [3, 4], his work was constrained by both a lack of modern electronics and theoretical understanding of cardiac dynamics. Understanding of fibrillation and its termination has advanced significantly in recent years. In the 1950's and 1960's, Hodgkin and Huxley [5] as well as FitzHugh [6] and Nagumo [7] developed the basis for the currently accepted mathematical models of membrane dynamics and excitability. Recently, large strides in understanding spatially extended cardiac tissue have come about due to the development of relatively high resolution mapping techniques that allow direct observation of spatial cardiac electro-dynamics [15]-[18]. It is now accepted by most researchers that the uncoordinated, seemingly random muscle contractions characteristic of ventricular or atrial fibrillation possess some degree of order [19]-[22].

Control of spatio-temporally complex behavior, in physical as well as biological systems, is an area of active research. Control of spatio-temporal complexity has been studied theoretically in coupled map lattices [8, 9] and the Ginzburg-Landau equations [10] as well as in optical systems [11, 12]. Experimentally, the control of spatio-temporal dynamics has been observed in flame fronts [13] and Taylor vortex flows [14].

The long term goal of the research presented in this dissertation is to devise methods for controlling the spatio-temporal complexity. I choose to work with cardiac muscle tissue, which is a physical realization of an excitable media that displays complex spatial and temporal disorganization during fibrillation. Experimental control of spatio-temporal complexity is challenging because there does yet exist a general set of procedures for achieveing such a goal using only small perturbations, although methods for controlling specific systems have been proposed and demonstrated [23]. In addition, this work is technically difficult because cardiac tissue varies greatly from animal-to-animal, the dynamics can vary between experimental runs, and the signals tend to be noisy.

My contribution to this research effort is to develop methods for controlling spatially localized behaviors observed in cardiac muscle tissue, and attempting to make an initial connection between controlling local behaviors and controlling spatially extended complex behavior. My approach is to study samples of cardiac muscle small enough so that spatial complexity is not important before trying to tackle the full problem of controlling whole-heart electrodynamics. To accomplish this goal, I explore an animal model testbed for analyzing local electrodynamics using cardiac muscle consisting of small pieces of periodically stimulated bullfrog (*Rana catesbeiana*) cardiac muscle. In addition, the test-bed gives an initial assessment of the importance of non-stationary tissue parameters in each experiment, animal-to-

animal variation, and helps develop expertise in electrophysiology. An experiment on *in vivo* sheep hearts is presented to explore a simple adaptation of small tissue control procedures to spatially extended cardiac tissue.

This Chapter is meant as an introduction to the study of control and cardiac dynamics in general and to the particular results of my research. The first section describes briefly the current state of research in controlling complex behavior in cardiac tissue. This is followed by a chapter-by-chapter overview of the main points of my dissertation. A glossary of terms is available in Appendix B.

1.1 The Heart and Nonlinear Dynamics

The mammalian heart is a four chambered mechanical pump. The chambers are divided left and right, atria and ventricle. The right two chambers take blood that is returning from the body and pump it to the lungs. The left two chambers then pump the blood coming from the lungs out to the body. The atria act as priming pumps to the main pumping chambers: the ventricles. The pumping action of the heart is accomplished by the muscle tissue that makes up the walls of the various chambers, which contract in response to stimulation. This stimulation normally comes from the sinus node (the main pace-maker of the heart). Clinically, each chamber can display fibrillation; I study atrial fibrillation because fibrillation can be sustained by the atria for some time without causing death, whereas ventricular fibrillation is typically fatal [1].

Cardiac muscle tissue is composed of many small cylindrical cells of approximately 100 μm in length and 15 μm in diameter. Each of these cells can be described as excitable, which means that they are stable in their rest state but a small but finite stimulus will cause a large but transient response. After stimulation, the transient response is unaffected by further stimulation for a period of time

until after the tissue recovers. This refractory period is a characteristic of an excitable medium. A typical response to pacing of a small piece of frog muscle tissue to stimulation I measured is shown in Fig. 1.1. The deflection of the transmembrane voltage away from and the return to the baseline voltage is called an action potential. The stimulation signal is shown at the bottom of the figure. An action potential duration (APD) is defined as the width of the deflection away from the baseline voltage. The diastolic interval (DI) is the time the muscle is able to recover between action potential.

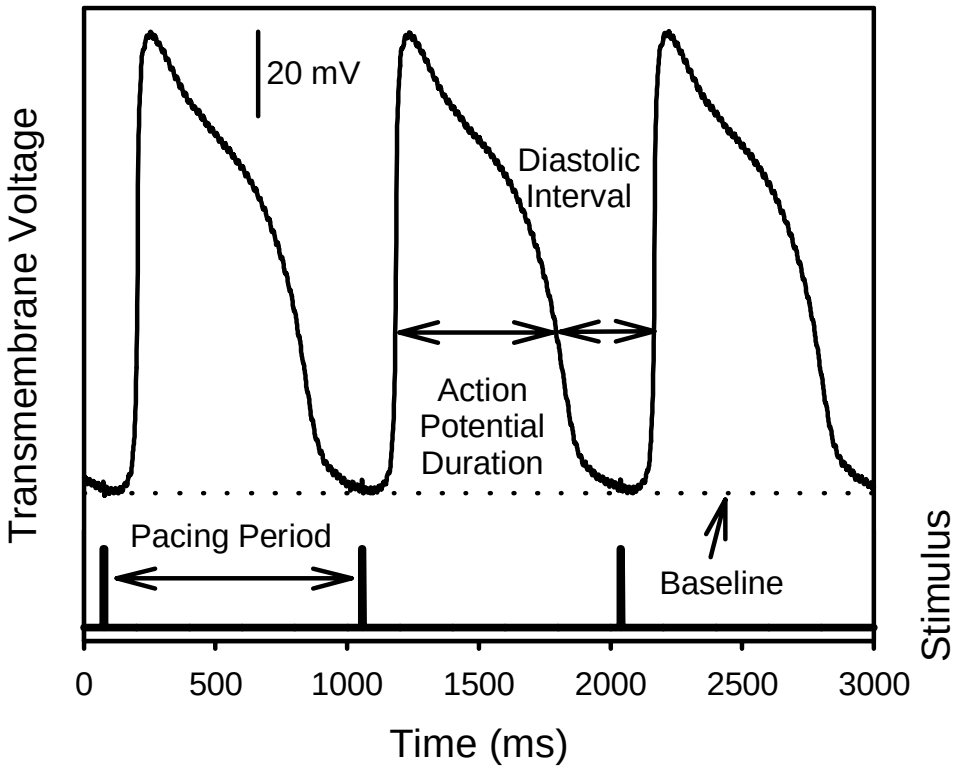

Figure 1.1: Temporal evolution of the transmembrane voltage of a bullfrog action potentials shown. The pacing period is the time between pacing stimuli (shown at the bottom). The action potential duration is the time between the upward deflection of the signal to the downward deflection. The diastolic interval is the time from the end of the previous action potential to the beginning of the next one.

The data shown in Fig. 1.1 is typical for small pieces of tissue. The contrast between normal cardiac behavior and the irregular dynamics encountered during fibrillation in large hearts is illustrated by Fig. 1.2 and Fig. 1.3 both collected from the right atria of a sheep. Both figures have several panels, each of which visualize a single time slice of the activity measured on the right atria with an array of electrodes. The gray points in each panel represent an electrode on the surface of the atria. The black dots indicate detected an activation. Arrows have been added to guide the eye of the time course of the wave. Figure 1.2 is of normal sinus rhythm, while Fig. 1.3 is a recording of a re-entry circuit captured during atrial fibrillation in the same animal. During normal sinus rhythm, the shape of the wave of electrical excitation is very simple, while during atrial fibrillation the shape of the wave is uneven and its speed varies widely from location to location. Notice that the panels in Fig. 1.2 differ in timing that those of Fig. 1.3, because the waves of activation travel slower during fibrillation than during normal sinus rhythm. The dynamics of real cardiac tissue is reminiscent of the behavior displayed in other spatially extended nonequilibrium systems, such as the Belousov-Zhabotinsky reaction and the aggregation of slime molds [28].

The control of nonequilibrium systems is of current interest to the nonlinear dynamics community. Control theory has been used in various engineering disciplines for a long time. Recently Ott, Grebogi and Yorke (OGY) [29] proposed that ability to stabilize any of the infinity of unstable periodic orbits embedded in chaos was both possible and perhaps desirable. Many people believe that there is chaos in the heart during fibrillation [22, 30, 31]. However, the time series that are analyzed are usually short and the data is noisy. Interestingly, Christini and Collins [32] have recently suggested that chaos control techniques can be used even in situations where the dynamics is driven by stochastic, rather than deterministic, influences;

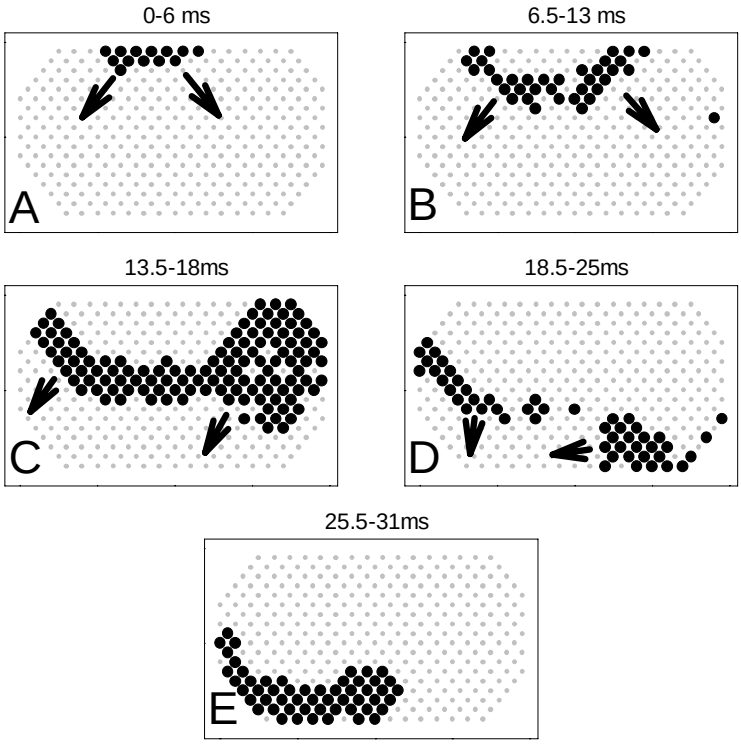

Figure 1.2: The panels A-E show the temporal evolution of a normal heart beat on the right atria of a sheep heart. The wave originates in the sinus node (off plaque in the upper left) and propagates across the atrial. Each of the panels reprensents 6 ms of time. The black dots show where the leading edge of activation was during that time slice. The plaque is approximately 7.5 cm $\times$ 3.5 cm and the wave of excitation travels arcoss it in 31ms. Each of these waves is separated in time by about 1 sec.

these chaos control techniques require only the existence of unstable periodic orbits. These results are intriguing for cardiac defibrillation because it suggests that small stimuli (perturbations), rather than large shocks, may be capable of controlling the dynamics of the heart.

The idea that small electrical stimuli can affect the dynamics of the heart is not new. It is well known that arrythmias such as atrial flutter and ventricular tachycardia can be initiated and terminated by one or more properly timed stimuli [33]. Unfortunately, attempts to interrupt atrial or ventricular fibrillation have been less

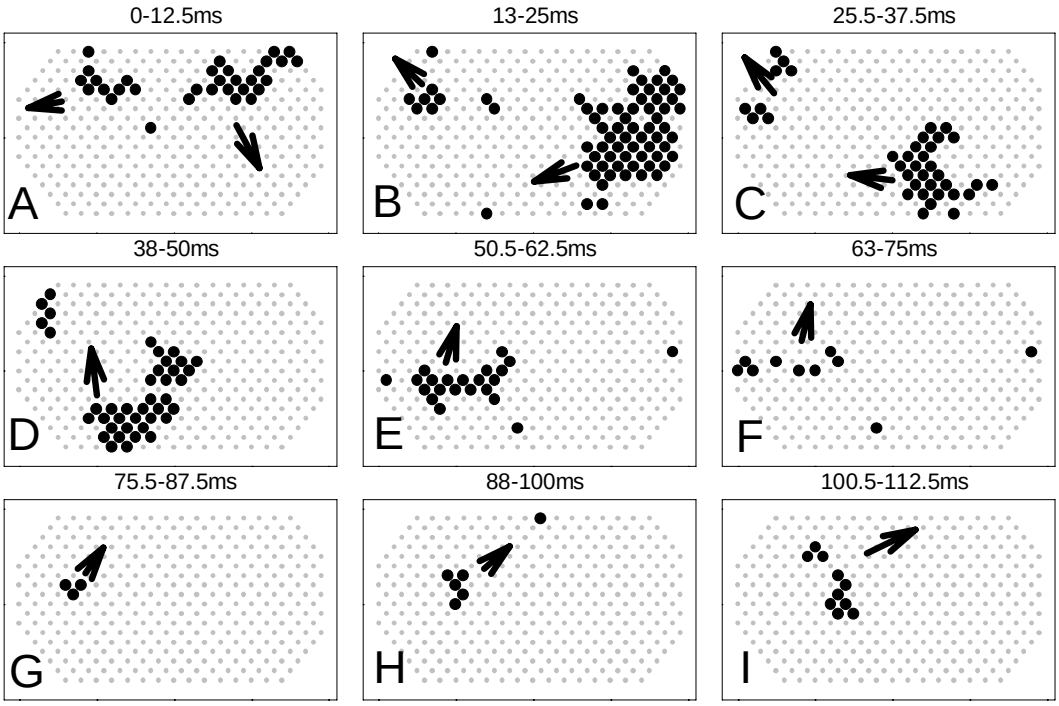

Figure 1.3: The panels A-I show the temporal evolution of a reentry circuit during fibrillation on the right atria of a sheep heart. The wave circulates around the surface of the atria. Each of the panels represents 12 ms of time. The black dots show where the leading edge of activation was during that time slice. The wave of excitation travels around the plaque in 120 ms. While this behavior is slower than normal sinus rhythm it is continuous.

successful. Allessie *et al.* [34, 35] successfully entrained the dynamics of a spatially localized portion of the myocardium during atrial fibrillation using rapid periodic pacing. However, this control procedure did not result in defibrillation, and complex dynamics reappeared after the pacing was terminated. Similarly, KenKnight *et al.* [36] captured the local dynamics during ventricular fibrillation. Both of these attempts to control fibrillation use an open-loop controller (periodic pacing). Open-loop control does not require any measurement of the state of the system, and its effectiveness relative to the tissue behavior is independent of when the controller is turned on.

Several groups have been trying to control complex cardiac dynamics using closed-loop control schemes developed to suppress low dimensional chaos. Closed-loop feedback controllers try to stabilize unstable steady states by applying small perturbations to an accessible parameter of the system using a measurement of the state of the system. The feedback scheme for controlling chaos, first proposed by OGY [29], is quite general, based on real-time measurement of the system dynamics, and does not require a detailed model of the dynamics. The key idea underlying the control scheme is to take advantage of the unstable dynamical states embedded within the system. Rather than making large changes to the system, the feedback technique stabilizes one of these unstable states. As the system approaches the desired state, the strength of the perturbations required to keep it there vanishes, so that the feedback signal can be as small as the noise level in the system. Variations of this method have been applied successfully to stabilize the dynamics of mechanical, electrical, optical, and chemical systems [37, 38].

Garfinkel *et al.* [39] have demonstrated that it is possible to stabilize cardiac arrythmias to a period-three behavior in a medicated small piece of the intraventricular septum of a rabbit heart *in vitro* by administering small, electrical stimuli using a variation of the OGY feedback control technique. Crucial to this strategy is the concept that the heart can display two different dynamical behaviors under essentially identical physiological conditions, such as normal sinus rhythm and fibrillation or tachycardia. More recently, Hall *et al.* [40] demonstrated that an adaptive controller can be used to suppress temporal instabilities in an atrial-ventricular nodal conduction system known to exhibit alternans, a behavior where the tissue response alternates. The control protocol is based on a comparison of consecutive interbeat intervals. This method is similar to the ones used in Chapter 3 to suppress alternans in cardiac muscle.

The results of Garfinkel *et al.* [39] and Hall *et al.* [40] only address specialized systems of the heart but not necessarily the muscle of atrial or ventricular walls, which are the primary substrate for fibrillation. While these results are intriguing, they only demonstrate that *temporal* complexity of a dynamical system can be controlled. There is not yet a general approach to controlling systems that display spatio-temporal complexity such as that displayed by the heart during fibrillation [19]-[22]. Toward this goal, Glass and Josephson [41] established criteria for annihilation of reentrant arrythmias; Biktashev and Holden [42] demonstrated that proportional feedback control can induce drift of spiral waves in a model of cardiac muscle; Aranson *et al.* [10] showed that external stimuli can stabilize meandering spiral waves; and Wantanabe and Gilmour [43] proposed a strategy that uses small stimuli to prevent cardiac rhythm disturbances. Most recently, Rappel *et al.* [44] demonstrated numerically that a grid of simple feedback controllers can prevent spiral wave break up in a 2-D model of cardiac behavior. In addition, preliminary research by Ditto and collaborators [23] suggests that it is possible to capture at least a portion of a fibrillating atrium during human trials using the same OGY variant Garfinkle *et al.* [39] used, where the heart dynamics is recorded and control stimuli are delivered through a quadrupolar electrode catheter inserted into the right atrium through the femoral vein. Due to the limited number of sensors, it could not be determined whether the entire atrium was controlled, and atrial fibrillation was terminated only rarely using this method.

There are several issues that must be addressed before the spatially extended control results can be used experimentally. In the work of Garfinkel *et al.* [39], Biktashev and Holden [42], and Watanabe and Gilmour [43], the use of a spatially uniform forcing function is assumed, a requirement that is unlikely to be satisfied in practice. Also, the results of Aranson *et al.* [10] and Glass and Josephson [41]

were obtained using a simplified model of cardiac dynamics whose properties are, in many aspects, different from the properties of cardiac muscle. The results of Rappel et al. [44] require each control point to continuously measure the transmembrane voltage, which is difficult in practice. Finally, experiments using many sensors at different spatial locations are needed to determine whether the preliminary work of Ditto and collaborators [23] was successful in capturing the entire atrium.

1.2 Thesis Overview

This dissertation documents my research on controlling complex behavior in cardiac muscle tissue. It is divided into seven chapters. Chapter 2 covers briefly concepts of cardiac dynamics and control that are necessary to appreciate the experimental sections. Chapters 3-5 detail my exploration of the behavior and control of small pieces of frog heart muscle. In Chapter 6 I present an investigation of controlling spatio-temporal complexity occurring in a fibrillating *in vivo* sheep atrium. Chapter 7 concludes with a summary of my results and a discussion of future directions for research. There are also several appendices that include derivations and some general material.

In Chapter 2, I develop the background of cardiac dynamics and control in an attempt to clarify both how cardiac dynamics is discussed and how I approach the problem of control. I explain briefly the origin of the signals that characterize the dynamics of the tissue and how they are measured. I show how a feedback controller works in a very simple model of local cardiac dynamics.

The experimental section of the dissertation begins in Chapter 3. I present the basic experimental system used to study local cardiac tissue behaviors and describe the analysis of the data. This system consists of a small piece of periodically paced bullfrog (*Rana catesbeiana*) cardiac muscle. The muscle is quiescent in the absence

of external pacing and small enough to prevent complex spatial effects. These features allow me to study the dynamics of the muscle tissue without the added effects of autonomous pace-making activity or spatial effects.

After this general introduction to the experimental system, I characterize the different types of behaviors I observe. Figure 1.4 shows a typical bifurcation diagram illustrating these behaviors as a function of pacing period. The bifurcation diagram is generated by sweeping the pacing period from a long value of 1000 ms to 250 ms in 50 ms steps (filled shapes) and then back (open shapes). For each step, I plot the observed action potential duration (APD). The arrows are added to guide the eye through the time course of the experiment. Under various conditions of periodic electrical stimulation (pacing), M stimuli can elicit N responses (M:N behavior). At several pacing periods, the tissue can exhibit behavior where one stimulus elicits one response or behavior where the tissue alternates in its response to every other stimuli. The tissue can also be in a state where it skips every other pace.

I find that bistability between 1:1 and 2:1 patterns exists in 17 of 23, or 74%, of the cardiac preparations. The window of bistability is situated over a range of pacing periods (PP) that lie near the natural period of a bullfrog's the resting heart ($\sim$ 1000 ms), and extends for $\sim$ 160 ms. The 2:2 behavior (alternans) occurs in 26 of 63 or 41% of cardiac preparations. In addition, I find that the stimulus that does not elicit a response in the 2:1 state does, in fact, have an effect on the tissue dynamics.

Also in Chapter 3, I introduce two different models of cardiac dynamics. These models reduce the complexity of ion flows and nonlinear conductances to simple one- and two-dimensional functions that map the present state of the system into the future. I demonstrate that these models provide a useful experimental guide even though they are not a complete description of local cardiac dynamics.

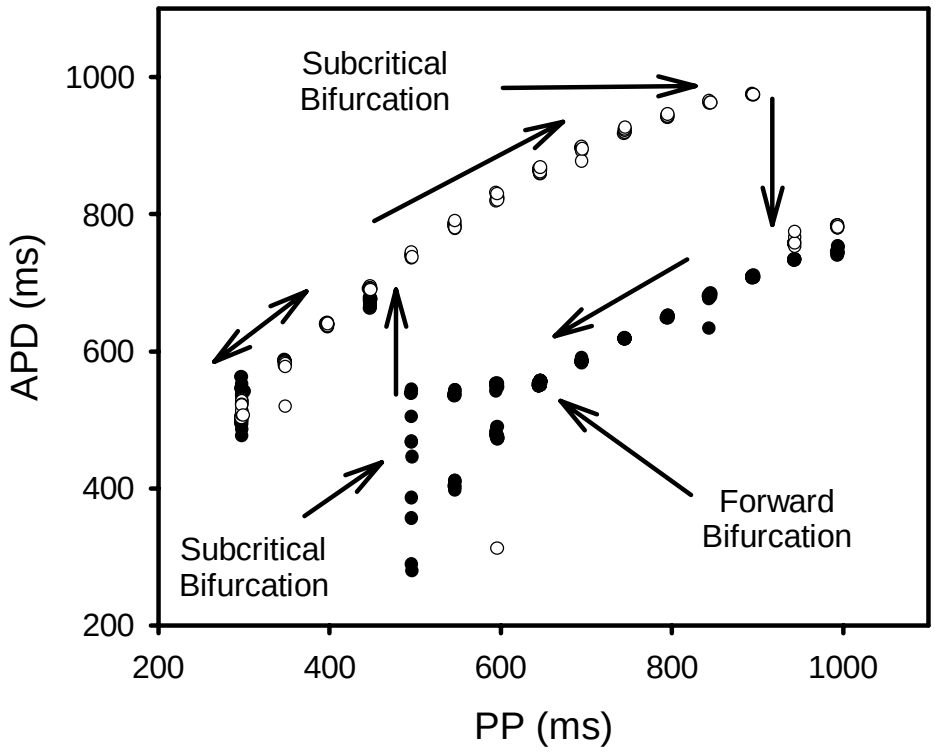

Figure 1.4: The bifurcation diagram of the response of small pieces frog ventricle muscle to periodic pacing. The solid circles are generated as the pacing period is decreasing, and the open circles are generated as the pacing period is subsequently increasing. The solid arrows are added to indicate the time course of the experiment.

In Chapter 4, I implement a feedback scheme to control one of the major behavior observed in small pieces of cardiac tissue: alternans. Alternans is a state where the behavior of the tissue alternates in response to periodic pacing. I stabilize the unstable 1:1 behavior using two variations of the feedback scheme known as time delay auto-synchronization (TDAS). The TDAS method uses the n^{th} action potential duration (APD_n) to characterize the state of the system and the pacing period as the accessible system parameter. An error signal ε_n is generated using the TDAS algorithm in a form given by

$$\varepsilon_n = \gamma(APD_n - APD_{n-1}), \tag{1.1}$$

where γ is the feedback gain. This controller uses the past behavior of the system as an approximation to the unstable state to be stabilized. The TDAS protocol has a very short memory that is it only uses information from the last two interbeat intervals, which allows it to track slow changes in the stability of the dynamics. When this control scheme is successful, APD_n=APD_{n-1}=APD^*, which is the desired state, and the error signal goes to zero for any gain γ.

The TDAS scheme may not be suitable for controlling whole heart behavior because, clinically the tissue is paced by some normally inaccessible autonomous system such as intrinsic pacemaking cells or by waves of excitation generated by complex behavior in some other location on the heart. In this situation, feedback controllers can only preempt the normal pace maker. This leads to a restricted version of TDAS. The error signal for the restricted TDAS is similar to TDAS except that it is constrained to be non-positive. Which for positive γ gives

$$\varepsilon_n = \begin{cases} \gamma(APD_n - APD_{n-1}) & if \quad APD_n < APD_{n-1} \\ 0 & if \quad APD_n \geq APD_{n-1} \end{cases} \tag{1.2}$$

thus ε_n<0 and the pacing period is only shortened. This type of control is discussed theoretically by Gauthier and Socolar [45].

Figure 1.5 shows the APD versus beat number from a control experiment using TDAS. When control is off (black points on left) the response of the tissue to periodic pacing alternates and the unstable 1:1 behavior is stabilized when control is switched on (gray points). Once control is turned off again (black points on right), the system returns to alternans.

In Chapter 5, I present a control experiment on the behavior most commonly observed: bistability. I show that it is possible to cause transitions between the two stable states by injecting a single pulse when the system of paced cardiac muscle is exhibiting bistability. I observe that it is possible to induce two types of 1:1-to-

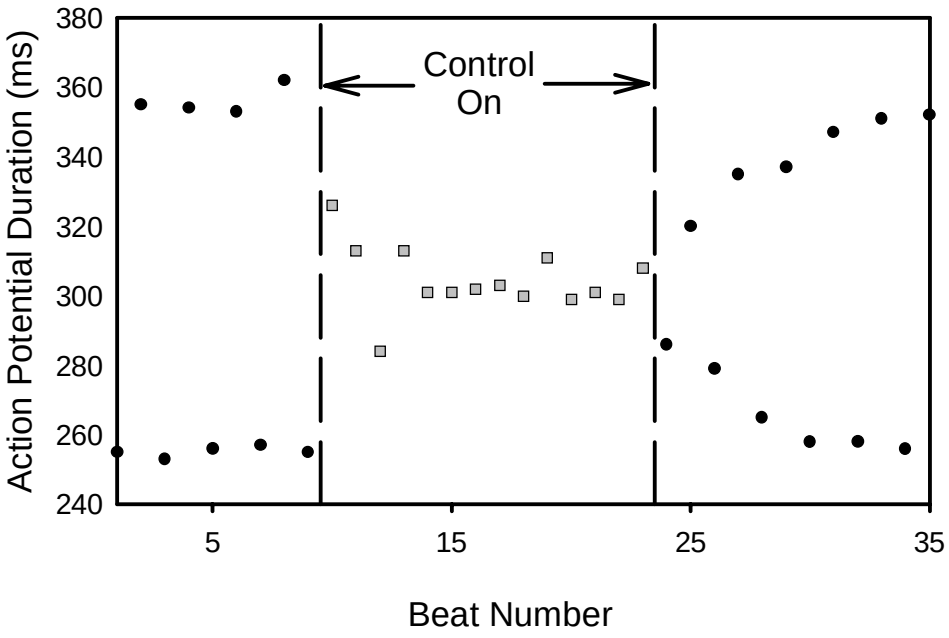

Figure 1.5: A beat by beat illustration of a TDAS control experiment. The action potential duration is plotted against beat number. While control is off (the black points) the tissue displys alternans. When control is turned on (the gray points) the alternans behavior is supressed and the normally unstable period one behavior is stabilized.

2:1 transitions observed, as well as two types of 2:1-to-1:1 transitions. One type of the 2:1-to-1:1 transitions is shown in Fig. 1.6. The transmembrane potential is shown at the top of the figure, while, the pacing signal is shown at the bottom of the figure. An extra stimulus is inserted between to regular periodic stimuli. I show that most of these transitions can be understood through use of the simplest mapping model of the tissue dynamics from Chapter 3, while an explanation of the other two transitions requires a fundamentally different type of theoretical model. These studies of the dynamics and control of small pieces of cardiac tissue are important for understanding the local mechanisms of cardiac arrythmias that may contribute to eventual control of conduction blocks, tachyrhythmia, and atrial and ventricular

fibrillation.

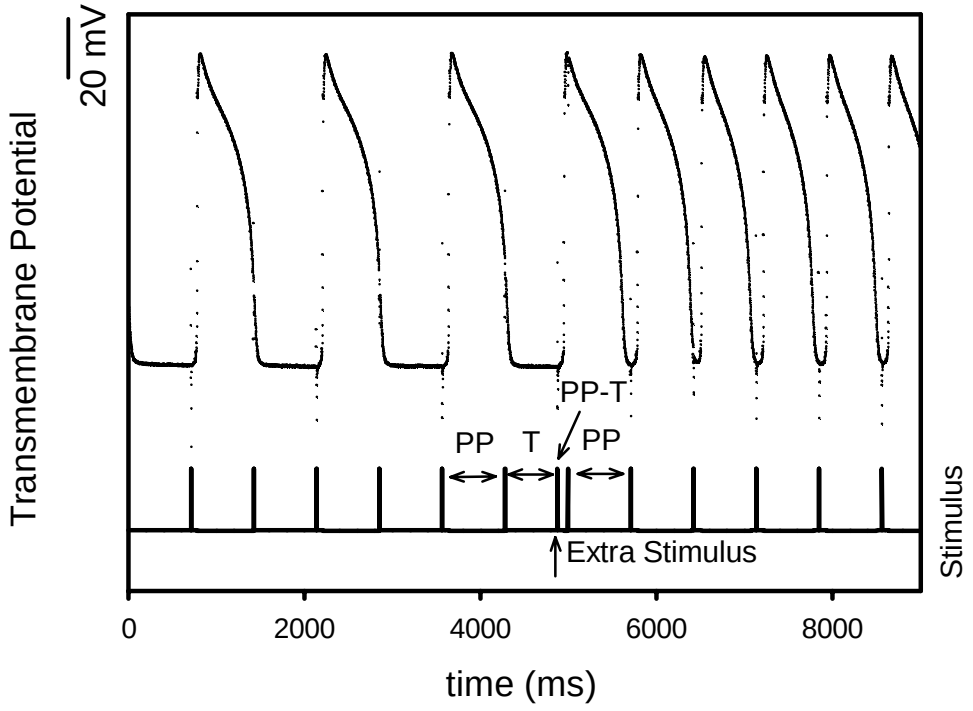

Figure 1.6: A 2:1→1:1 transition can be caused by a single injected stimuli. The pacing sequence is shown at the bottom of the figure. The pacing period (PP) is marked. The extra stimuli is T ms after the regular stimulus.

In Chapter 6, I present an initial study designed to control complex spatio-temporal behavior in an *in vivo* sheep heart. This research was preformed in collaboration with the Duke Cardiac Electro-Physiology Laboratory in the Biomedical Engineering department. This study allows investigation of control of cardiac dynamics in a preparation that is much closer physiologically to an *in vivo* human heart. I use an electronic mapping system to measure both temporal and spatial response of the tissue to control during fibrillation. The results of these control experiments using TDAS-like controller have thus far been inconclusive.

In Chapter 7, I outline the successes to date and discuss some issues to be ad-

dressed by future theoretical and experimental research. The underlying assumption to be tested by future studies is that fibrillation can be controlled using feedback control methods at one or a few spatial locations on the heart. To test this assumption will require several steps. The first step is to continue to study small pieces of cardiac muscle where spatial complexity is not important. In these studies, precise experiments are compared quantitatively to ionic-based cardiac mathematical models in order to extend theoretical understanding of real tissue. The next steps involve exploring theoretically these techniques to one two and three dimensional models of cardiac muscle. In addition, I believe it would be useful to attempt refinements of my initial sheep experiments.

The appendices contain several important pieces of practical information. They are intended to serve two purposes. They provide a place of quick reference for relevant numbers and derivations that are used in this dissertation. In addition, some experimental details that are relevant for future researchers can be found there.

Chapter 2

Fundamentals of Controlling Cardiac Dynamics

The long term goal of this research is to develop methods for controlling the spatio-temporal disorganization that arises in human hearts during fibrillation. The nonlinear dynamics community hypothesizes that feedback methods designed for controlling complex *temporal* dynamics using small perturbations will be able to control complex spatio-temporal dynamics occurring in the heart [23, 46, 8, 47]. While controlling spatio-temporal complexity is interesting from a fundamental point of view, a control technique must be more effective or use less energy to defibrillate the heart than the present techniques that rely on large shocks for it to be clinically practical. To be experimentally practical, a technique cannot measure the dynamics and apply control perturbations at every location on the heart because this would be unachievable in any realistic setting. For these reasons, researchers, such as Ditto *et al.* [23], focus on closed-loop control techniques that use information from one spatial location and apply small perturbations to the same location in an attempt to suppress complex spatio-temporal behaviors.

Closed-loop controllers have been used to suppress *temporally* complex dynamics in a variety of systems [29, 48]. A closed-loop (feedback) controller attempts to suppress complexity by employing a circular process of observing the dynamics and adjusting a parameter of the system to change the dynamics in a desired manner. The basic building blocks of the control process are shown in Fig. 2.1. Initially, the dynamical system produces complex behavior that is undesirable. The dynamical system in this research consists of cardiac muscle tissue. A measurement of the

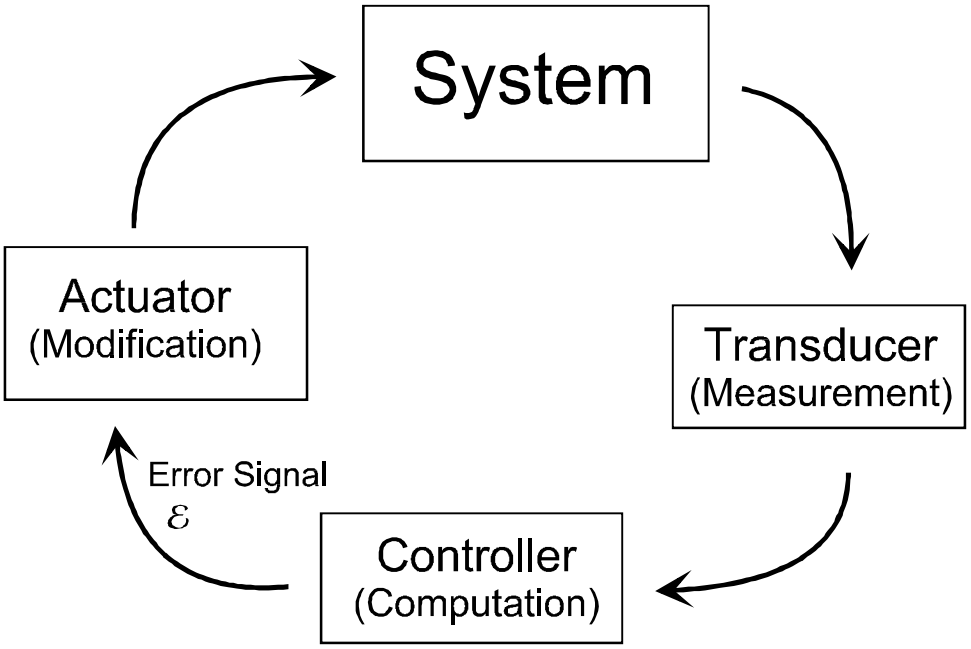

Figure 2.1: Circular process of feedback controllers. The state of the system to be controlled is measured with the transducer. A calculation of the difference between the current state and the desired state is used to generate an error signal. The actuator adjusts some system parameter in order to minimize this difference.

dynamics of the system is made with the transducer. The signal from this measurement is used by the controller to compute an error signal, which is the difference between the current state of the system and the desired state. The error signal is applied to the actuator to modify a system parameter that changes the dynamics in order to reduce the error signal. If the controller is successful, this measurement and correction loop continues until the system displays the desired behavior, producing a zero error signal.

Applying this simple concept of feedback control to a fibrillating heart reveals the challenges inherent in spatially extended systems and biological system. In an extreme situation where the cardiac cells are not coupled to each other, the dynamics of each individual cell must be measured to fully quantify the dynamical state of

this heart. Similarly, one control actuator per cell is needed to completely control the dynamics of each cell. Consequently, the control algorithm in general needs to be nearly infinite dimensional. However, coupling between cells links their dynamics, effectively reduces the number of observation points and actuators and the complexity of the controller needed to effect control. For example, in the opposite limit of infinitely strong coupling, the spatial problem would reduce to controlling the dynamics of a single spatial location, and only one measurement transducer and actuator would be needed.

The basic questions for controlling cardiac muscle then become: how many locations and actuators are necessary, and what control algorithm will suppress complex activity. The approach taken by several researchers [23, 46, 8] is to apply feedback control at a few spatial locations in extended systems displaying complex dynamics and observe the resulting behaviors. Preliminary research by Ditto *et al.* [23] suggests that it is possible to capture at least a portion of a fibrillating atrium during human trials using a closed-loop method, where the heart dynamics is recorded and control stimuli are delivered through a catheter inserted into the right atrium. Due to the limited number of sensors, it could not be determined whether the entire atrium was controlled. In addition, atrial fibrillation was terminated only rarely using this method.

In this chapter I explain the four parts of the control process depicted in Fig. 2.1 with special emphasis on controlling a model of cardiac muscle dynamics in order to motivate the experiments in the later chapters. In section 2.1, I discuss the dynamics of cardiac muscle (the target system) at the cellular level, summarizing the origin of the transmembrane voltage and ionic currents that are used to characterize the state of the cardiac muscle tissue. Section 2.2 is dedicated to understanding how electrodes (the transducer) measure transmembrane voltages and related signals. In

the final section, I combine the calculation and actuation processes and present a example of how feedback control can suppress alternations in a simple mathematical model of the dynamics of a single cardiac muscle cell.

2.1 Basic Cardiac Dynamics

On a macroscopic level, heart muscle contracts in a coordinated fashion causing blood to flow. In more complicated situations, such as fibrillation, this contraction can become uncoordinated. In order to understand how controllers can estimate and affect the state of the muscle it is important to understand how the microscopic dynamics give rise to the properties of the macroscopic cardiac muscle. While this subject is covered in much more detail elsewhere [49], it is important to include a brief treatment here to provide a basic understanding of the system highlighted in the control loop shown in Fig. 2.2.

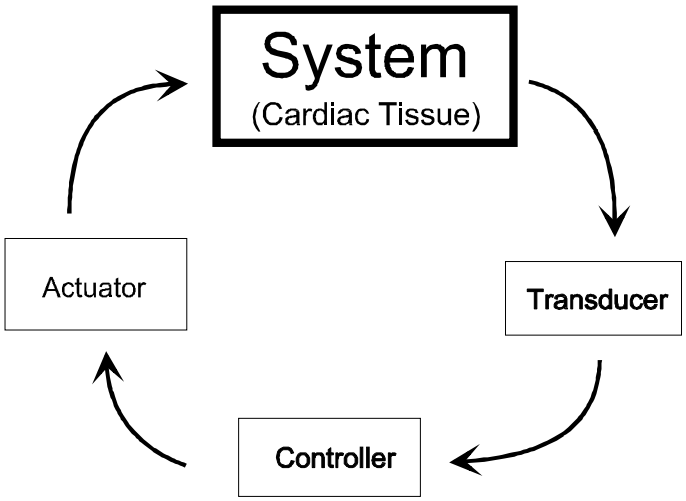

Figure 2.2: Cardiac muscle tissue is the system that produces the unstable dynamics in the feedback loop.

In this section, I explain cardiac electrodynamics starting from the cellular level.

I start with the structure of the cellular membrane. Next, I explain the membrane mechanics that produce an action potential. Finally, I explain how waves of excitation propagate through cardiac tissue.

2.1.1 Membrane Dynamics

The contraction of the muscles of the heart change the volume of the atria and ventricles causing the pumping of blood. This contractions are caused by a shape change of several proteins inside the cell. The shape change of these proteins is caused by the exposure to Ca^{2+} that occurs when the cell becomes activated [1].

The activation of cardiac muscle cells involves a complex interaction of voltage-sensitive proteins embedded in the cell walls and ions in the solutions that surround and fill the cellular structure of the muscle tissue. A cartoon of a cardiac membrane is shown in Fig. 2.3. The intracellular and extracellular solutions contain different concentrations of ions, mostly potassium (K^+), sodium (Na^+), chloride (Cl^-), and to a lesser extent calcium (Ca^{2+}). The concentration gradient of each species of ion across the cell membrane causes a voltage difference across the membrane. At rest, this difference is approximately -80 mV. The resulting chemical potential difference drives the activity of the cell. The interior and exterior regions are separated by a cell wall (a lipid bilayer) approximately 3 nm thick that is impermeable to the ions. Proteins in the membrane selectively carry ions across the membrane under certain conditions of voltage and concentration.

The voltage across the membrane depends on the interaction between the non-linear conductances of the proteins and the transmembrane voltage. If the voltage difference across the membrane decreases below a critical level, some of the protein gates open allowing ions to rush through. This causes other channels to open or close, thereby changing their conductances. The response of the cardiac tissue to

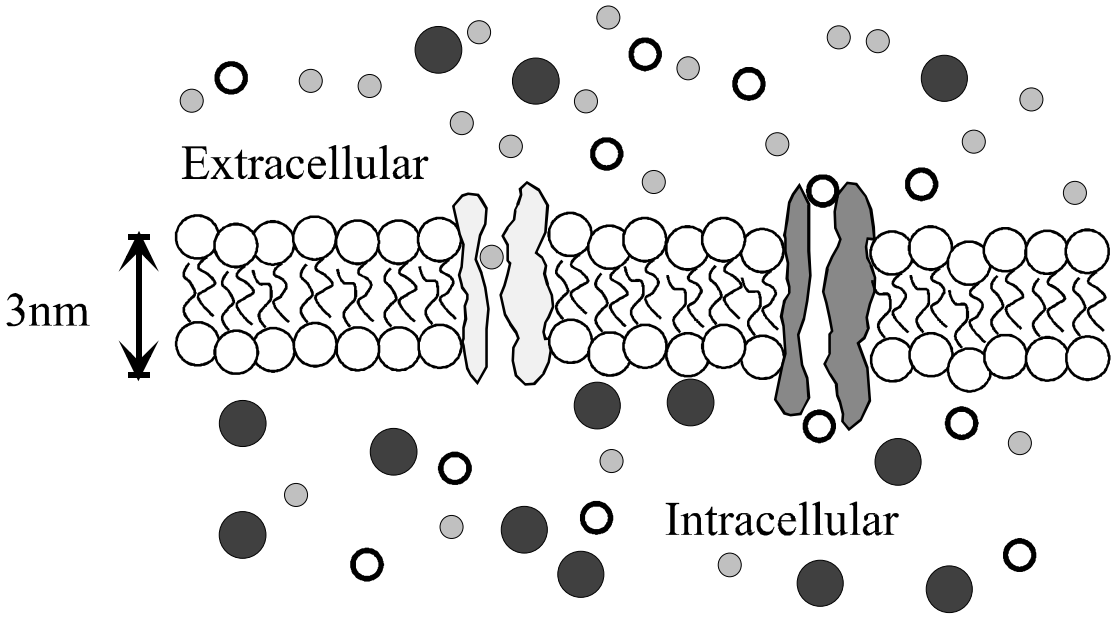

Figure 2.3: A drawing of a cardiac membrane. The membrane consists of a lipid bilayer with embedded proteins. The lipid bilayer keeps the solution that fills the cellular structure separate from the solution that surrounds the tissue. The ions are transported across the membrane wall by proteins that act as ion-selective voltage-sensitive channels and pumps.

stimulation is a result of the voltage dependent conductances of the protein channels that govern ion transfer across the membrane. A set of protein pumps try to reestablish the original balance of ions by pumping ions back to their original concentrations. These ion flows result in the time course of the transmembrane voltage from a bullfrog muscle shown in Fig. 2.4. The initial quick depolarization (upward deflection) is caused predominantly by a rapid influx of sodium ions. Potassium ion flows predominantly account for the repolarization (downward deflection). This transient depolarization and subsequent repolarization is called an action potential. The action potential's maximum height is typically about 100 mV. In a bullfrog the duration of an action potential is typically between 300 and 900 ms.

The electrodynamics of the cell membrane can be modeled by an electric circuit

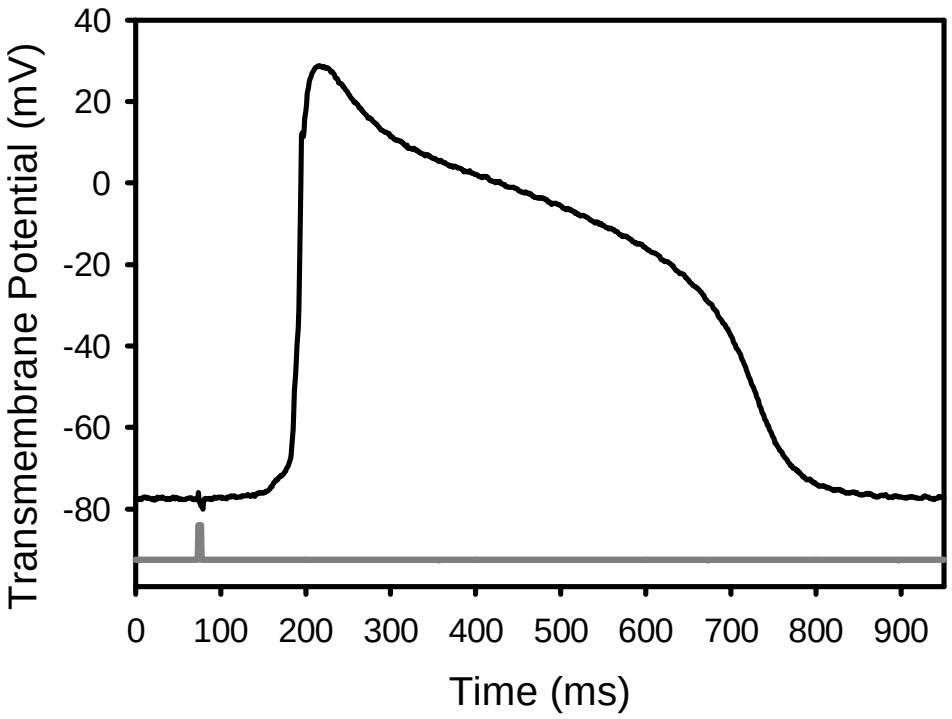

Figure 2.4: Temporal evolution of the transmembrane potential in a bullfrog cardiac cell in response to a brief stimulus. The transient depolarization of the membrane (black curve) is called an action potential. The stimulus is shown at the bottom of the figure (gray curve).

shown schematically in Fig. 2.5. Each ion flow across the membrane can be treated as a current through a series combination of a battery and a variable conductance. The battery represents the voltage generated by the equilibrium concentration gradient of that ion. The variable conductances represent the voltage-dependent ion-selective proteins in the membrane that move ions across the membrane. The additional current through the resistor and capacitor represents a voltage independent ion flow across the membrane and the capacitance of the membrane itself.

Modelling the ion flows across a membrane including the nonlinear conductances involves a large number of differential equations. Often this type of model requires numerical solution. The mathematical details of these descriptions depend on the

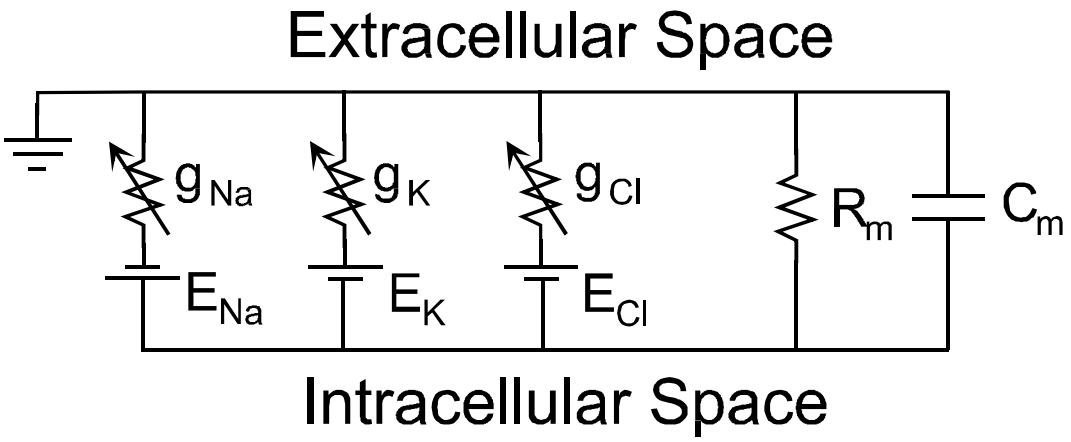

Figure 2.5: An equivalent circuit model of cardiac cell. The ion flows across the cellular membrane can be modeled by a simple circuit. The batteries represent the Nerst potential of the resting concentration of each type of ion. The variable conductances represent the protein gates that open and close in response to the various voltage levels.

species of animal [50, 51] and the specific type of tissue [51, 52]. However, more detailed ionic models do not necessarily improve our understanding of tissue dynamics. While the description of ionic flows can differ from species to species and among tissue types, it appears that all cardiac muscle tissue behaves similarly.

Generally, cardiac muscle tissue can be described as an excitable medium. An excitable medium is a system that is stable to infinitesimal perturbations. However, if the system is perturbed with a stimulus greater than some small (but finite) threshold the system will display a large, transient response. During this response, the system is unaffected by further stimulation. Similarly, cardiac tissue is stable in its polarized state. However, when stimulated with a pulse larger than some threshold, the cardiac muscle tissue will respond with an action potential. During an action potential, while the equilibrium ion concentrations are being re-established and the protein channels are not yet reset, further perturbations have little effect

on the tissue. The time while the tissue cannot be re-excited is called the refractory period.

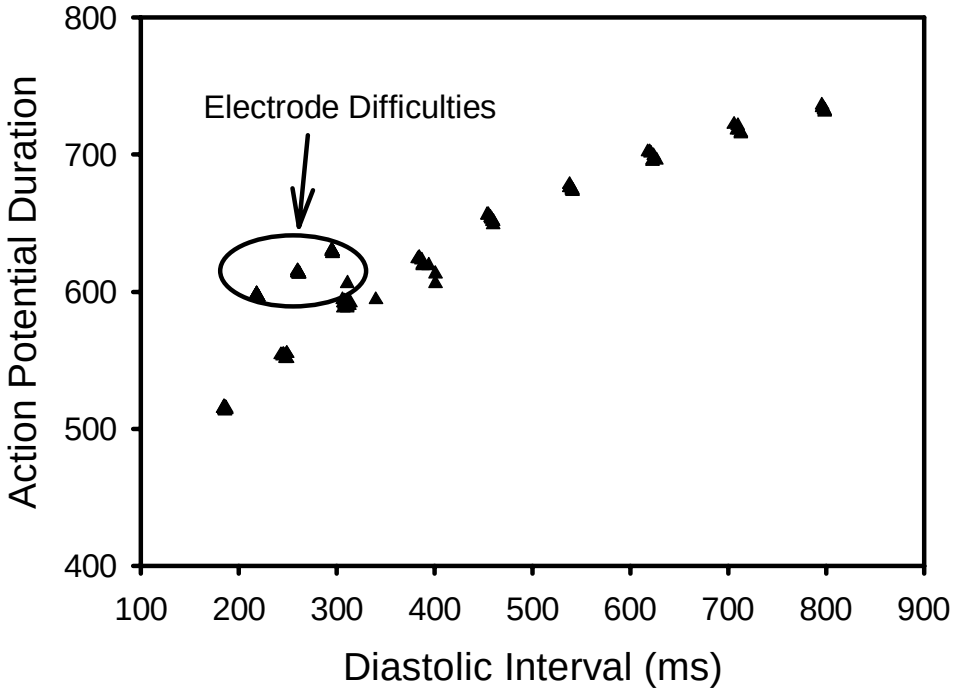

Figure 2.6: An experimentally restitution curve I recorded from bullfrog cardiac muscle relating the action potential duration to the proceeding diastolic interval.

Since all cardiac muscle tissue behaves roughly the same regardless of the specifics of the shape of its action potential, researchers often consider its activity in terms of the duration of the action potential and not it shape. Experimentally, the duration of the action potential (denoted by APD) is seen to depend on the length of time the tissue has had to reset to its equilibrium ion concentrations between stimuli. The relevant time is from the end of one action potential to the beginning of the next, called the diastolic interval (DI). The APD is assumed to be a function of the DI such that $APD_n = f(DI_n)$. This view is supported by considering the ionic origin of the action potential. The ionic pumps take some time to restore the equi-

librium ionic balance. If the tissue is stimulated before this balance is restored the action potential is shortened. This view clearly discards much information about the specific nature of the tissue, but is useful to understand the gross features of cardiac dynamics.

The relationship between APD and the preceding DI is called a restitution relation. Figure 2.6 shows the relationship between APD and DI for a small piece of periodically paced bullfrog cardiac tissue. The tissue is periodically paced at various periods, and at each period the steady state action potential duration and the resulting diastolic interval is observed. Notice the slope of the restitution relation begins to level off for long DI, and there is a maximum APD.

The restitution relation describes qualitatively the bifurcation structure of small pieces of real tissue. However, as I will show in Chapter 3 and 5, this description does not capture all of the observed effects in paced cardiac muscle tissue. Regardless, whole tissue dynamics are much richer than those observed in small pieces of tissue, due to coupling between cells.

2.1.2 Propagation of action potential

The muscles of the heart consists of many millions of small cylindrical cells in a complex arrangement. While each of these cells can be described as above there is the additional complication of coupling between cells. A cardiac muscle cell is coupled to its neighbors through gap junctions, or channel proteins at the end of the cell. These channel proteins connect to the channel proteins in the neighboring cell, providing a path for ions to flow inside the cellular structure. This path couples the ionic concentration of a cell through diffusion to the cells around it.

The ionic coupling between cells is responsible for the propagation of waves of excitation. Stimulation of one cell causes the membrane to depolarize because of

a local sudden change in the ionic concentrations. The voltage difference between neighboring cells induces a current from the next cell, which causes a small depolarization in that cell. This depolarization is enough to cause an activation in that cell and the process continues. A detailed review of the mathematics of this process is presented by Henriquez [53].

It is interesting to note that the refractory period of individual cells cause waves to propagate in only one direction. Cells in front of a wave of excitation have not yet been activated, while those behind have recently been excited and consequently are refractory. This also explains why waves annihilate each other when they collide, instead of passing through each other.

2.2 Measurement of Cardiac Signals

As discussed earlier, effective control of uncoupled cardiac muscle cells, would require a measurement of the state of each cell. In addition, to fully know the state of each cell it would be necessary to measure all the ion concentrations. In practice this is impossible. While it would be difficult to measure continuously ion concentrations, there are several widely used techniques for measuring voltages. Measuring the state of the cardiac muscle system is the transducer step highlighted in Fig. 2.7.

In this section, I discuss some common techniques for measuring electrical activity in cardiac cells. First, I introduce microelectrodes that allow a direct measurement of the transmembrane potential from a single cell. Then I introduce monophasic action potential (MAP) electrodes. Next, I describe general extracellular measurements. These electrodes do not measure the transmembrane voltages, but rather the voltage on the surface of cells that results from the ion currents. Finally, I present a voltage-sensitive dye technique that seems to hold much promise in

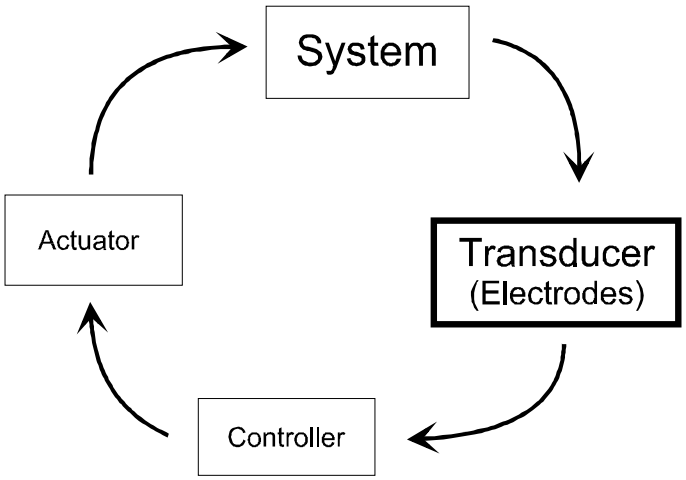

Figure 2.7: Electrodes fullfill the role of transducers in the feedback loop used to control cardiac muscle tissue.

certain situations. The first three techniques I use in various experiments. Further details in the use of all these techniques are presented in Appendix C and in Geddes [54] and Franz [55] or for voltage sensitive dyes in Ebner *et al.* [56].

2.2.1 Microelectrodes

A microelectrode is one of the best devices for measuring the internal state of a cardiac muscle cell. The microelectrode provides a direct electrical connection to the internal cellular solution [54]. The theory of operation for microelectrodes is quite simple. A microelectrode consists of a pipette with a tip sharp enough (approximately 1 μm in diameter) to puncture a single cardiac cell. After being punctured, the cell membrane often closes around the tip of the microelectrode, forming a good seal. Inside the microelectrode is a salt solution that provides a conductive salt bridge between the inside of the cell and the other end of the pipette where a silver electrode is placed. However, because microelectrode tips are so small, they are prone to break if the cardiac muscle moves. This limits their

usefulness in measuring signals from contracting cardiac muscle.

A sequence of action potentials from a periodically paced bullfrog ventricle recorded using a microelectrode is shown in Fig. 2.8. This signal has been multiplied by a factor of ten by an amplifier. Using this technique it is possible to observe the initial negative voltage of the inside of a cell, as well as the classic action potential shape with the fast depolarization and slower repolarization.

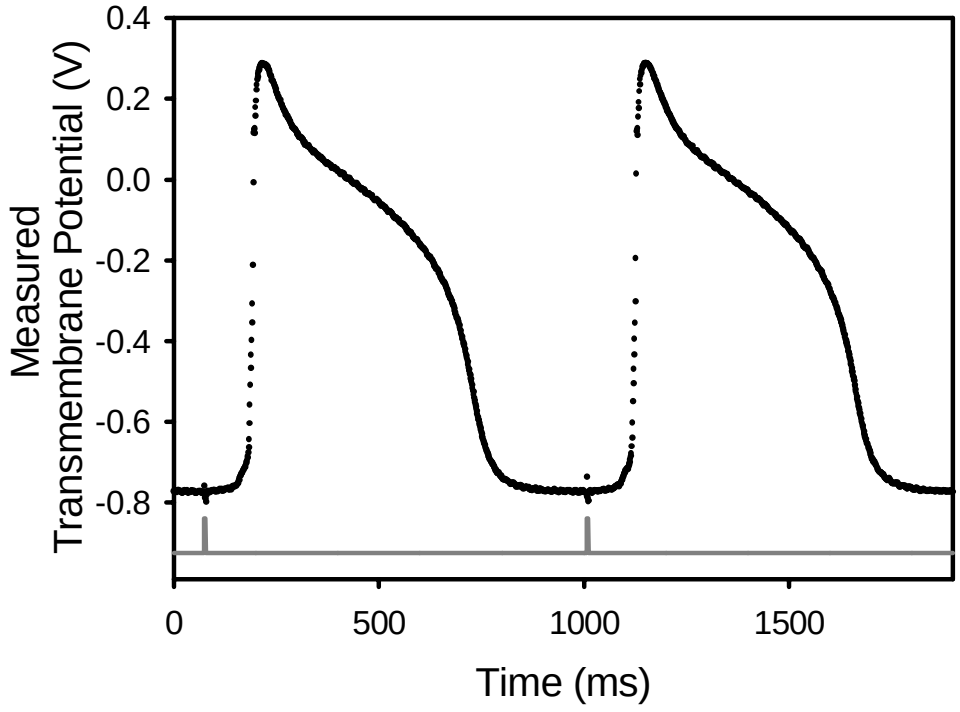

Figure 2.8: The temporal evolution of a microelectrode signal. The signal is recorded from a small peice of periodically paced bullfrog ventricle muscle. The pacing signal (period 950 ms) is shown at the bottom of the figure. The transmembrane voltage was amplified by a factor of ten by the differential amplifier and then digitized with 12-bit resolution over 2 to -2 volts range at 2000 samples/sec.

2.2.2 MAP Electrodes

The monophasic action potential (MAP) electrode has some of the benefits of microelectrodes. The signal is monophasic, with a single polarity deflection just like a microelectrode signal. This gives a signal that has a shape with a clearly defined beginning and end. However, the signal shape is not exactly the same as the transmembrane potential observed with microelectrodes. The distortion of the action potential morphology is offset by the fact that this technique is better for measuring activity from moving cardiac muscle.

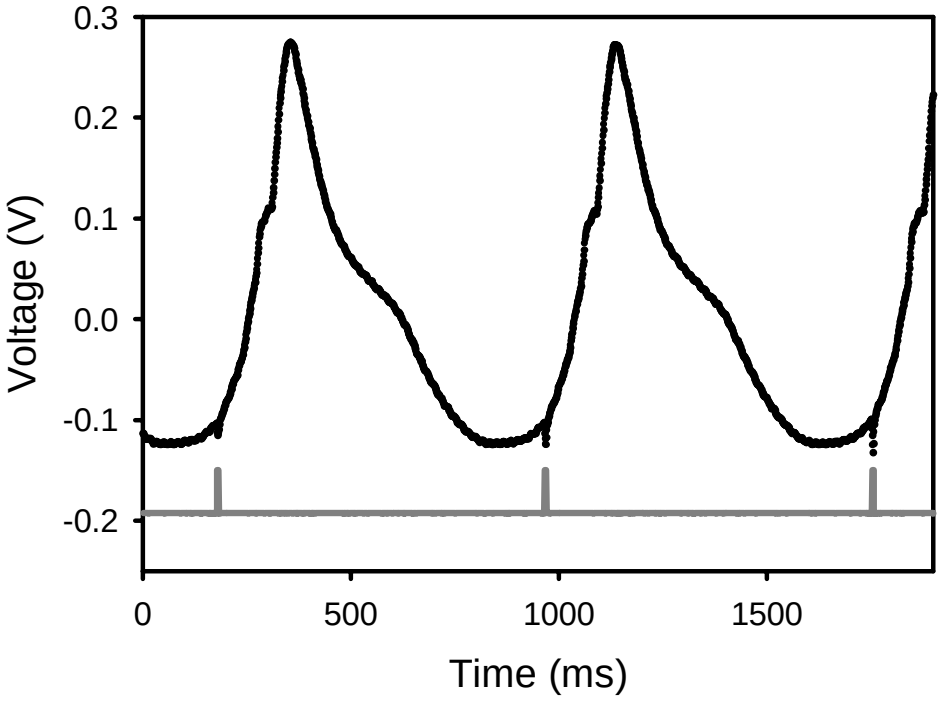

Figure 2.9: The temporal evolution of the signal from a MAP electrode. The signal is recorded from a small peice of periodically paces bullfrog ventricle muscle. The pacing signal (period 800 ms) is shown at the bottom of the figure. The signal was amplified by arbitrary gain and then digitized with 12-bit resolution over 2 to -2 volts range at 2,000 samples/sec.

A MAP electrode is technically an extracellular electrode; however, the signal

it produces is similar to the microelectrode signal. An extracellular measurement is one that is taken from the outside of the cell as opposed to across the cellular membrane. The basic theory of the MAP electrode is that damage to the tissue caused by one of two electrodes creates, at least temporarily, a low resistance path to the interior of the cell [55]. A differential measurement is made between the electrode causing the damage and a nearby electrode connected to the exterior of the cell. The signal from this configuration shows a positive voltage signal when an action potential is observed.

A recording made from a MAP electrode is shown in Fig. 2.9. Notice that the deflections away from the baseline look almost like the action potential measured from a microelectrode. However, the signal shapes are not exactly the same even though these measurements were made from a frog just as in Fig. 2.8.

2.2.3 Extracellular Electrodes

The most commonly used type of electrode to observe cardiac muscle cell's electrical activity are extracellular electrodes. For example, EKG signals are an extracellular measurement. This technique is common because it is very easy to implement. All that is required to obtain an extracellular signal is a wire to collect current and an amplifier to enlarge the signal. This technique is particularly useful because many simultaneous extracellular measurements can be conveniently made.

In contrast to microelectrodes and MAP electrodes, both of which try more or less directly to measure the transmembrane voltages, extracellular electrodes measure the effect of currents leaving the cell. Extracellular techniques take advantage of the fact that the solution bathing the cell has a slight electrical resistance and the ions flowing in and out of the cell cause the voltage on the surface of the cell to vary with respect to a distant electrode in the solution. Analyzing the cell as a core con-

ducting cable (as discussed further in Appendix C) suggests that the current across the cell membrane is roughly the second derivative of the transmembrane voltage. This indicates that the voltage at the surface of the cell relative to a distant ground is proportional to the second derivative of the transmembrane voltage. However, an extracellular electrode cannot distinguish the current from one cell from another cell. Consequently, the extracellular signal is properly thought of as the sum of signals from several cells nearby that are all responding with slightly different phases, depending on when they were activated.

An extracellular recording from a bullfrog is shown in Fig. 2.10 and is compared with a transmembrane measurement recorded simultaneously. While the morphology of the two signals is quite different, the beginning and end of the action potential is clear from the extracellular signal. Unfortunately, the deflection in the extracellular signal that signifies the repolarization is not always detectable. If the repolarization slope is more gentle with smoother inflections, as it is in sheep atria, the second derivative is very small.

2.2.4 Voltage Sensitive Dyes

Voltage sensitive dyes allow a spatial measurement of the transmembrane voltage of cardiac tissue at many spatial locations simultaneously. This is possible because the dyes can penetrate the cell and become embedded in the cell membrane. When the tissue is illuminated with the right frequency of light, voltage variations in across the membrane cause different amounts of fluorescence in a voltage sensitive dye. This fluorescence can be detected and the transmembrane voltage can be determined. However the signals are usually small and the dyes can be toxic to the tissue [56].

The use of voltage sensitive dyes is an emerging technology that promises to revolutionize the measurement of transmembrane voltages. These dyes, with the

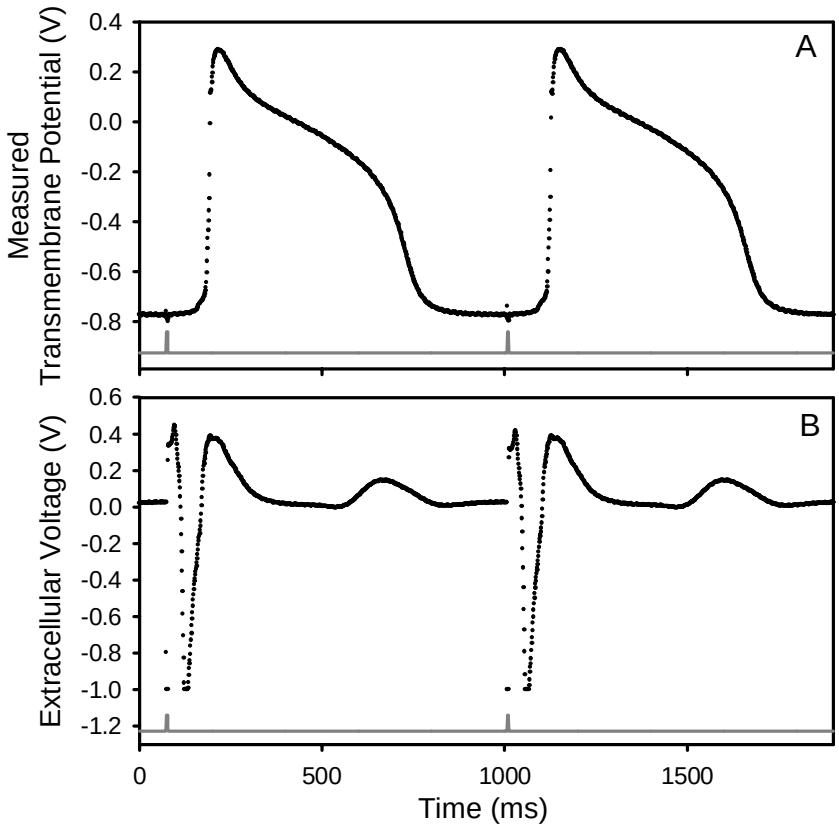

Figure 2.10: A comparison between a signal from a microelectrode (A) and a signal from an extracellular electrode (B). Both these signals were recorded simultaneously from the same frog ventricle and both are relative to a ground wire in the physiological solution. The pacing signal (period 950) is shown at the bottom of each panel. The microelectrode signal was ampilified by a factor of 10, while the extracellular signal was amplified arbitrarily to approximately 2 volts peak to peak.

associated illumination and recording system, will allow measurement of the transmembrane potential at several locations. They have been used with success to observe with high resolution both cardiac and brain slice tissues [56, 57, 58]. They represent one possible future direction for research in controlling cardiac dynamics *in vitro* in larger pieces of cardiac tissue where the extended spatial characteristics play a more crucial role.

2.2.5 Measurement Summary

It is worth noting that the choice of measurement techniques tends to govern how the dynamics of cardiac tissue are viewed. For example, if microelectrode techniques are used, then it is easy to view the action potential as a continuous complex shape, governed by a complex ion flows, and best described with a set of ordinary or partial differential equations with many ionic variables. If extracellular electrodes are used to monitor the activity of cardiac tissue, then only timing information is readily available. This leads to considering the dynamics of cardiac tissue as a map that relates one activation to the next.

2.3 Control of Local Cardiac Dynamics

To complete the control process outlined in Fig. 2.11, it is necessary to process the information about the system and actuate the system to promote some desired state. By way of explanation, I present a mathematical model of single cell dynamics and control. The dynamics of this model become unstable to an alternating behavior (alternans) as the pacing period is shortened. I illustrate control using proportional feedback. This is accomplished by slightly varying the pacing period around its minimal value (actuation).

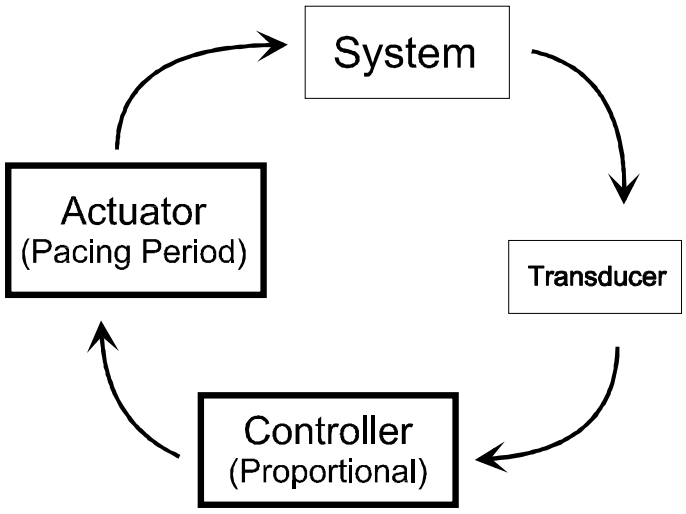

Figure 2.11: An example of how the control and actuation stage of the control process is exemplified by a simple model of a cardiac muscle cell dynamics.

2.3.1 Simple model of periodically paced cardiac muscle

To develop a mathematical model of single cell dynamics, I assume that the action potential duration of a single cell is a function of the diastolic interval. This restitution relationship is given by the function f such that $APD_n = f(DI_{n-1})$. The experimentally observed shape of this restitution relationship (an example is shown in Fig. 2.6) can be described by the function,

$$APD_n = APD_{\max} - Ae^{-DI_{n-1}/\tau}, \tag{2.1}$$

where $APD_{\max}$, A and τ are parameters that are determined experimentally. This function is a monotonic increasing function of its argument DI_{n-1} that saturates to a limiting value for large DI_{n-1}. An example theoretical restitution relation is shown in Fig. 2.12 as a solid line.

To complete this simple model of cardiac dynamics, I assume that the tissue whose restitution is described by (2.1) is periodically paced. The pacing period (PP) must be equal to one action potential duration and one diastolic interval.

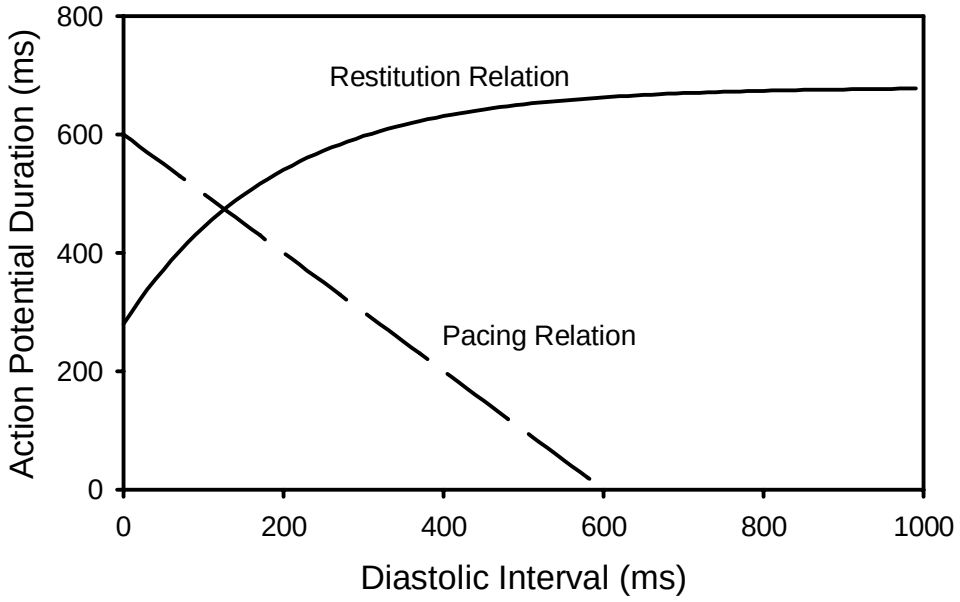

Figure 2.12: A simple model of cardiac behavior can be derived from the restitution relation (solid line) and the pacing relation (dashed line). The restituion curve describes how the APD_n is related to the DI_{n-1}. This restitution relation was generated from equation (2.1) with parameters APD_{max}= 680 ms, A = 313 ms, and τ = 207 ms. The pacing relation (dashed) relates how DI_n is related to APD_n. This curve is produced using equation (2.2) for PP = 600 ms.

Solving for the diastolic interval gives,

$$DI_n = PP - APD_n. \tag{2.2}$$

This pacing relationship between APD_n and DI_n is drawn in Fig. 2.12 as a dashed line. Combining (2.1) and (2.2) equations gives,

$$APD_n = APD_{\max} - Ae^{-(PP-APD_{n-1})/\tau}, \tag{2.3}$$

which maps APD_{n-1} into APD_n. This mapping has a fixed point APD^* where $APD_n = APD_{n-1}$. This fixed point corresponds to the 1:1 behavior observed in cardiac muscle tissue where every stimulus elicits an identical action potential. The action potential and the diastolic interval of this cardiac model system are given by the intersection of the two curves in Fig. 2.12. Notice that the location of this intersection and the consequent fixed point depends on the pacing period.

The mapping is a compressed description of the physical events that occur during periodic pacing of cardiac muscle tissue. The muscle tissue is stimulated, which elicits a response of duration APD_n. After an amount of time equal to PP from the first stimulus the second stimulus occurs, allowing the tissue a diastolic interval $DI = PP - APD_n$. The diastolic interval dictates the next action potential duration.

The fixed point APD^* of the mapping (2.3) loses stability when the pacing period is decreased too far. This behavior is similar to real cardiac tissue that is not able to respond fast enough to produce stable 1:1 behavior, when paced too fast. As the PP is shortened and the fixed point becomes unstable, the map dynamics begins to alternate, a behavior that corresponds to the 2:2 behavior or alternans in real tissue. The stability of our simple cardiac model can be determined expanding the mapping (2.3) in a Taylor series around its fixed point, where $APD_n = APD_{n-1}$

$= APD^*$. Letting $APD_n = APD^* + dAPD_n$ gives

$$\begin{aligned} APD^* + dAPD_n &= f(APD^* + dAPD_{n-1}) \\ APD^* + dAPD_n &= f(APD^*) + \lambda * dAPD_{n-1} + H.O.T. \\ dAPD_n &= \lambda * dAPD_{n-1} + H.O.T. \end{aligned}$$

where λ is defined as the derivative of f evaluated at APD^* and is called the Floquet multiplier of the fixed point;

$$\lambda = -\frac{A}{\tau} e^{-(PP - APD^*)/\tau}. \tag{2.4}$$

At every iteration of the mapping, a small deviation grows by a factor of λ. The fixed point is unstable when λ has magnitude greater than one. Using the values that generated the theoretical restitution curve in Fig. 2.12 in equation (2.4), I find for PP values greater than 631 ms the magnitude of λ is less than one and the 1:1 behavior is stable. For PP less than 631 ms the 1:1 behavior is unstable, and the system alternates.

Figure 2.13 shows a bifurcation diagram for this mapping. At each PP the map is iterated to determine the asymptotic behavior of the map. The resulting APD are plotted against the parameter PP. Notice that in this bifurcation diagram there is a transition at PP=631 ms from a 1:1 behavior where all APD_n are the same to alternating APD_n. This type of bifurcation is called a forward or supercritical bifurcation [59]. The unstable fixed point solution is drawn in Fig. 2.13 with a dashed line.

2.3.2 Proportional control

The 1:1 behavior still exists when the pacing period is selected to place the model dynamics in a regime that produces alternans ($PP < 631$ ms), it is just unstable.

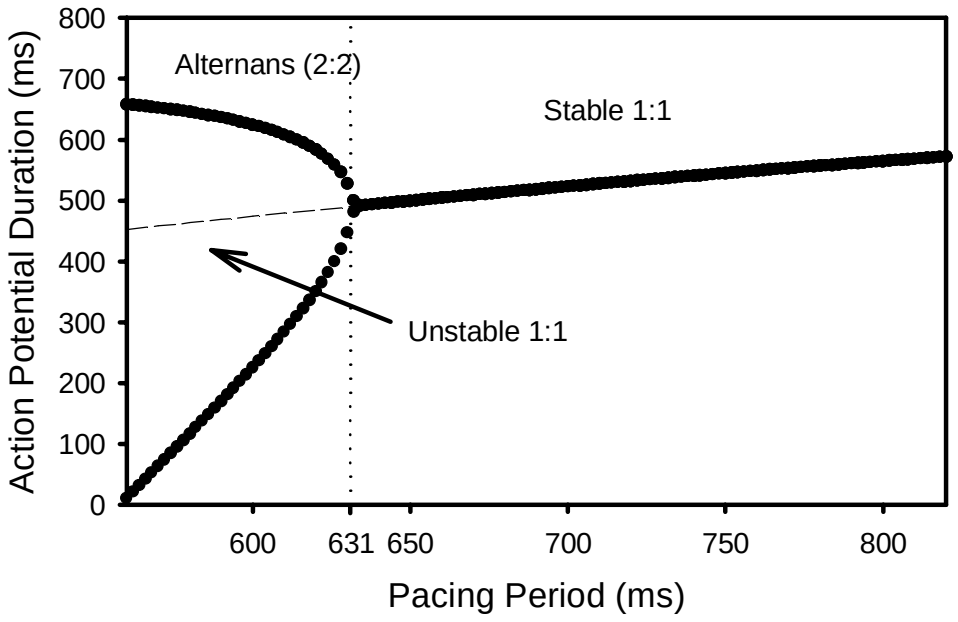

Figure 2.13: A bifurcation diagram of the simple model of point for pacing period greater than 631 ms. For periods less than that the 1:1 dynamics is unstable and the system alternates.

A feedback controller can stabilize the fixed point of the map (the 1:1 state) and suppress alternans. Here, I illustrate control mathematically using proportional feedback. The pacing period serves as the accessible system parameter that the controller actuates to suppress the alternans.

Proportional control seeks to minimize the difference between the current state of the system and a reference state. To stabilize the fixed point of the mapping (2.3), I use the unstable fixed point APD^* as the reference state. The algorithm generates an error signal defined by,

$$\varepsilon_n = -\gamma(APD_n - APD^*), \tag{2.5}$$

where APD^* is the fixed point, and γ is the gain parameter that is freely adjustable.

The controller affects the simple mapping by modifying the n^{th} pacing period

by an amount ε_n. Therefore the n^{th} pacing period is given by,

$$PP_n = PP + \varepsilon_n,$$

where PP is the nominal pacing period. Notice that if the dynamics of this model is on the fixed point, ε_n=0, PP_n=PP, and the system is unperturbed. Therefore, the controller does not modify the existence or location of the fixed point, only its stability. Applying this controller to the mapping (2.3) gives a system of two equations:

$$\begin{aligned} APD_n &= APD_{\max} - Ae^{-(PP+\varepsilon_{n-1}-APD_{n-1})/\tau}), \\ \varepsilon_n &= -\gamma(APD_n - APD^*). \end{aligned}$$

Expanding around the fixed point and eliminating higher order terms gives

$$\begin{aligned} dAPD_n &= \lambda * dAPD_{n-1} - \lambda * \varepsilon_{n-1}, \\ \varepsilon_n &= -\gamma * dAPD_n, \end{aligned}$$

where λ is defined as before. It is possible to solve the set of equations by combining them to give

$$dAPD_n = \lambda(1+\gamma) * dAPD_{n-1}.$$

For this new system to be stable, γ must be chosen such that $\|\lambda(1+\gamma)\| < 1$.

It should be noted as an aside that generally, the application of control results in a system plus control that is higher in dimension than the system without control. The Floquet multiplier of the fixed point of the system plus control can then be found directly by computing the eigenvalues of the linearized system plus control. It is also possible to determine whether or not the Floquet multipliers of this system plus control have magnitude greater than one without solving for them by using the Schurr-Cohen criterion [60].

A simple control experiment illustrating how proportional control works is shown in Fig. 2.14. The model cardiac system is iterated for a nominal pacing period of 600 ms. At this period the Floquet multiplier of the fixed point is -1.08, so the model produces alternans. At the first vertical dashed line proportional control is turned on with γ=0.1. Initially, perturbations are made to the pacing period stabilizing the fixed point. When the dynamics is on the fixed point the error signal goes to zero. The fixed point again becomes unstable and the dynamics start to return to alternans when control is turned off again (the second vertical dashed line).

2.4 Summary

A closed-loop or feedback controller works by employing a circular process of observing the dynamics of the target system and adjusting a parameter of the target system to change the dynamics in a desired manner. The target system (periodically paced cardiac tissue) produces complex behavior that is undesirable. A transducer makes a measurement of the dynamics of the system. This measurement is used by the controller to compute an error signal. The error signal causes the actuator to modify a system parameter to change the dynamics in order to minimize the error signal. If the controller is successful then this measurement and correction loop continues until the system displays the desired behavior, producing a zero error signal.

The model and controller in this chapter are designed for small pieces of tissue, but we are ultimately interested the control of complex spatio-temporal dynamics. However, it is unknown how to modify or if its possible in general to use a temporal controller to control spatial dynamics. There is some indication that these controller have some positive effect on spatio-temporal complexity [23]. Another problem is that during spatially complicated behaviors the stimulation of the local tissue is

not periodic and the pacing timing is not available for modification. In addition, simple feedback controllers designed to stabilize unstable states are unable to modify bistability which is a highly prevalent behavior. In chapter six I describe a set of experiments that attempt to overcome these difficulties in a whole sheep heart experiment. This experiment, while inconclusive, points out the specific difficulties to overcome in future experiments.

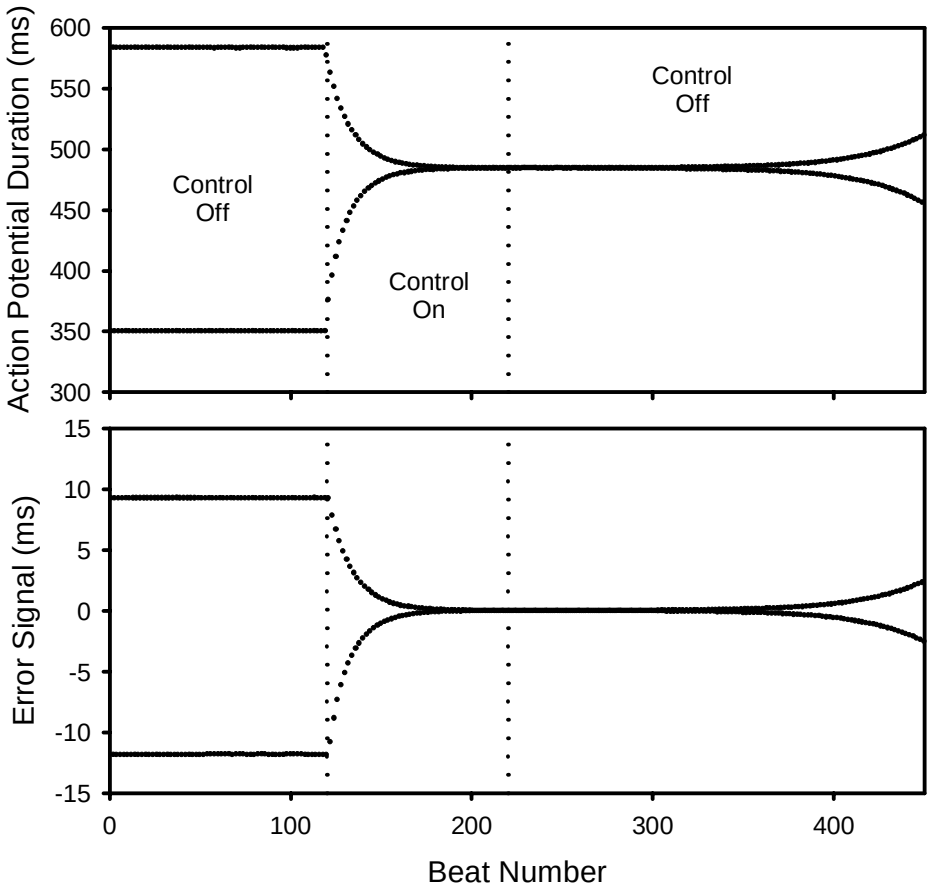

Figure 2.14: The temporal evolution of the simple model of periodically paced cardiac tissue. The pacing period PP is selected in a regime where the system produces alternans (600 ms). At the top of the figure is the APD versus beat number and at the bottom of the figure is the error signal versus beat number. Between the two dotted vertical lines control is on.

Chapter 3

Dynamics of small pieces of cardiac muscle

As discussed in the introduction to this dissertation, the long term goal of this research program is to devise methods for controlling or suppressing spatio-temporal disorganization occurring in human hearts during fibrillation. The general approach is to investigate methods developed by the nonlinear dynamics community for controlling chaos using small perturbations. In this chapter and the next two, I try to understand the dynamics of small pieces of tissue where spatial complexity is not important. This work has implications for controlling whole heart dynamics. For example, I found a correlation between windows of bistability and unsustained reentry in whole sheep atria *in vivo*, during initial experiments conducted by my collaborators in biomedical engineering and myself [65]. In addition, Karma *et al.* [24] has found a connection between the initiation spatio-temporal complexity and a local bifurcation to alternans (a period doubling bifurcation) using a mathematical model of cardiac muscle.

In the sections that follow, I present an exploration of tissue dynamics during rapid pacing. The experimental setup consists of a small piece of frog heart tissue (ventricular myocardium) and various support systems. The bullfrog ventricular muscle is periodically paced with an external electrical stimulator. This test-bed gives an initial assessment of the importance of parameter variation during experiments and animal-to-animal variation as well as experience in cardiac electrophysiology. In addition, I use this test bed system to determine types and prevalence of local tissue bifurcations. This information is important because control protocols

need to be designed to deal with commonly encountered behaviors. This chapter ends with the analysis of simple mathematical models that give some insight into the observations and develops a framework for later use.

3.1 Small piece of tissue test bed

I investigate *in vitro* the response of small pieces of bullfrog (*Rana catesbeiana*) cardiac muscle to periodic electrical stimulation to determine the prevalence of different rate-dependent behaviors. Under various conditions of periodic electrical stimulation (pacing), M stimuli can elicit N responses (M:N behavior). A wide range of these responses have been observed where the specific type of behavior depends on the type of cardiac tissue, animal species, or stimulus parameters, such as frequency [63], amplitude [68], and shape [120]. I concentrate on rate-dependent behaviors in cardiac muscle because of the wide range of excitation rates that occur in both healthy and pathological cardiac tissue (See Table A.6). Previous studies [68] have focused on multiple experiments in tissue samples taken from a few animals. In contrast, I explore the range of dynamical behaviors in a large number of animals.

In these experiments, the heart is excised from adult animals of either sex whose length ranges between 4 and 8 inches. The animals are anesthetized using 1 mg/L 3-aminobenzoic acid ethyl ester (MS-222) mixed with cold tap water, double pithed, and dissected by cutting along the ventral side of the body. A detailed description of this procedure can be found in [64]. The heart is excised and the auricles (frog atria) and pacemaker cells cut away. All procedures are approved by the Duke University Institutional Animal Care and Use Committee (IACUC). After the pacemaker cells are cut away, a small piece of ventricular myocardium (typically $3\times3\times5$ mm) is removed, placed in a chamber, and superfused with a recirculated physiological solution.

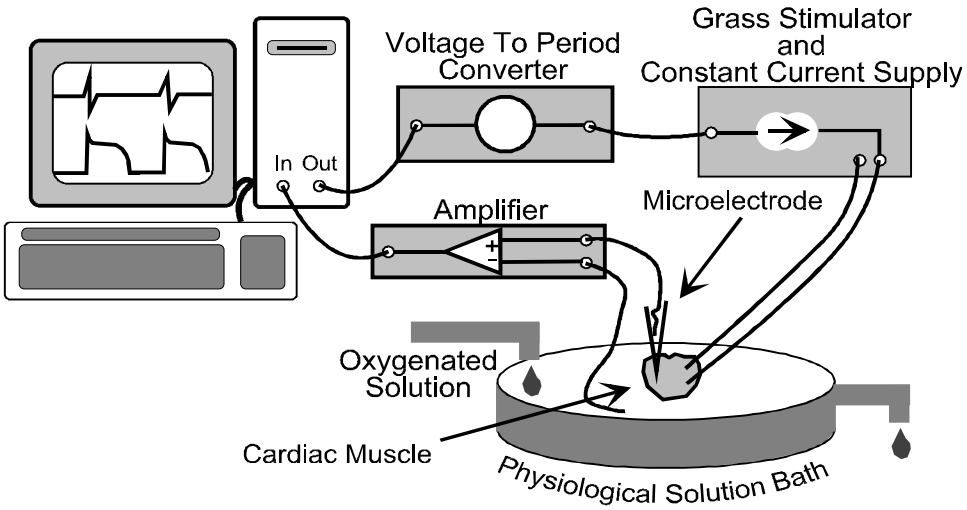

Figure 3.1: The experimental setup to investigate the dynamics of rapidly paced cardiac tissue. This setup consists of three subsystems. The first is the tissue bath system shown at the bottom of the figure. The physiological solution is flowed (100 ml/min) across the tissue, re-oxygenated, warmed (or cooled) and then recirculated. The second subsystem is the pacing system. The computer generates a voltage that a voltage-to-period converter and Grass stimulator turn into a train of constant current pulses. These current pulses are applied to the tissue through two tungsten wires. The final subsystem is the recording system. The microelectrode records transmembrane potentials. The signal from this electrode is recorded along with the pacing signal by the computer.

The tissue size is small enough so that is acts synchronously and does not show spatio-temporal effects. Tissue of this size is approximately 10 times the conservatively estimated passive length scale computed using the core conductor cable theory and approximately 1/10 of a dynamical length scale based on the action potential duration and propagation velocity (see Appendix C). Occasionally, some autonomous beating activity from the tissue was observed. I believe that this was an ectopic focus which is a cell that activates periodically causing stimulation. Trimming some tissue off the region of the ventricle that was attached to the atria often rectified the situation, indicating that there were still some pacemaking cells

attached.

The excised tissue is placed in a custom designed support system. This system is intended to maintain the vitality of the cardiac tissue. The support system consists of an open-top chamber with a wax bottom where the cardiac tissue is pinned down. A Fischer Scientific peristalsis Mini-Pump flows physiological solution into the chamber and across the tissue. The physiological solution that superfuses the cardiac tissue is held in a 250 ml Pyrex bottle. This solution contains 110 mM NaCl, 2.7 mM KCl, 1.5 mM $MgCl_2$, 1.8 mM $CaCl_2$. This combination of salts provides the correct ionic concentrations necessary for excitability. In addition the solution contains 5.6 mM glucose for energy and 30 mM $NaHCO_3$, 2.8 mM Na_2HPO_4 and 1 mM HEPES all of which preserve the pH at 7.4±0.1. In most experiments (∼80% of hysteresis loops) 5-20 mM of 2-3-butanedione monoxime (DAM) is added to the physiological solution to reduce the mechanical motion of the tissue due to contractions. Riccio *et al.* [89] have shown that the DAM alters the dynamics of the heart muscle, however, I have performed this experiment both with and without DAM and have not observed any change in the preparation response. To oxygenate the superfusate and provide carbonate buffering the solution is continuously bubbled with 95% O_2 and 5% CO_2. The details of how the solution was designed are in Appendix E. The Pyrex bottle is submersed in a water bath that is maintained at a temperature of 20±2 °C by a NESLAB RTE-210 heater/chiller.

The physical setup of the pacing and recording systems is shown in Fig. 3.1. The tissue, quiescent in absence of an applied stimulus, is paced with 4 ms square pulses generated by a computer-controlled Grass S48 stimulator with a Grass PSIU6 constant-current isolation unit. The synchronization signal that operates the Grass Stimulator is produced by a voltage-to-period converter I constructed (Fig. 3.2). Stimuli are applied through two (51 μm diameter) tungsten wires set about 2 mm

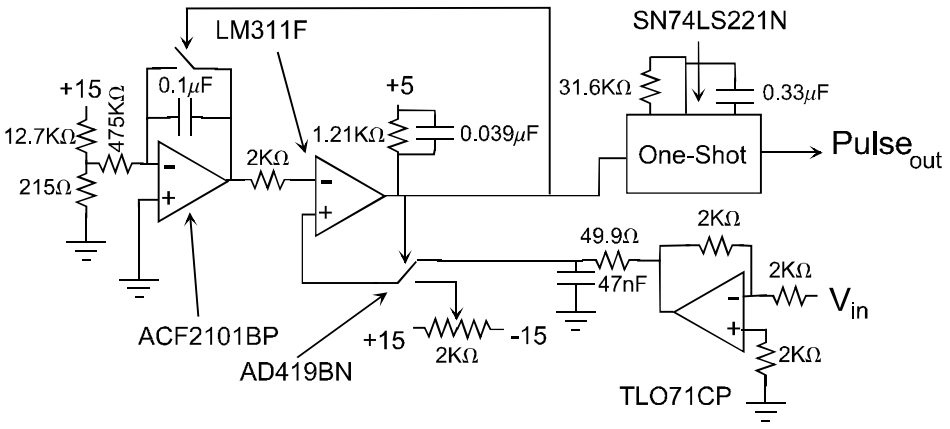

Figure 3.2: The voltage-to-period conversion circuit. The basic operation of this circuit is to integrate a DC voltage up to a threshold voltage that is externally controller. I after the integrator's output voltage crosses the threshold it is rest and a TTL pulse is generated. The experimentally observed relation between the input voltage and the output time is Time (V) = 0.191*V_{in}(V)+0.015

apart on the tissue surface. The current amplitude of the applied stimulus is typically twice the minimum amplitude necessary to obtain a response [49]. Under these conditions, simple dynamical responses (typically 1:1, 2:1, and 2:2 states) are observed. To allow the tissue time to recover from the trauma of the dissection before initiating data collection, the tissue is paced at $\sim$ 1000 ms intervals for about 20 min. The temporal evolution of the amplified intracellular signal and stimulus waveform are digitized at a sample rate of 1 or 2 kHz.

The computer control of the system is accomplished using a combination of a Intel 166 MHz Pentium based computer running National Instruments LabView 4.1 for Microsoft Windows 95 and a National Instruments AT-MIO-16E-2 multifunction data collection card. A flow chart of the custom LabView software that controls this experiment is shown in Fig. 3.3. The first loop in the code governs the sweep across decreasing pacing periods. At each pacing period the transients are allowed to settle. Then the computer records the tissue dynamics, and the period is decremented. The

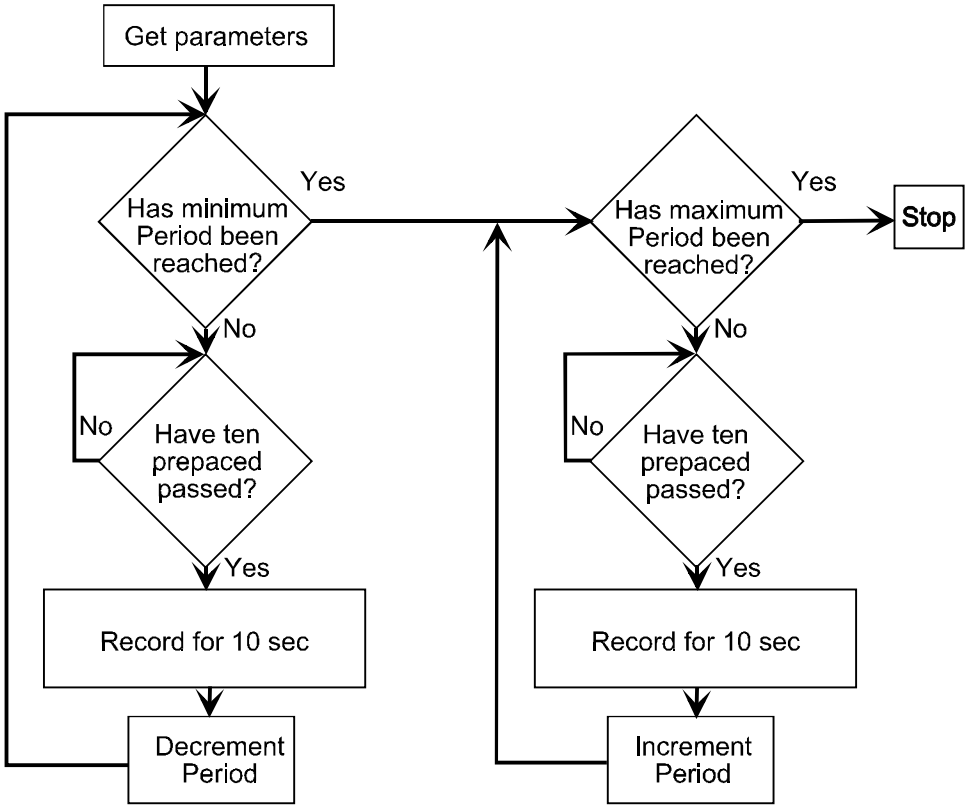

Figure 3.3: A flow chart of the temporal sequence of operations of the labview pacing program. The program flow is broken up into two parts. The first records the response of the periodically pace tissue to decreasing periods. The second part of the program records the response of the tissue to increasing periods.

second loop in the code similarly governs the increasing pacing period part of the protocol.

The state of the cardiac tissue was observed using microelectrodes. This technique is described briefly in Chapter 2 and in more detail in Appendix E. A transmembrane potential difference recording using a microelectrode is shown in Fig. 3.4. The intracellular (transmembrane) voltage is measured within 1-2 mm of the stimulus electrodes. The signal was amplified with a DAGAN 8100 10$\times$ preamplifier.

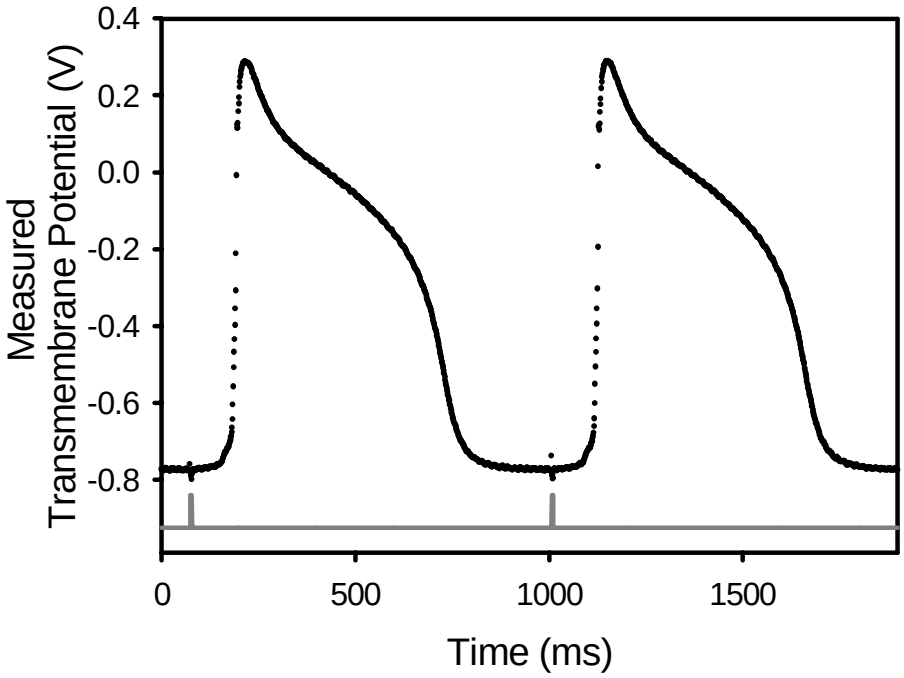

Figure 3.4: A signal from a small piece of periodically paced bullfrog ventricle muscle obtained using a microelectrode. The pacing signal is shown at the bottom of the figure. The pacing period was 950 ms. The signal was amplified by a factor of ten by the differential amplifier and then digitized with 12-bit resolution over 2 to -2 volts range at 2000 samples/sec.

Measurement of the time evolution of the transmembrane potential allows me to determine the action potential duration (APD), the duration of the deflection of the transmembrane potential away from its rest state in response to a stimulus. The APD is determined at 70% of peak height (which I find gives less scatter in our experimental data than the more common cutoff of 90%) using a custom software routine. I also measure the diastolic interval (DI), defined as the interval between the repolarization after an action potential and the start of the next response.

This experimental setup allows the exploration of rate dependent dynamics of small pieces of cardiac tissue. This exploration is important when trying to un-

derstand what causes the breakup of cardiac arrythmia into the spatio-temporal complex dynamics of fibrillation.

3.2 Characterization of the Small Tissue System

A typical method for investigating the dynamics of small pieces of cardiac tissue is to measure the time for cells to repolarize after depolarization by a brief electrical stimulus (this time interval is known as the action potential duration, APD) as the interval between stimuli (pacing period, PP) is varied slowly. When the tissue is paced slowly, each stimulus elicits one action potential, with all APD equal (1:1 pattern). Faster pacing results in a decrease in both DI and APD, a property of cardiac muscle known as restitution.

As PP is decreased, there is a minimum diastolic interval θ where the tissue becomes unable to recover fast enough after each stimulus to respond to the next. The combination of θ and APD is defined as the refractory period, during which the tissue apparently does not respond to applied paces. If the tissue is unable to respond to every stimulus, it then enters a 2:1 pattern in which one response occurs for every two stimuli. Occasionally, a 2:2 pattern (responses of alternating duration) intervenes between the 1:1 and 2:1 states [85]. I observe hysteresis between these dynamical states as the pacing interval is swept up and down.

The coexistence of two stable states at the same PP is seen in Figs. 3.5a and 3.5b, where I show the temporal evolution of the transmembrane potential for a PP of 600 ms in the same tissue preparation. Figure 3.5a is recorded after the PP is slowly varied from 1200 ms to 600 ms, and Fig. 3.5b is recorded after the PP is slowly varied from 300 ms to 600 ms. This observation demonstrates that the tissue can display two different behaviors at the same PP.

A bifurcation diagram is a convenient way to summarize observations of the

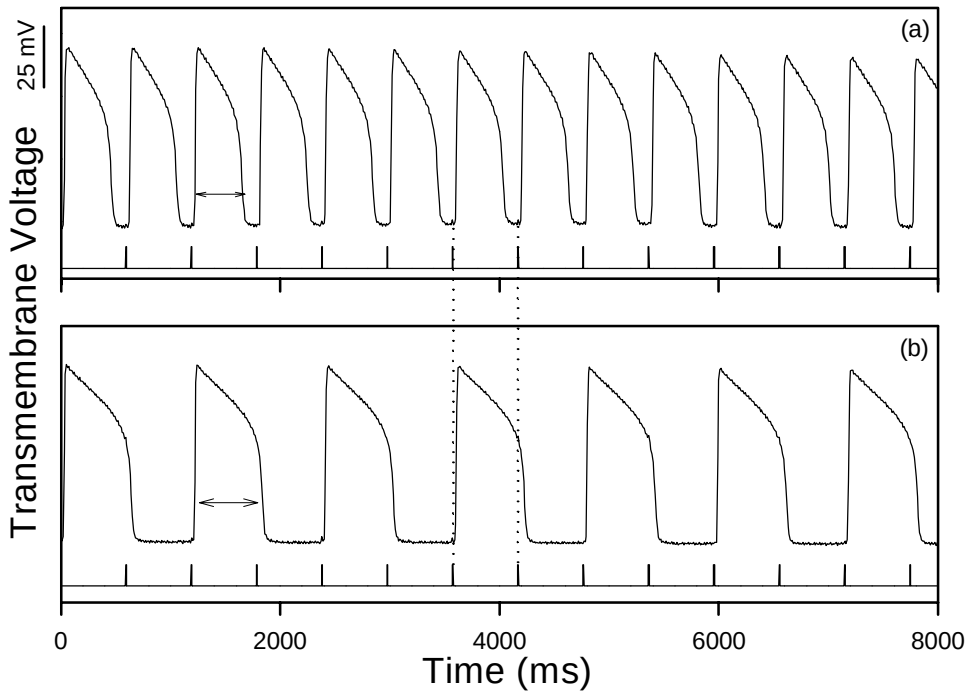

Figure 3.5: Time evolution of transmembrane potential during a typical hysteresis experiment. The stimulus waveform is shown at the bottom of each diagram. (a) The tissue exhibits 1:1 dynamics for slow pacing during a PP downsweep. This time series is taken from the data used to generate points on Fig. 3.6 (open circles) at a PP of 600 ms. (b) The tissue exhibits 2:1 dynamics (closed triangles in Fig. 3.6) for the same PP used in (a), but during an upsweep. Arrows indicate measured APD. Vertical dotted lines illustrate the correspondence between stimulus intervals in (a) and (b).

long-term dynamical behavior of the tissue as PP is varied slowly. I obtain such a diagram by recording APD while adjusting PP across a wide range of physiological values, from 1200 to 300 ms in 100 or 50 ms intervals (downsweep), and then from 300 to 1200 ms, again in 100 or 50 ms steps (upsweep). For each PP, the response of the tissue to the first 5-10 stimuli is discarded in order to eliminate transients and the subsequent behavior is recorded for up to 10 seconds. After discarding transients, the width of each action potential is determined at 70% of full repolarization and plotted at each PP.

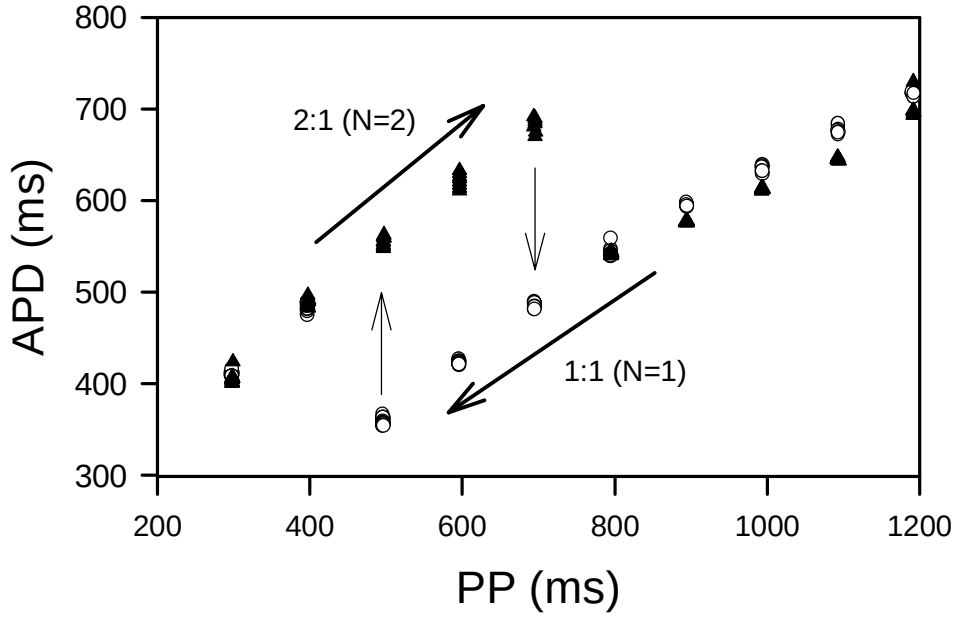

Figure 3.6: A bifurcation diagram showing 2:1→1:1 hysteresis. Open circles are APD measurements as the PP is swept downward (i.e., the tissue is driven faster); closed triangles show APD during the PP upsweep.

Figure 3.6 shows a bifurcation diagram for the experimental preparation in Fig. 3.5. For long PPs, the tissue responds in a 1:1 pattern. The APD decreases for decreasing PP (open circles). As PP is decreased from 500 to 400 ms, an abrupt increase in the APD occurs, highlighted by the thin vertical arrow, indicating the bifurcation from a 1:1 to a 2:1 pattern. After the smallest PP of our pacing protocol is achieved, the PP is increased slowly (closed triangles). The tissue remains on the 2:1 branch for a wide range of PP values which elicited 1:1 response during the downsweep. At a PP between 700 and 800 ms, the tissue response makes an abrupt transition back to 1:1 behavior. The presence of hysteresis indicates that this transitions is either a subcritical or a saddle node bifurcation [59].

For some preparations, the tissue undergoes a different set of bifurcations, as shown in Fig. 3.7. During the downsweep (open circles), a 1:1 → 2:2 transition

occurs, followed by a bifurcation from 2:2 to the 2:1 branch, indicated by a vertical arrow. During the upsweep (closed triangles) the tissue remains on the 2:1 branch, eventually returning to the 1:1 regime. Note that the 1:1 $\rightarrow$ 2:2 transition is a supercritical bifurcation, while the 2:2 $\rightarrow$ 2:1 transition is a saddle-node (or subcritical) bifurcation, like the 1:1 $\rightarrow$ 2:1 transition shown in Fig. 3.6. In all tissue preparations which show 2:2 behavior, bistability is also observed. Bistability between 1:1 and 2:1 dynamical states has been reported previously both in periodically paced bullfrog myocardium [3] and spontaneously beating aggregates of embryonic chick heart cells [70].

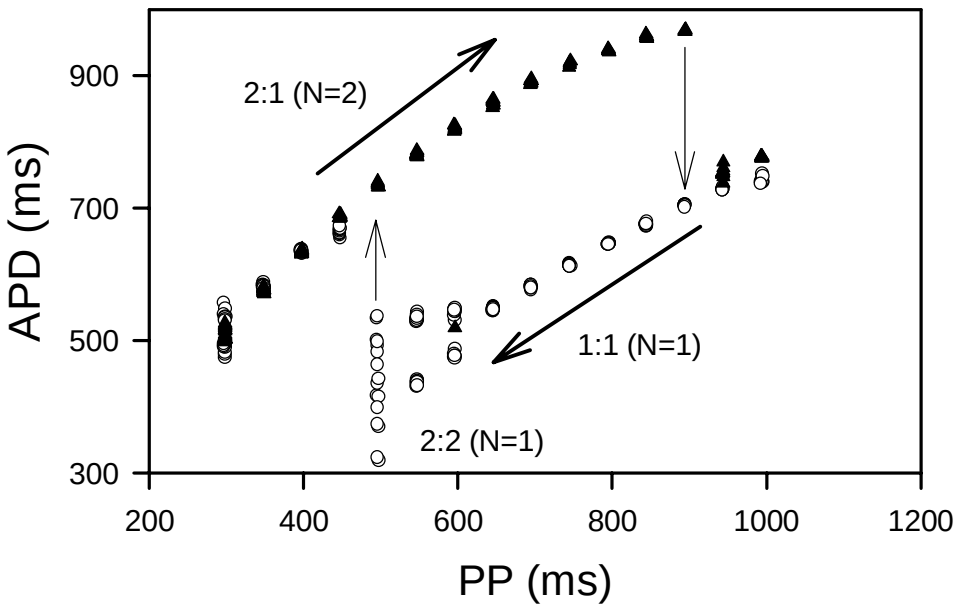

Figure 3.7: Observations of alternans, bistability and hysteresis from tissue taken from a different animal than that used to generate the data in Fig. 3.6. Thick arrows show the direction of the PP sweep; thin arrows indicate the 2:2$\rightarrow$2:1 and 2:1$\rightarrow$1:1 transitions. Note that several data points appear almost on top of each other for each PP, representing slight variations in measured APD.

Alternans and bistability are observed to occur with different probabilities. In one set of experiments I found that bistability between 1:1 and 2:1 patterns exists

in 17 of 23, or 74%, of the cardiac preparations. The window of bistability was situated over a range of pacing periods (PP) which lay near the natural period of the resting heart ($\sim$ 1000 ms), and extended for $\sim$ 160 ms. I found that 2:2 behavior (alternans) occurred in 8 of 23 or 35% of cardiac preparations. In this experiment in all cases where 2:2 behavior was observed, bistability also occurred between 2:2 and 2:1 dynamics.

The size of the hysteretic windows of various preparations, including regions of 2:2$\leftrightarrow$2:1 hysteresis ranges from 50 to 400 ms with an average of 157 $\pm$ 67 ms. Note, however, that our PP step size is 50 or 100 ms; it is possible that animals in which I do not observe hysteresis actually possess hysteretic windows below the resolution of our experiment. In two of the 23 animals, I studied two different pieces of ventricular epicardium. The overall dynamics in both pieces of tissue from a single animal were qualitatively similar, though the specific location of the bifurcations varied.

In a later set of experiments, I found similar rates of occurrence of both bistability and alternans. During the experiments conducted to test control alternans (Chapter 4), I found that 18 out of 40 animals showed alternans (45%). This value is within the 90% confidence interval of the previously observed alternans frequency. Adding the statistics for alternans together brings the observed percentage to 41%. I did not pace, however, the tissue fast enough to cause a bifurcation to 2:1 dynamics. Similarly, in experiments designed to explore transitions between bistable states, I observed 9 of 12 (75%) animals slowed bistability.. Unfortunately, I did not record the prevalence of alternans. Both of these additional observations support the generic nature of these dynamics in rapidly stimulated local tissue.

3.3 Map Based Model Of Local Cardiac Tissue

A qualitative understanding of my observations may be obtained from simple mapping models of localized cardiac dynamics such as that suggested by Nolasco and Dahlen [71] and later generalized by Guevara *et al.* [63]. In such models, the action potential duration APD_{n+1} is typically expressed as

$$APD_{n+1} = f(N * PP - APD_n), \tag{3.1}$$

where N is the smallest integer satisfying the condition $N * PP - APD_n > \theta$. Note that the 1:1 and 2:2 patterns observed in the experiments correspond to $N = 1$, and the 2:1 pattern corresponds to $N = 2$. This is basically the same model that I used in Chapter 2. For some tissue preparations, including bullfrog ventricular muscle [71], a function of the form

$$f(DI_n) = APD_{\max} - Ae^{-DI_n/\tau}, \tag{3.2}$$

where $DI_n \equiv N*PP-APD_n$, gives good agreement with experimental observations, where $APD_{\max}$, A, and τ are tissue-dependent constants.

To find model parameters that fit the observations shown in Fig. 3.6, I require that the model undergoes 1:1→2:1 and 2:1→1:1 transitions at the observed transition points (PP_u, APD_u) and (PP_d, APD_d) in the experiment. In addition, I require that the model does not undergo a bifurcation to a 2:2 state. Along with the definition of θ as the smallest possible DI then these conditions become,

$$PP_u - APD_u = \theta \tag{3.3}$$

$$PP_d - APD_d = \theta \tag{3.4}$$

$$APD_u = f(PP_u - APD_u) \tag{3.5}$$

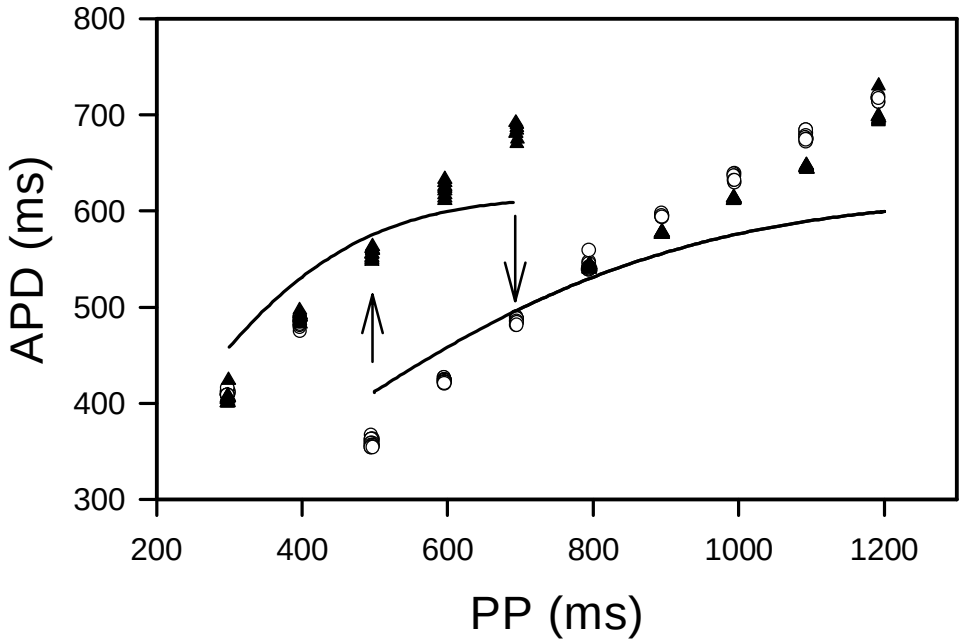

Figure 3.8: Comparison between the predictions of the simple mapping model and the experimental observations shown in Fig. 3.6. The solid line is obtained by iterating (3.1) where $f(DI)$ is of the form (3.2), and parameters $APD_{max} = 616$ ms, $A = 313$ ms, $\tau = 207$ ms, and $\theta = 86$ ms. The upward arrow indicates the 1:1→2:1 transition; the short downward arrow indicates the 2:1→1:1 transition in the observed data and the one-dimensional model.

$$APD_d = f(2PP_d - APD_d) \tag{3.6}$$

$$f'(\theta) = -1. \tag{3.7}$$

Combining Eqs. (3.3)-(3.6) gives,

$$\begin{aligned} PP_u - PP_d &= APD_u - APD_d \\ &= f(2PP_u - APD_u) - f(PP_d - APD_d) \\ &= f(PP_u + \theta) - f(\theta) \\ &= Ae^{-\theta/\tau}(1 - e^{-PP_d/\tau}). \end{aligned} \tag{3.8}$$

Using (3.7) to solve (3.2) for A gives,

$$A = \tau e^{\theta/\tau}$$

and that along with (3.8) gives,

$$PP_u - PP_d = \tau(1 - e^{-PP_d/\tau}).$$

However, these conditions are not sufficient to determine τ. I determine τ by least squares fitting the system of equations to the data on the 1:1 branch.

To find a least squares fit of a model equation to data generally requires an iterative procedure. First a chi-square (χ^2) is produced by summing for of all the data the difference squared between the actual APD_i^* and the predicted APD_i^* from the model equation. Therefore χ^2 is given by,

$$\chi^2 = \sum_{\substack{data \\ points}} [APD_i^* - g((APD_i^*, PP_i), \vec{C})]^2,$$

where APD_i^* is the ith measured APD, PP_i is the ith pacing period, and $\vec{C} = (APD_{max}, A, \tau)$ is a vector where each element is one of the model equation parameters. To minimize χ^2, it is necessary to iteratively adjust the parameters to make χ^2 smaller. This is possible by changing the parameter vector along the gradient of χ^2 with respect to the parameters. So at each new step the new parameter vector is given by,

$$\vec{C}_{new} = \vec{C}_{old} + \nabla_{\vec{C}}\chi^2 * step\ size,$$

where the step size is selected to be as large as a possible without the process losing stability.

Figure 3.8 shows a comparison between our experimental observations shown in Fig. 3.6 and the theoretically predicted bifurcation diagram generated using the simple mapping given by Eqs. (3.1)-(3.2). While it is seen that bifurcations occur at the correct PP values, there is a significant discrepancy in the observed and predicted values of the APD's. It is important to note that this simple model is exquisitely sensitive to small parameter changes. Decreasing τ by as little as

10% yields a map that bifurcates to 2:2 behavior before the transition to the 2:1 branch. This underscores the potential pitfall of adhering to rigid choices of parameter regimes when developing or implementing models of biological systems.

I have investigated the discrepancy between the simple one-dimensional model and the observed data, and find that it is impossible to find a smooth function f that depends only on the diastolic interval $DI_n = N * PP - APD_n$ that both fits accurately the data of the $N = 1$ branch and reproduces the appropriate bifurcation diagram. In addition, I observe in some animals that the stimulus that does not elicit a response in the 2:1 state does, in fact, have an effect on the tissue dynamics. This can be seen in Fig. 3.9, which shows the dependence of f on DI_n for the data displayed in Fig. 3.6. It is seen that one value of DI can give rise to two different values of APD, depending on whether the tissue response is on the $N = 1$ (solid line) or $N = 2$ (dotted line) branch. Thus the stimulus which does not elicit a response in the 2:1 pattern does in fact alter the tissue dynamics, and the observed data cannot be described by a single-valued function. Furthermore, the observed stability of the 1:1 branch is inconsistent with the fit to the $N = 1$ (solid line) branch using Eqs. (3.1)-(3.2). The 1:1 pattern generated by the model must be unstable when the slope of f is greater than unity. However, the observed 1:1 pattern is stable when the rate of decrease in APD with respect to a decrease in DI is larger than unity.

To correctly account for the observed stability, a model must include at least one other dynamical variable. The difference-differential model, proposed by Chialvo and Jalife [121], includes a memory term M describing the long-term evolution of the tissue properties. Their model is simplified by converting the differential part of the model into another difference equation by polling its value at the pacing period. In addition their model has a latency equation that models propagation,

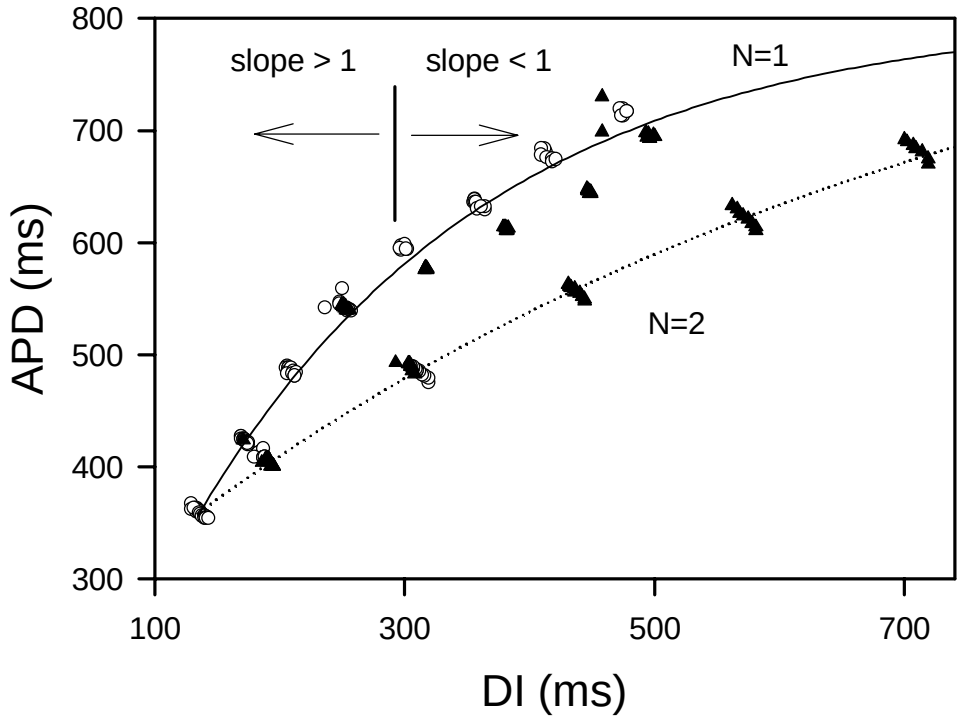

Figure 3.9: Action potential duration as a function of diastolic interval for the data shown in Fig. 3.6. Open circles indicate downsweep; closed triangles indicate upsweep. Data separates into two distinct branches, one corresponding to $N = 1$ and the other to $N = 2$. The solid and dotted lines were added to guide the eye. Vertical line at DI=285 ms indicates the diastolic interval at which the slope of the $N = 1$ branch becomes greater than unity. The solid (dotted) curve guide the eye along the $N = 1$ ($N = 2$) branch.

which I ignore because I assume that the tissue acts synchronously and there are no propagation effects. Under these simplifications this model reduces to

$$\begin{aligned} APD_{n+1} &= c_1(1 - M_n)[1 - c_2 e^{(N*PP - APD_n)/\tau_1}], \\ M_{n+1} &= [1 + (M_n - 1)e^{-APD_n/\tau_2}]e^{(N*PP - APD_n)/\tau_2}, \end{aligned} \tag{3.9}$$

with N determined as above. A least squares fit of the fixed points of (3.9) to the data on the $N = 1$ branch (open circles in Fig. 3.6) is illustrated by the dotted lines in Fig. 3.10.

The least squares fitting procedure used here is similar to the procedure used on the simple mapping. The main difference is that the data does not include a measurement of the memory variable M. However because I am fitting to the fixed points of (3.9), M_{n+1} equals M_n. This allows the fixed point M^* to be solved for a function of the data vector (APD^*,PP) giving,

$$M_i^* = e^{(N*PP_i - APD_i^*)/\tau_2}(1 - e^{-APD_i^*/\tau_2})/(1 - e^{(N*PP_i - APD_i^*)/\tau_2 - APD_i^*/\tau_2}).$$

This equation can be substituted into the first equation of (3.9) giving,

$$APD_i^* = g((APD_i^*, PP_i), (c_1, c_2, \tau_1, \tau_2)),$$

g can be derived from (3.9). The chi square (χ^2) of this difference is defined by,

$$\chi^2 = \sum_{\substack{data \\ points}} [APD_i^* - g((APD_i^*, PP_i), (c_1, c_2, \tau_1, \tau_2))]^2.$$

Chi-square χ^2 can be minimized using the gradient method described earlier.

This model clearly fits the $N = 1$ branch data better than the simpler model. However, there is little agreement between the model and observed APD values on the $N = 2$ branch, and the transition from the $N = 2$ to the $N = 1$ branch occurs at a much longer PP than that found experimentally. In addition, this model accounts for the observed stability of the N=1 branch, but it can not take care of difference between N=1 and N=2 branches. This suggests that significant improvements must be made to this model before it can completely describe the experimentally observed results.

3.4 Conclusion

In this chapter, I developed an animal model test-bed for exploring dynamics of cardiac muscle. I found that periodically paced small pieces of tissue show a surprising level of complexity. The tissue dynamics in response to shortening pacing

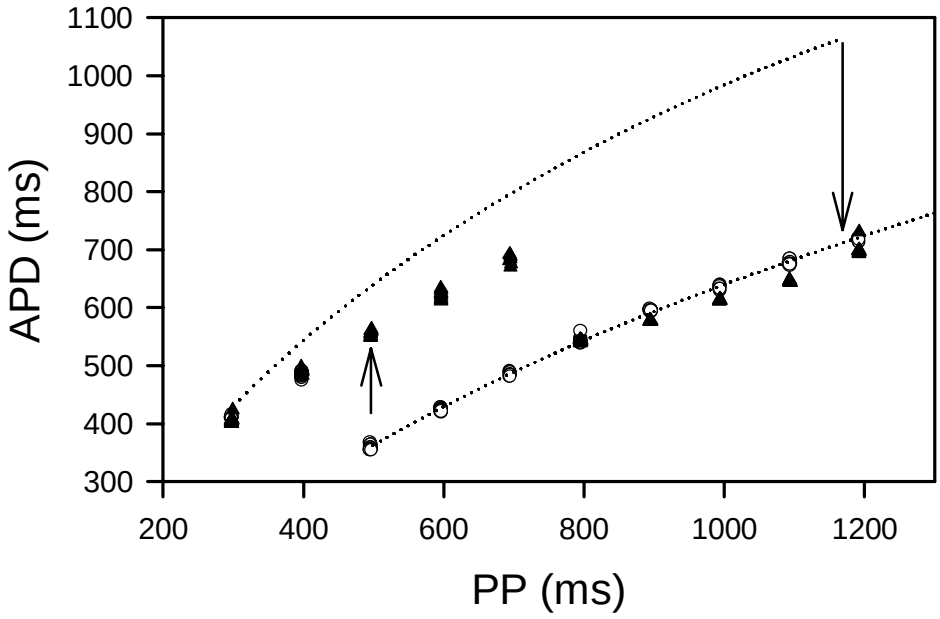

Figure 3.10: 2-D model fit to the bifurcation diagram shown in Fig. 3.6. The line indicates a fit using the two-dimensional mapping model (3.9), with c_1=1359 ms, c_2=2.64, τ_1=51 ms, τ_2=1080 ms and θ = 136 ms. The upward arrow indicates the 1:1→2:1 transition; the long downward arrow indicates 2:1→1:1 transition in the two-dimensional model.

periods can undergo a bifurcation from 1:1 to 2:2 dynamics, then to 2:1 and follows a different path as the pacing period is lengthened again. Using this test-bed I observe that rapidly paced cardiac tissue displays three behaviors; 1:1, 2:2, and 2:1. The animal-to-animal variation I observe indicates that both the existence of alternans and the size of the hysteretic window depend sensitively on the tissue characteristics. However, since these experiments are conducted over a number of months, and for animals of various sizes, I conclude that the observed prevalence of these behaviors is generic in *Rana catesbeiana*. Most significantly, my findings indicate that bistability is highly prevalent in bullfrog cardiac tissue, and thus optimal controllers must be designed with sufficient flexibility to deal with bistability as well unstable periodic orbits.

I present two simple mapping models of local cardiac dynamics that give some insight into the observations. I find the mapping approach to modeling cardiac dynamics has problems accurately modeling the observed bifurcation structure. A realistic 1-D map model similar to that used by many researchers [71, 63] cannot both fit the data well and have correct set of bifurcations. While the more complicated 2-D model from Chialvo *et al.* [121] somewhat solves this problem, neither model can account from the observed deviation of the N=1 (1:1 dynamics) and N=2 (2:1 dynamics) branches of dynamics. This is because both models assume that the skipped pace in 2:1 dynamics has no effect.

Chapter 4

Feedback Control of Alternans

Patterns of alternans in the T-wave of the electrocardiogram [67] have been correlated with vulnerability to ventricular fibrillation in human patients. In addition, alternans in models of cardiac muscle dynamics has been implicated in the initiation of spatio-temporal complexity similar to fibrillation [61]. These observations have encouraged researchers to understand how alternans can lead to spatio-temporal instabilities in cardiac tissue [61, 62] as well as attempt to control this behavior [44, 40].

Several research groups in the nonlinear dynamics community have attempted to use feedback methods designed for controlling complex *temporal* dynamics to control complex spatio-temporal dynamics [23, 46, 8, 47]. Recent research on controlling spatio-temporal complexity has focused on closed-loop control techniques that use information from a few spatial location [23, 44] and the application of small perturbations. Closed-loop controllers, which use the process shown in Fig. 4.1, have been used to suppress *temporally* complex dynamics in Lasers [48] and fast electronic circuits [83]. To achieve the goal of controlling spatio-temporal complexity, it is crucial to develop a understanding of how control stimuli interact with local cardiac muscle that is producing alternans.

Closed-loop or feedback controllers attempt to stabilize an unstable state of the system by making small adjustments to an accessible system parameter based on an estimate of the distance in phase space from the current state of the system to a desired state. The simplest feedback controller is the proportional controller. This control scheme uses the difference between the current state of the system and

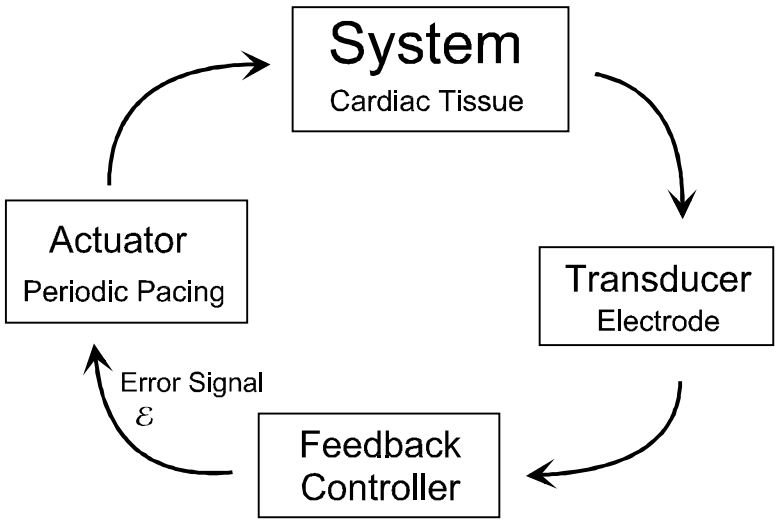

Figure 4.1: Feedback control process

a fixed reference state (known *a priori*) as the error signal. Proportional control scheme is easy to understand and implement, however, if the parameters of the system drift and the reference state changes the proportional controller is unable to adapt. An adaptive controller, Time Delay Autosynchronization (TDAS), was introduced by Pyragas [87]. This controller does not require that the desired state be known *a priori*. Instead, TDAS compares the current state of the system to a past state, in effect using the past state as an approximation for the reference state. Because TDAS uses the past dynamics as a reference state, it is able to compensate for slow changes in the reference state automatically [95, 78]. This type of controller has been used to suppress chaotic fluctuations in fast electronic circuits [83], CO_2 lasers [88], and AV nodal conduction [40]. Recently, a grid of these controllers was found to be able to suppress spiral wave breakup in a 2-D computer simulation of cardiac dynamics [44].

In this chapter I use a TDAS protocol to control alternans in the periodically paced bullfrog cardiac muscle test bed described in Chapter 3. In the first section

of this chapter I describe the experimental setup the system in Fig. 4.1. In the next section I introduce TDAS and Restricted TDAS as the feedback controller in Fig. 4.1. Both of these control schemes are based on a comparison of consecutive interbeat intervals to generate an error signal. The pacing protocol is adjusted by an amount proportional to this error signal. Finally, I present the results of the control experiments.

4.1 Experimental Setup

The system I use to study the control of alternans is artificially paced small pieces of cardiac muscle tissue without intrinsic pacemakers. This tissue is paced rapidly to produce alternans following the suggestion of Nolasco and Dahlen [71]. Using small pieces of cardiac tissue allows the study of muscle dynamics exclusively without the complications of spatially complex dynamics or pacemaker cells that stimulate the tissue. The experimental setup is similar to the test-bed system presented in Chapter 3. The only difference is that a control loop has been added to the physical setup as shown in Fig. 4.2.

The sequence of operations in this experiment are somewhat different that in Chapter 3. The tissue is paced at $\sim$ 1000 ms intervals for about 20 min before initiating data collection to allow the tissue time to recover from the trauma of surgery. The bifurcation structure of the tissue is determined using the protocol established in the experimental section of Chapter 3. (Recall that the types of responses to pacing are denoted M:N, where M paces elicit N different responses.) The frog cardiac muscle tissue does not always display alternans, but if it does I record the pacing periods that generate 2:2 behavior. After the range of pacing periods that elicit 2:2 (alternans) is established, the tissue is paced with a constant period in this range. The controller is turned on manually and the tissue response

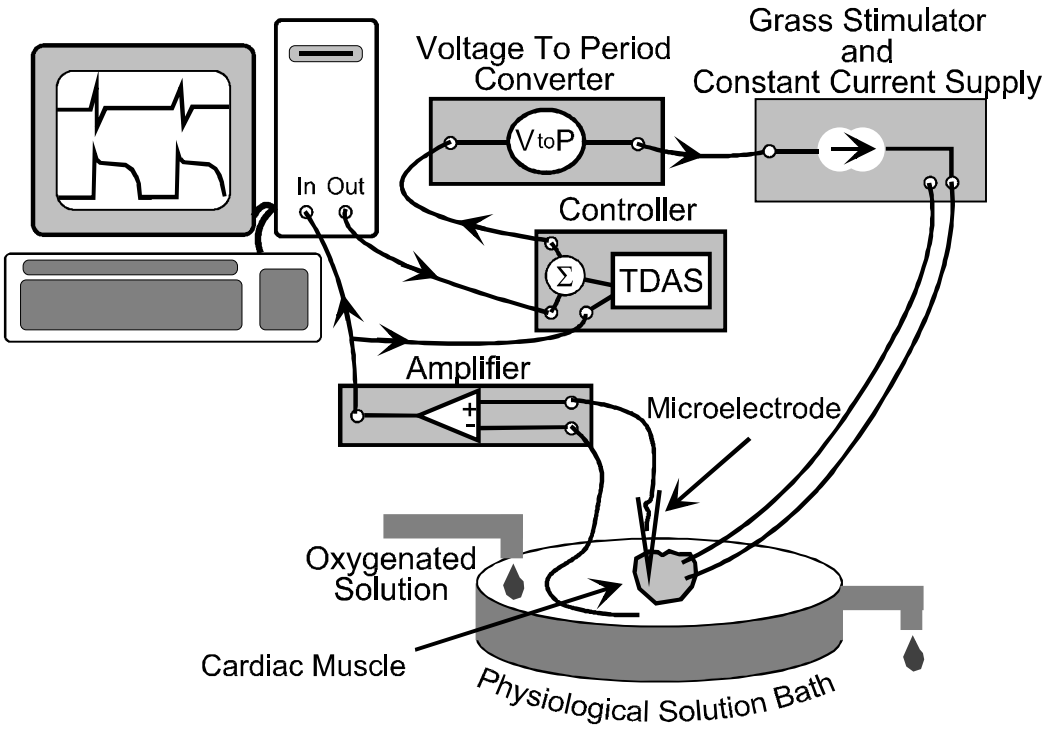

Figure 4.2: Experimental control setup used to induce and control alternans in a small peice of cardiac muscle. This setup is similar to the simple pacing experiment described in Chapter 3. The major difference is that there is now a controller that generates an error signal that is added to signal sent to the voltage-to-period converter. This error signal effects the timing of the n^{th} pacing period.

is recorded using the computer as before.

Figure 4.3 shows a bifurcation diagram from an animal that displays alternans as the pacing period is slowly decreased from 1000 to 300 ms in 50 ms steps. The tissue response to each pace is recorded for 10 seconds after the first 5-10 stimuli are discarded to eliminate transients. At long pacing periods, the tissue responds with a 1:1 behavior where every stimulus elicits an identical action potential. Most of the time, for shorter pacing periods the tissue undergoes a saddle-node (or subcritical) bifurcation from the 1:1 state to a 2:1 state. However, a small fraction of the time, as the pacing period is shortened the 1:1 behavior loses stability and the muscle dynamics undergoes a forward bifurcation to alternans. In this figure the 1:1 to 2:2 bifurcation occurs at a pacing period of 500 ms. In addition this tissue undergoes a further bifurcation to 2:1 dynamics at a pacing period of 350 ms.

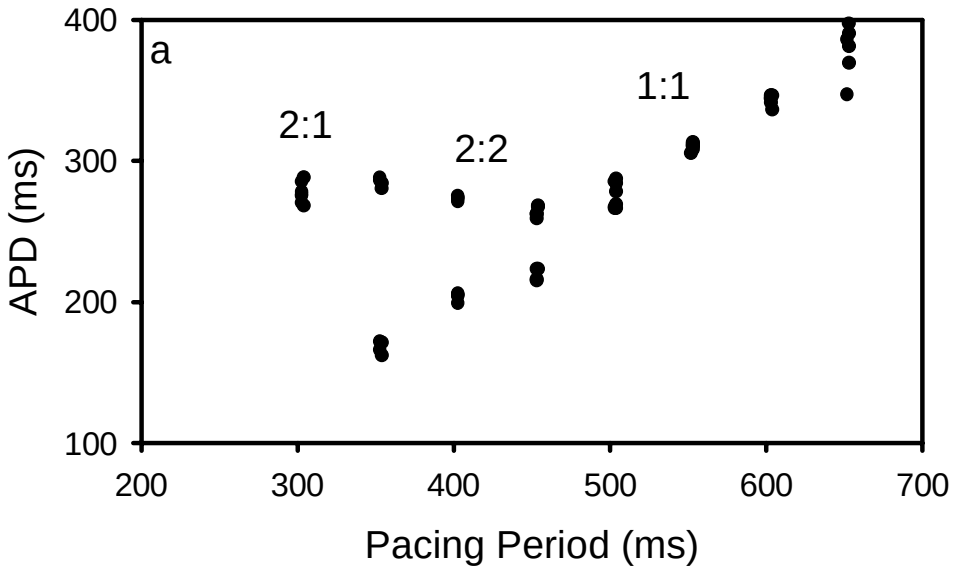

Figure 4.3: A typical bifurcation diagram for a small piece of periodically paced bullfrog showing alternans. The dynamics of the tissue is measured with a microelectrode. For long pacing periods (PP>500 ms) the muscle tissue displays 1:1 dynamics. Between 500 ms and 350 ms the dynamics of the cardiac tissue alternate. At 300 ms the dynamics bifurcates from 2:2 dynamics to 2:1 dynamics.

I characterize the state of the system using either a microelectrode or a suction-type monophasic action potential (MAP) electrode. The microelectrodes and the MAP electrodes are described in Sec. 2.1 and Appendix E. When a MAP electrodes is used, it is attached to the tissue within 2-3 mm of the stimulus electrodes. The signal from the damaging lead (inner ring) of the electrode is subtracted from the reference lead (outer ring) and amplified to about 1V peak to peak using a Tektronix 5A22N differential amplifier before recording. The details of the construction and use of the suction-type MAP electrode can be found in Appendix E. I find the MAP electrode signal characterizes the system well enough for the feedback algorithms to successfully control the system.

Measuring the temporal evolution of the voltage allows me to determine the action potential duration (APD). Regardless of the type of electrode, an action potential is defined as a deflection of the potential away from its rest state in response to a stimulus. The APD serves as the dynamical variable used to characterize the state of the system.

The duration of an action potential is experimentally determined using a custom built detector circuit. This circuit integrates a fixed voltage for a time equal to the APD. The voltage at the end of the action potential is proportional to the APD. The circuit diagram for the detector is shown in Fig. 4.4. The signal (V_{in}) is compared to a reference voltage that is set manually to a level that is approximately 50% of peak height of the action potential. When the signal crosses this threshold a digital line is pulled low until the signal recrosses the threshold. In addition, a set of TTL (transistor logic) clock pulses is generated by the detector marking the beginning of an action potential.

The width of the digital pulse marking the action potential is converted into a voltage by the time-to-voltage circuit shown schematically in Fig. 4.5. The digi-

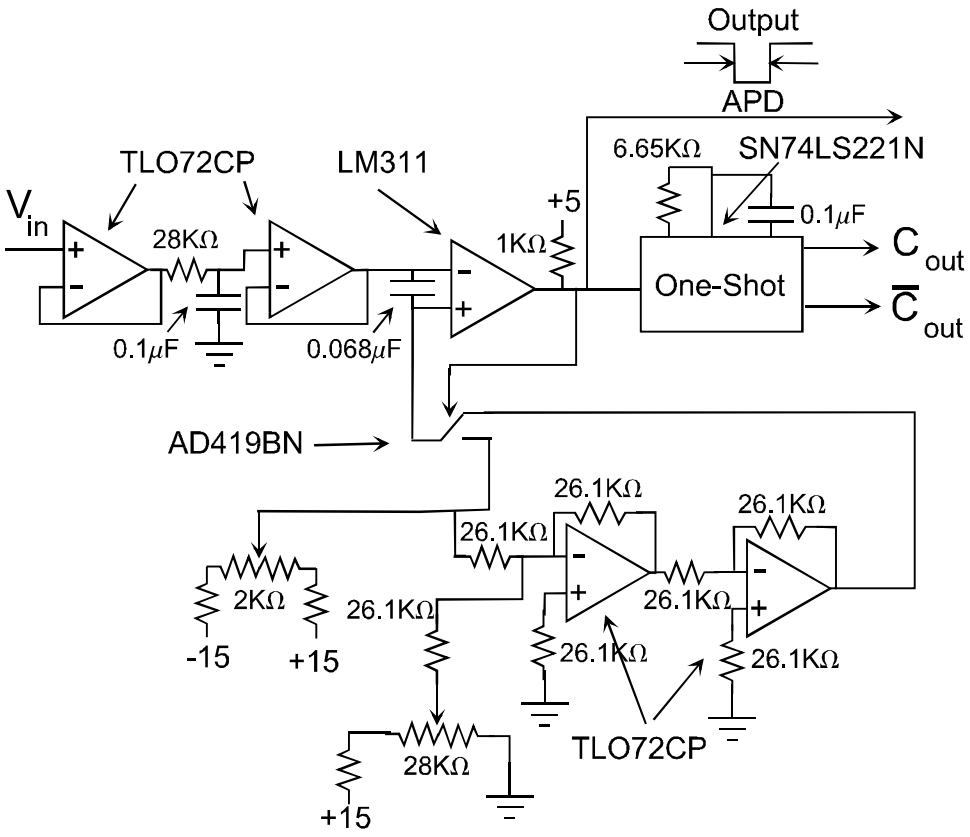

Figure 4.4: A circuit diagram of the action potential detector. The signal (V_{in}) amplified from the microelectrode is filtered and then compared (using a schmitt trigger) to a threshold value. The threshold value is set manually to be approximately 50% of the height of the action pootential. A threshold crossing causes a digital line to transition low. This low value is maintained until the repolarization of the action potential. In addition, a clock pulse (C,$\bar{C}$) is generated as the tissue initially depolarizes.

tal signal that represents the action potential sets and resets an integrator that is integrating a constant voltage. The clock pulses generated by the activation propagates the voltage stored in this integrator into a set of sample-and-hold integrated circuits. These sample-and-holds store the voltage values that are proportional to APD_n and APD_{n-1}.

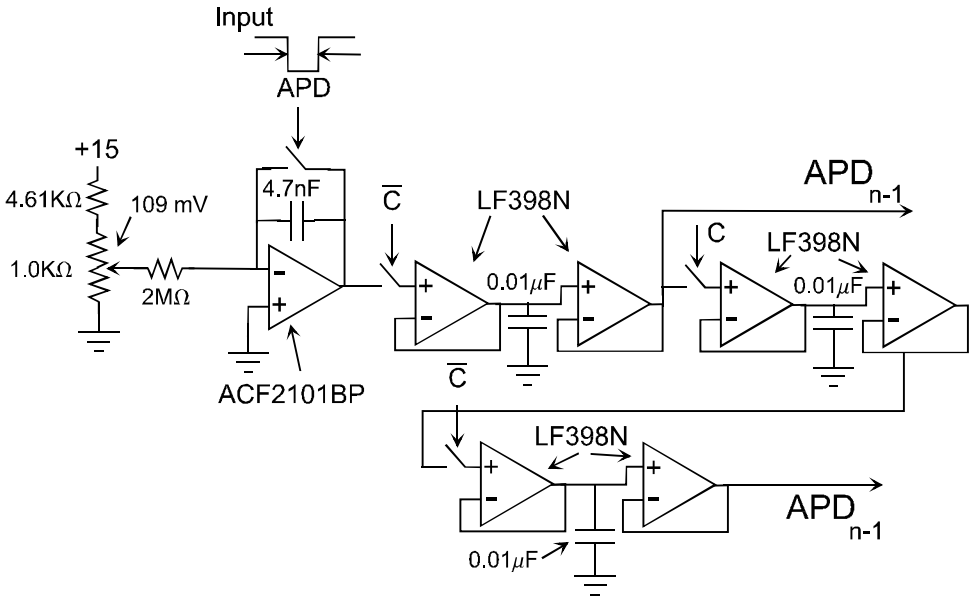

Figure 4.5: A circuit diagram of the time to voltage converting circuit. The sample and hold integrated circuits provide this circuit with a two level stack memory. A fixed voltage is integrated while the action potential is being detected. The integrated voltage is set by the voltage divider. During all of these experiments this voltage was set to 109 mV, which gives an integration slope of 11.5 mV/ms. At each clock pulse (C,$\bar{\text{C}}$), the output voltage of the integrator is propagated down a line of sample-and-holds.

4.2 Control Schemes

In this section I present TDAS and a restricted version of TDAS. For both controllers the pacing period (PP_n) is used as the accessible system parameter. The adjustment of the pacing period is accomplished by summing the error signal with the constant

voltage signal that sets the pacing period in the voltage-to-period converter shown in Fig. 4.2. The n^{th} pacing period PP_n is perturbed around its nominal value PP, giving,

$$PP_n = PP + \varepsilon_{n-1.}.$$

4.2.1 Time Delay Autosynchronization

To generate an error signal ε_n, TDAS does not require that the desired state be known *a priori*. The error signal, which is given by

$$\varepsilon_n = -\gamma(APD_n - APD_{n-1}),$$

where γ is the gain, compares the current state of the system (APD_n) to a past state (APD_{n-1}). In effect, this controller uses the past state as an approximation to the reference state.

When this control scheme is successful, $APD_n = APD_{n-1} = APD^*$, which is the desired state. Note also that the error signal goes to zero for any gain γ if $APD_n = APD_{n-1}$; therefore, the controller does not effect the desired state of the system, only its stability. Because this controller uses the difference between the current interbeat interval and the previous interbeat interval it is able to automatically track slow changes in the stability of the dynamics.

Experimentally, the calculation of the error for the TDAS scheme is very simple. The two voltages corresponding to APD_n and APD_{n-1} from the time-to-voltage converter (Fig. 4.5) are subtracted from one another. The difference voltage is amplified by an amount γ and buffered. A switch allows the resulting error voltage to be added to the voltage that the computer generates that controls the period of the pacing.

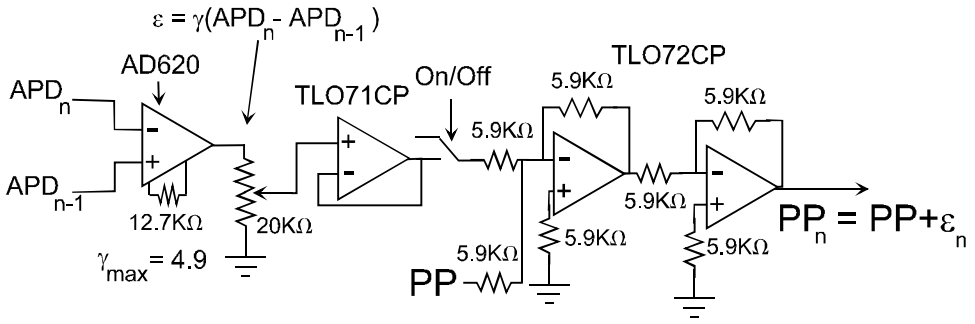

Figure 4.6: TDAS control circuit diagram. Two voltages proportional to the duration of an action potential are subtracted using a instrumentation amplifier (AD620) and the difference is amplified by a factor γ, which is set with a ten-turn potentiometer. The resulting that sets PP_n voltage is summed with the constant voltage that sets PP for voltage-to-period converter. The resulting gain γ is equal to 1.1*(setting on the ten-turn potentiometer), assuming the voltage-to-period converter constant is 0.191 ms/mV.

4.2.2 Restricted Time Delay Autosynchronization

While studying control techniques such as TDAS applied to cardiac muscle is interesting from a basic science perspective, eventually, I want to apply these techniques to a whole heart *in vivo*. The application of control schemes *in vivo* is complicated by the presence of the autonomous pacing that originates either from the heart's pacemaker or as waves of excitation from complex spatio-temporal dynamics. In a whole heart preparation during fibrillation the pacing period is not accessible. Each location on the heart is stimulated by its neighbors. To adjust the pacing period I can only stimulate the tissue to generate a response. This stimulation can only shorten the interbeat intervals. It would be difficult to lengthen the pacing periods in this situation as the TDAS algorithm might require. However, control protocols that only shorten the pacing period can be easily implemented through the injection of an extra stimulus just before the regular stimulus. The refractory nature of cardiac muscle will cause the tissue to respond to the injected stimuli and ignore the

regular stimulus as if the normal pace had arrived early. To mimic this behavior in this test bed I restrict the TDAS controller so that it only shortens pacing periods.

The restricted TDAS's error signal is similar to TDAS except that it is constrained to be negative. Which for $\gamma>0$ gives

$$\varepsilon_n = \begin{cases} -\gamma(APD_n - APD_{n-1}) & \text{if } APD_n \geq APD_{n-1} \\ 0 & \text{if } APD_n < APD_{n-1} \end{cases}$$

thus $\varepsilon_n<0$ and the pacing period is only shortened. This restriction transforms the linear TDAS into a nonlinear controller.

The restricted version of TDAS is similar to TDAS in several respects. The error signal goes to zero if the cardiac muscle is displaying the desired dynamics, because $APD_n=APD_{n-1}$. In addition, the restricted TDAS controller is also able to track changes in the dynamics of the cardiac tissue.

The implementation of the restricted TDAS is similar to TDAS. The two voltages corresponding to APD_n and APD_{n-1} from the time-to-voltage converter (Fig. 4.5) are subtracted from one another. This difference voltage is amplified by an amount γ and buffered. The resulting voltage is checked by a comparator to see if it is negative. Only if the error signal is negative is it added to the computer generated pacing voltage.

4.3 Results using TDAS

I attempt to suppress alternans using feedback control once a range of pacing periods that elicit alternans is determined. Figure 4.8 shows a complete TDAS control experiment. A MAP electrode voltage measurement (Fig. 4.8a) and the error signal (Fig. 4.8b) are plotted as a function of time. Figure 4.8c shows the corresponding pacing periods plotted against beat number. The tissue is paced at a nominal period of PP=500 ms. The vertical dashed lines indicate where control is turned on or off.

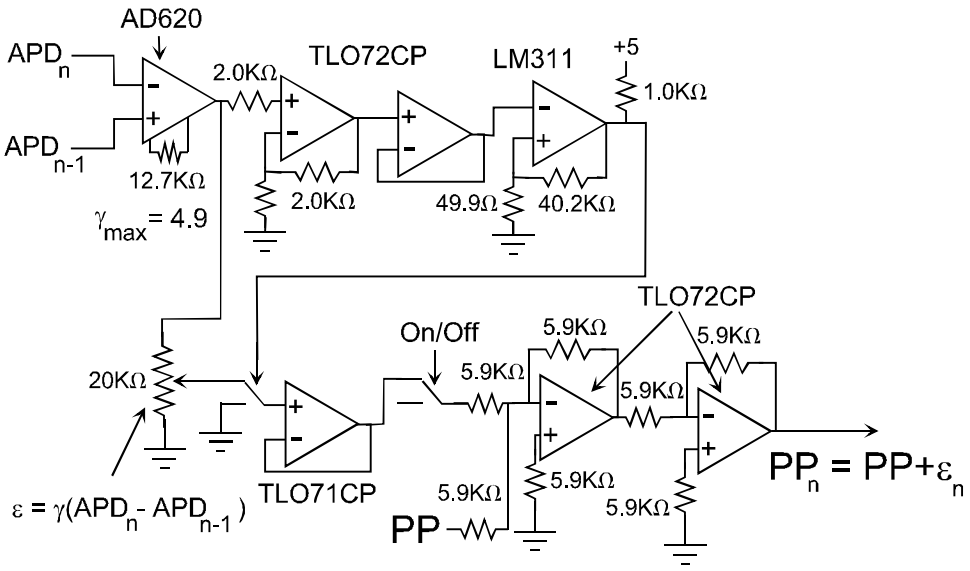

Figure 4.7: Restricted TDAS control circuit diagram. Tho voltages proportional to the duration of an action potential are subtracted and the difference is amplified by a factor γ, which is set with a potentiometer. The resulting voltage is compared with zero and only negative voltages are passed. This negative voltage is summed with the set voltage for voltage-to-period converter. The resulting gain γ is equal to 1.1*(seting on the ten-turn potentiometer), assuming the voltage-to-period converter constant is 0.191 ms/mV.

The gain of the controller is $\gamma = 1.54$. With control off (on the far left) the APD_n alternate between approximately 110 and 180 ms. Soon after control is turned on (in between the dashed lines) the controller causes the pacing period to vary by as much as 20%. It is seen in Fig. 4.8 that after an initial transient, the pacing period returns to its nominal value and the behavior of the tissue follows the 1:1 dynamics with an APD^*=132 ms. The error signal ε_n is less than 0.5% of the nominal pacing period (PP). The 1:1 dynamical state is unstable after control is turned off (to the right of the dashed lines) and the system rapidly returns to alternans.

After control is turned off and the tissue dynamics is in the neighborhood of the

unstable 1:1 state, the behavior can be approximated by

$$dAPD_n = -\mu\ dAPD_{n-1} \tag{4.1}$$

where $dAPD_n$=APD_n-APD^* and μ is the Floquet multiplier characterizing the unstable state. Assuming when the control is turned off that there is some initial distance between the dynamics of the system and the 1:1 behavior $dAPD_0$ (due to noise), then equation (4.1) becomes,

$$dAPD_n = (-\mu)^n\ dAPD_0. \tag{4.2}$$

I estimate μ = -1.3 by fitting the first four data points after control is turned off to equation (4.2). Note that any $\|\mu\| > 1$ indicates the 1:1 state is unstable as mentioned in Chapter 2.

Out of 18 animals, 40 showed alternans. In 2 of the 18 animals there were technical difficulties in the experiment that prevented application of control. In 14 out of 16 attempts I found it was possible to control alternans with TDAS. During successful control of alternans to the unstable 1:1 state, the typical variation of the APD_n was suppressed to less than 2% of the average APD_n from an alternation of as much as 15% of the average APD_n. For comparison, the variation of the APD_n during stable 1:1 behavior at long PP is approximately 2% of the average APD_n.

I find that the alternans can be suppressed and the 1:1 state stabilized using a range of feedback gains, which can be quickly visualized by plotting a 'domain of control.' The domain of control is mapped out by determining the ranges of values of the feedback gain γ that successfully stabilize the alternans as a function of the bifurcation parameter PP. The domain of control of the TDAS algorithm is shown in Fig. 4.9b. In general, decreasing the pacing period PP results in decreasing the range of gains that successfully control the alternans. This result is consistent with

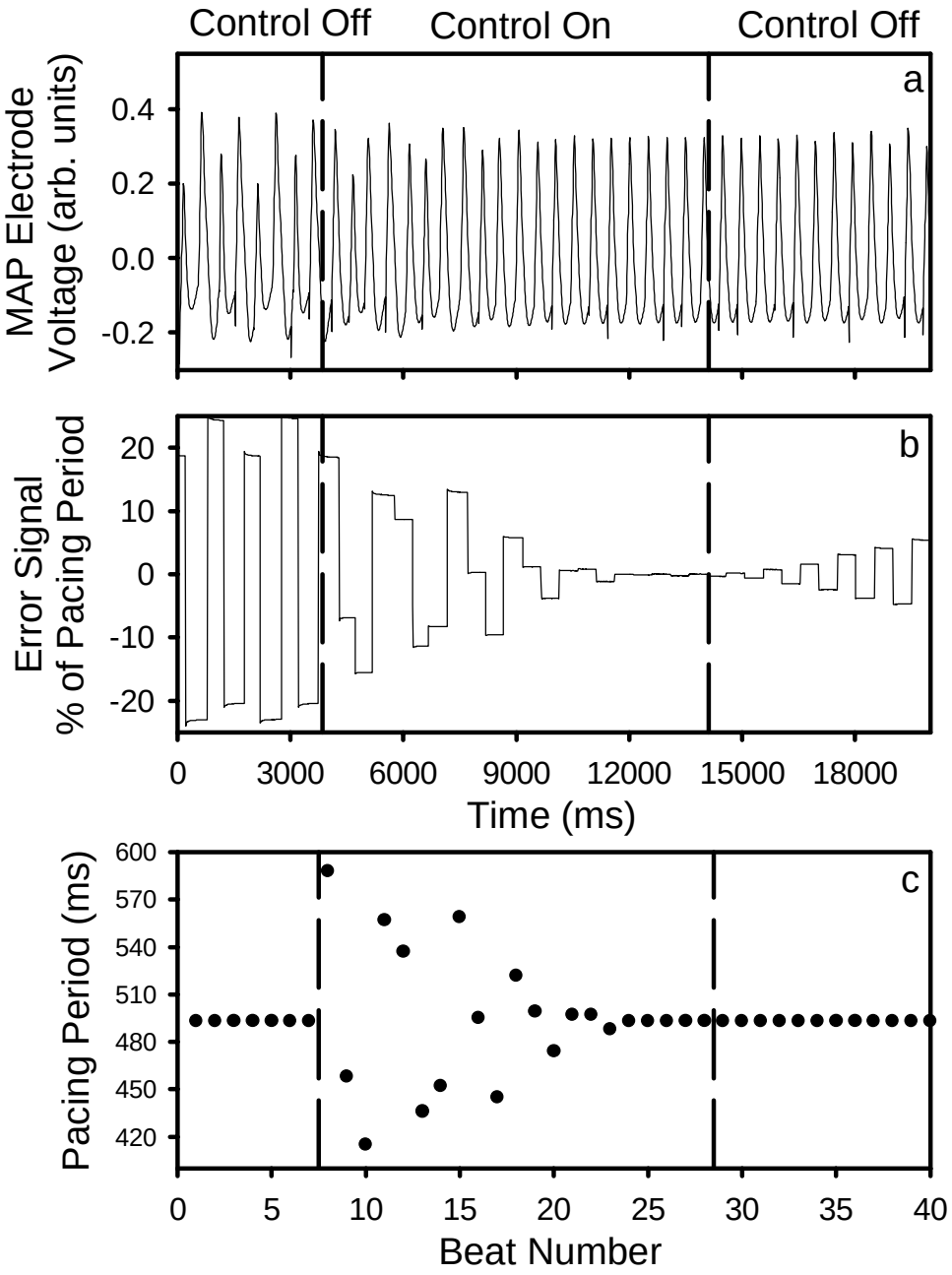

Figure 4.8: The MAP electrode signal (a), the error signal (b), and the pacing period (c) from a TDAS experiment. These signal show how the TDAS controller supress alternans by varying the pacing period. The pacing period is 500 ms and the gain $\gamma = 1.54$.

the idea that the 1:1 state becomes more unstable (its Floquet multiplier gets larger) as PP decreases because of the normal restitution properties of cardiac tissue. The existence of a domain is important because it allows control without accurate *a priori* knowledge of the optimal gain for this system.

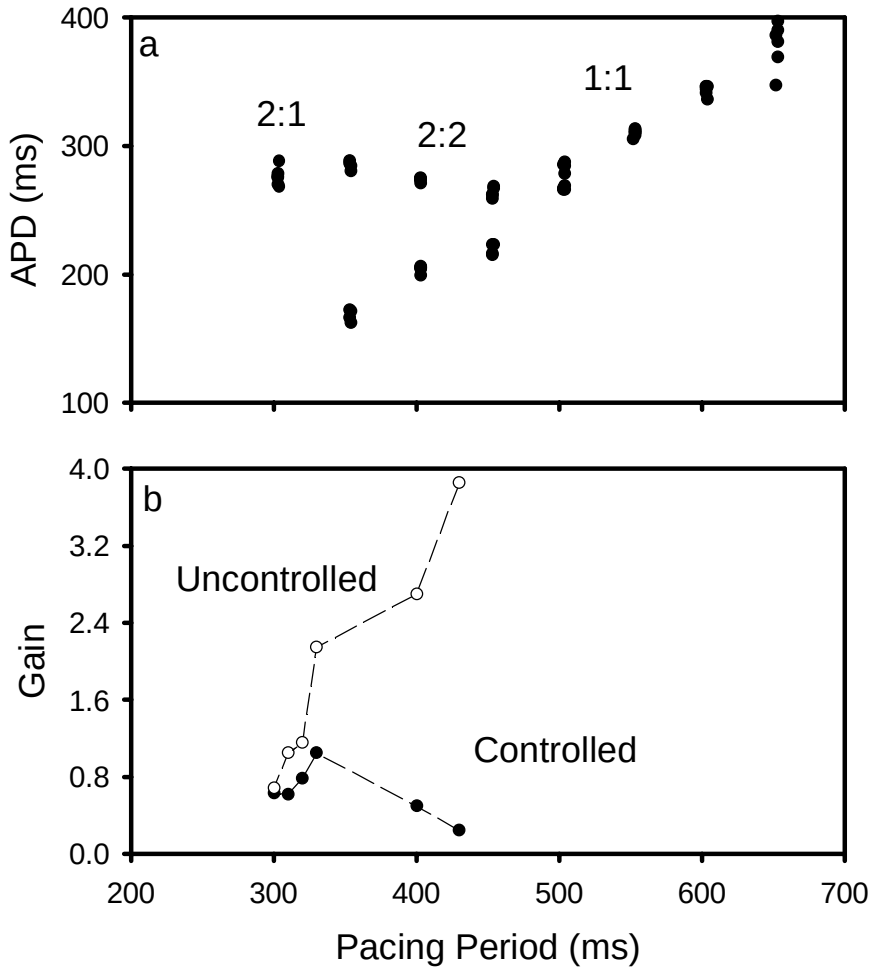

Figure 4.9: A bifurcation diagram and domain of control for TDAS applied a piece of periodically paced bullfrog venticle. The bifurcation diagram in panel (a) shows that the dynamics of the tissue bifucate to alternans at $PP = 500$ ms. The domain of control in panel (b) shows that as the tissue paced with a shorter period the region of successful control gains shrinks.

The stability of the 1:1 behavior of myocardial muscle is sensitive to changes in

tissue parameters caused by fluctuations in temperature, aging, tissue adaptation and other environmental factors. The TDAS scheme is able to track changes in the excitability of the tissue as seen in Fig. 4.10. In this figure control is turned on and then back off three times, and the resulting APD is plotted versus beat number. During the time course of this experiment the pacing period and all other experimental conditions were held constant but the tissue properties drifted by some mechanism that was not determined. The drifting could be the result of the cumulative effects of ion depletion (or build up) caused by rapidly pacing the tissue for long periods of time. The grey points indicate control is on and the black points indicate control is off. Each time the control was turned on, the gain of the controller was held constant at $\gamma = 2.9$. The APD^* of the 1:1 state drifted from 338ms in Fig. 4.10a, to 300 ms in Fig. 4.10b, and finally to 291 ms in Fig. 4.10c. The size of the alternations also varies, initially alternating between 329-352 ms, then alternating between 255-355 ms, and ending at values between 285-299 ms. In addition, the estimated Floquet multiplier of the 1:1 state varies with values of 1.21, 1.28, and 1.51 for the panels a, b, and c respectively. Throughout the experiment, however, the controller was able to return the system to 1:1 dynamics.

4.4 Results using Restricted TDAS

Interestingly, while restricting TDAS might seem to hobble the effectiveness of the controller, I observe that this is not true. In 12 out of 15 animals, I am able to stabilize 1:1 dynamics using the restricted TDAS as compared with 14 out of 16 for the unrestricted TDAS. A time series showing control of alternans using a restricted TDAS protocol is illustrated in Fig. 4.13a. The error signal shown in Fig. 4.13b is always less than or equal to zero. To the left of the dashed vertical line control is on and to the left control is off. Using the restricted TDAS I observe two apparently

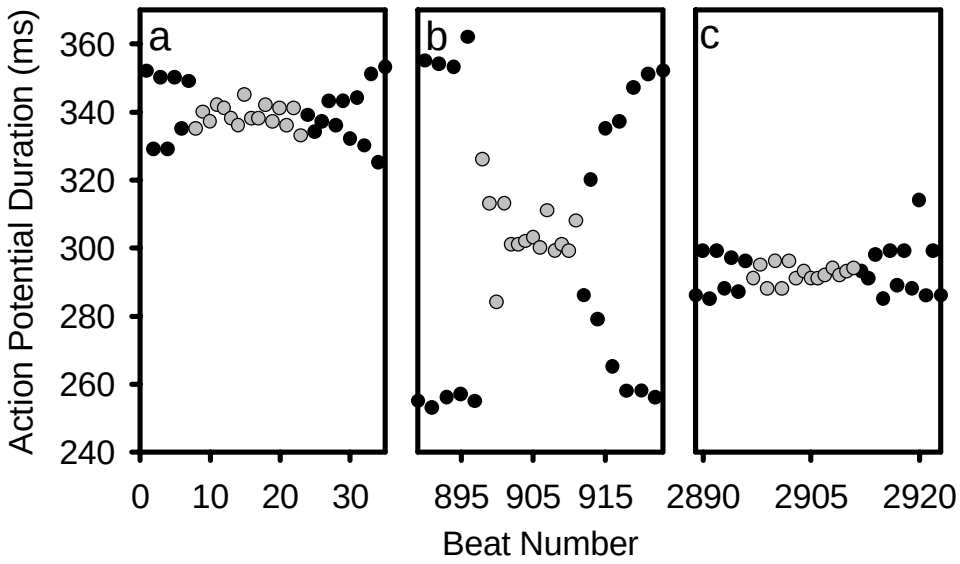

Figure 4.10: A plot of APD versus beat number for a long experiment showing the ability of TDAS to track changes in the dynamics. The pacing period was 540 ms. and the gain was 0.66.

distinct domains of control in 3 out of 11 animals.

A theoretical discussion of this restricted TDAS controller is found in Gauthier and Socolar [45]. They apply the restricted TDAS scheme to a simple 1-D mapping given by,

$$\begin{aligned} X_n &= -\mu X_{n-1} + \varepsilon_{n-1} \\ \varepsilon_n &= \begin{cases} -\gamma(APD_n - APD_{n-1}) & if \quad APD_n \geq APD_{n-1} \\ 0 & if \quad APD_n < APD_{n-1} \end{cases} , \end{aligned} \tag{4.3}$$

where μ is the Floquet multiplier of the mapping's fixed point at $X^* = 0$. They show that the restricted TDAS controller is able to control this mapping when μ is much larger than TDAS is able to successfully control. The domains of control for the simple system (4.3) are shown in Fig. 4.11. The dotted region is the domain of control for TDAS and the regions that are bounded by solid lines are the domain of control for the restricted TDAS. Notice in this simple 1-D system (4.3) that there

are multiple domains of control using the restricted TDAS while TDAS has only one domain of control.

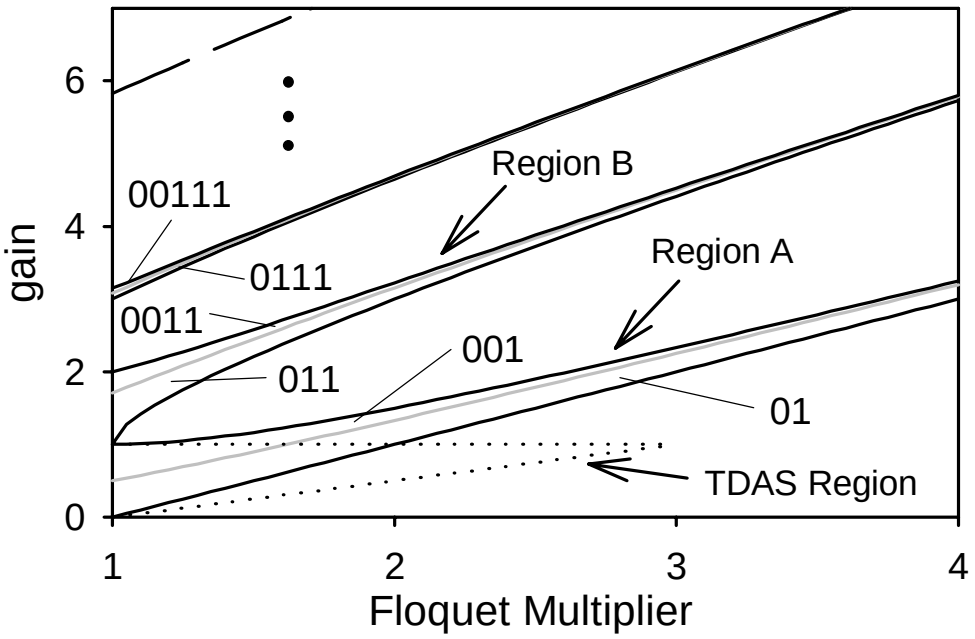

Figure 4.11: Domains of control for TDAS and restricted TDAS applied to a simple unstable fixed point. Notice that there are multiple domains for the restricted TDAS. This figure is from Gauthier and Socolar

The analysis done by Gauthier and Socolar [45] showed that in each domain of control a different sequence of symbols described the dynamics of the mapping plus restricted TDAS control. In the largest domain (region A in Fig. 4.11), which lies nearest the TDAS domain, the system responds with a repeating sequence of '01' or '001' symbols, where a '1' corresponds to control being applied ($\varepsilon_n < 0$) and '0' indicates control is not applied ($\varepsilon_n \equiv 0$). The dynamics of the next largest domain (region B in Fig. 4.11) is described by the sequences '0011' and '011'.

Experimentally, I observe both multiple domains and symbol sequences similar to those from regions A and B of Fig. 4.11 when I use the restricted TDAS algorithm. In 3 of 11 animals where restricted TDAS is successful I observe a second set of gains

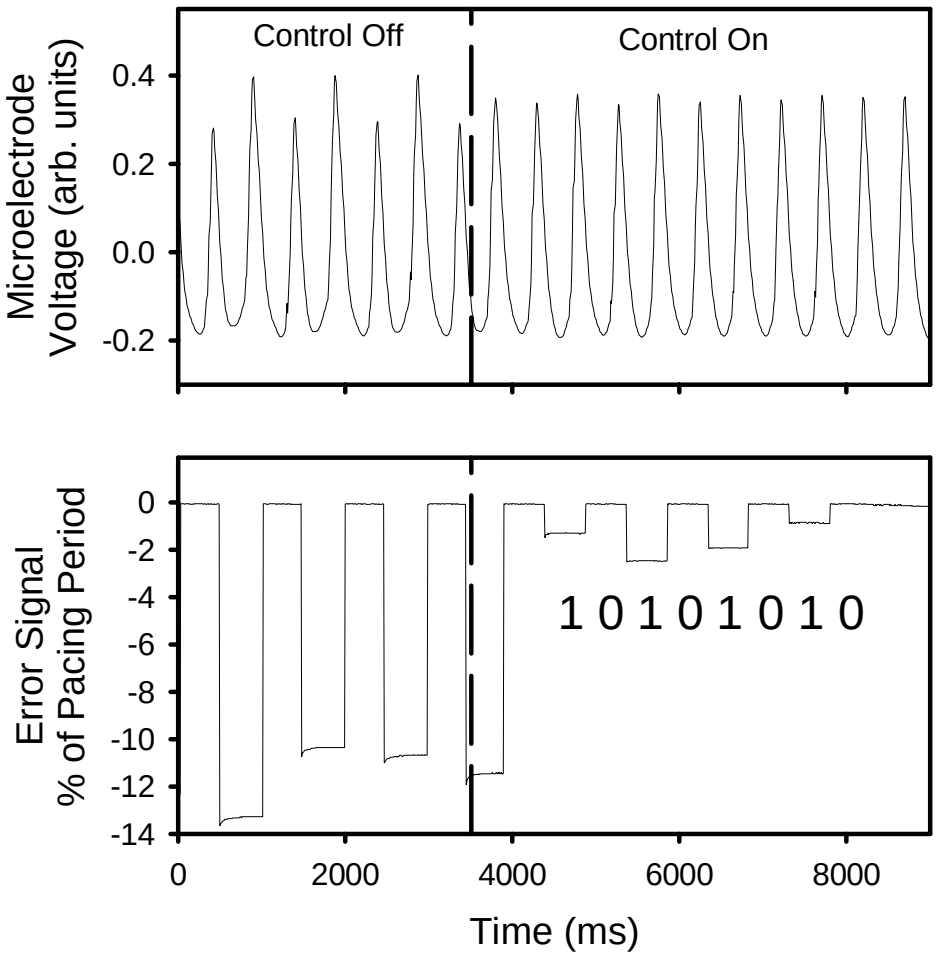

Figure 4.12: A time series of the signal from a MAP electrode (a) and the error signal from the restricted TDAS controller (b) during a control experiment. The tissue is paced at 575 ms. The gain is 4.4 When control is on (to the left of the vetricle dashed line) the cardiac tissue dynamics are very close to the 1:1 behavior. This recording was taken from the second domain of control. Notice that the symbol sequence is '01.'

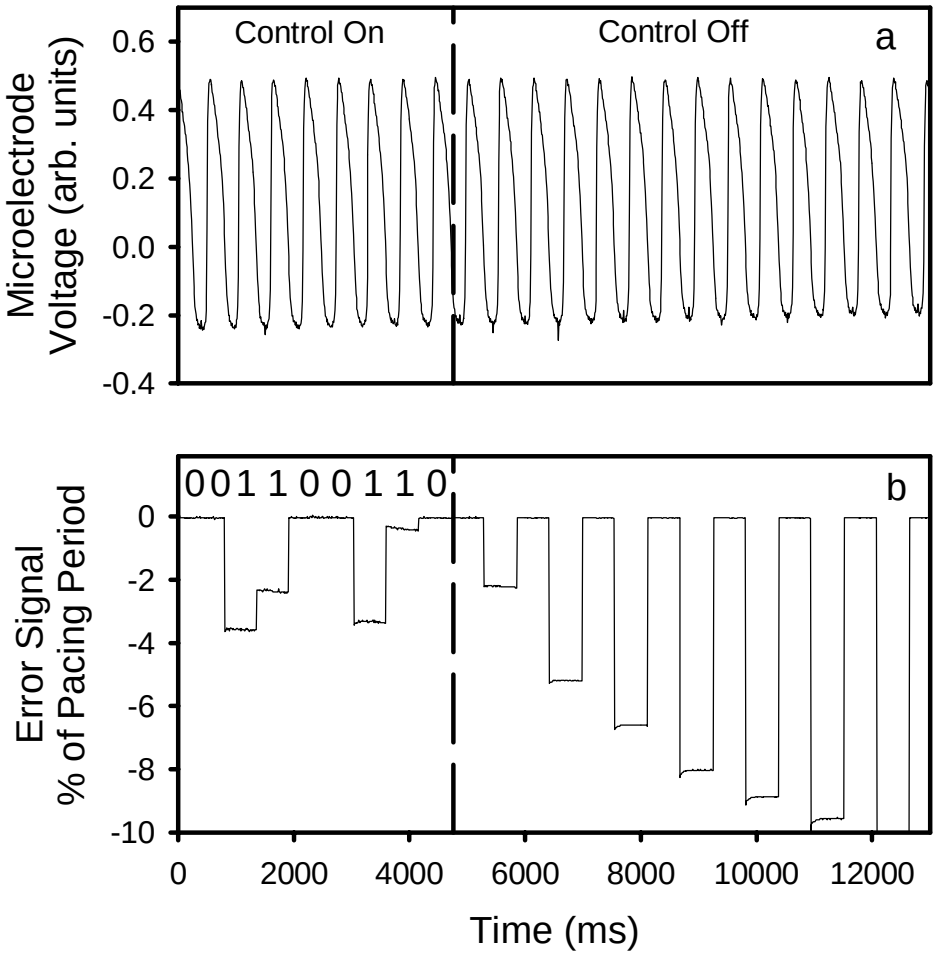

Figure 4.13: A time series of the signal from a MAP electrode (a) and the error signal from the restricted TDAS controller (b) during a control experiment. The tissue is paced at 575 ms. The gain is 4.4 When control is on (to the left of the vetricle dashed line) the cardiac tissue dynamics are very close to the 1:1 behavior. This recording was taken from the second domain of control. Notice that the symbol sequence is '0011.'

larger than the first is able to suppress alternans. Gauthier and Socolar [45] suggest that there are other domains of control for larger gain, however, I never observe a third domain.

The symbol sequences from two control experiments on cardiac tissue is show in Fig. 4.12 and Fig. 4.13. Figure 4.12 illustrates the dynamics seen in 12 out of 15 animals, which corresponds to region A in Fig. 4.11. The symbol sequence observed in this figure is '01.' In most experiments the dynamics I observe look like a mixture of '01' and '001' sequences. Figure 4.13 illustrates the symbol sequences from the second domain of control I observe. Notice that the dynamics follow the '0011' sequence similar to region B in Fig. 4.11. The theory from Gauthier and Socolar is for a simple 1-D mapping. However, the symbolic descriptions seem to describe reasonably well the dynamics of real tissue.

4.5 Summary

To achieve the long term goal of controlling fibrillation, I believe it is crucial to understand how controllers interact with local tissue instabilities. Instability to alternans has been correlated with vulnerability to ventricular fibrillation clinically [67] and observed numerically to give rise to spatio-temporal complexity [61]. Therefore, in this chapter I explored the effectiveness of two versions of TDAS controlling alternans in the cardiac tissue test bed introduced in Chapter 3.

I found that TDAS was able to control alternans in 14 out of 16 animals. In addition, I observed that TDAS was able to adapt to changing excitability in cardiac tissue. This ability may make this technique particularly suited to controlling complex behavior in biological systems like cardiac tissue.

I also found that restricting TDAS to only shortening the pacing period did not significantly hamper its effectiveness. In 12 out of 15 animals I was able to suppress

alternans with the restricted TDAS. This observation indicates this is a promising technique for in vivo studies where the control is limited to injecting stimuli to shorten pacing periods. In addition, I observed that there are multiple domains of control, which are similar to those predicted by Gauthier and Socolar [45].

Chapter 5

Induced transitions in bistable cardiac muscle

The eventual goal of research on controlling spatio-temporal complexity in cardiac tissue is to prevent or suppress fibrillation in humans. The conventional wisdom is that spatio-temporal complexity is initiated via a local tissue bifurcation to alternans [19, 24, 63]. This alternating state is believed to cause a spatial variation in the excitability of the cardiac muscle tissue that causes the wave of excitation to break up into fibrillation. However, I have found in my experimental investigations that small pieces of periodically paced cardiac muscle display bistability much more often than alternans. In addition, I observed during experiments with collaborators in Biomedical Engineering that the genesis of spatially complex waves correlate with an edge of observed windows of bistability [65]. Both of these observations suggest that local transitions between bistable states in muscle tissue dynamics is one possible cause of spatial complexity.

Bistability in cardiac tissue is not a new phenomenon. Lorente *et al.* [68] have shown that the dynamics of rapidly paced cardiac tissue is bistable with respect to the pacing current. In addition, Mines [3] and Guevara [70] have both observed that it is possible to induce transitions from stable 1:1 behavior to stable 2:1 behavior by removing one pace from the periodic pacing train. Mines also observed that it is possible to elicit a 2:1 to 1:1 transition with an injected stimulus.

This chapter describes a series of experiments demonstrating that it is possible to induce transitions between bistable states in the periodically paced frog cardiac muscle. In the first section I describe the experimental setup. In the next section

I present the results of my characterization of the timing of the successful extra stimuli. I find injecting a stimulus into the periodic pulse train can cause transitions in both from 1:1 to 2:1 dynamics and from 2:1 to 1:1 dynamics. In addition, I also observe that there are multiple types of transitions. Surprisingly, I also find that during 1:1 dynamics, it is possible to modify the dynamics of the tissue even if it is in the refractory period. For the 2:1 to 1:1 transitions, I show that the simple mapping model of cardiac dynamics can qualitatively predict which injected stimuli will successfully elicit transitions.

5.1 Experimental Protocol

The experimental setup is the same as the test-bed system presented in Chapter 3. This setup allows the study of muscle dynamics exclusively without the complications of spatial complexity or internal cells that stimulate the tissue. The pacing protocol is different than in Chapter 3. There are two phases to the pacing protocol in this chapter. The first phase attempts to characterize the tissue similar to chapter 3 with the aim of identifying windows of bistability. Once the range of pacing periods that elicit bistability is known, I manually set the pacing period in this range and try to elicit transitions between the states by injecting extra stimuli into the periodic pulse train. The transmembrane voltage is measured using a micropipette as discussed in Chapter 2 and Appendix E and used in Chapter 3.

A typical bistable window is shown in Fig. 5.3. Open circles show APD as the PP is slowly and incrementally decreased, as described in Chapter 3. At PP=660 ms, a saddle node (or possibly a subcritical bifurcation) [59] occurs from 1:1 to 2:1 dynamics (left upward-pointing arrow). The tissue continues to exhibit 2:1 behavior as the PP is decreased further. At PP=300 ms, the tissue jumps briefly to a 3:1 pattern (far left up-and-down arrow). At this point, I begin to incrementally

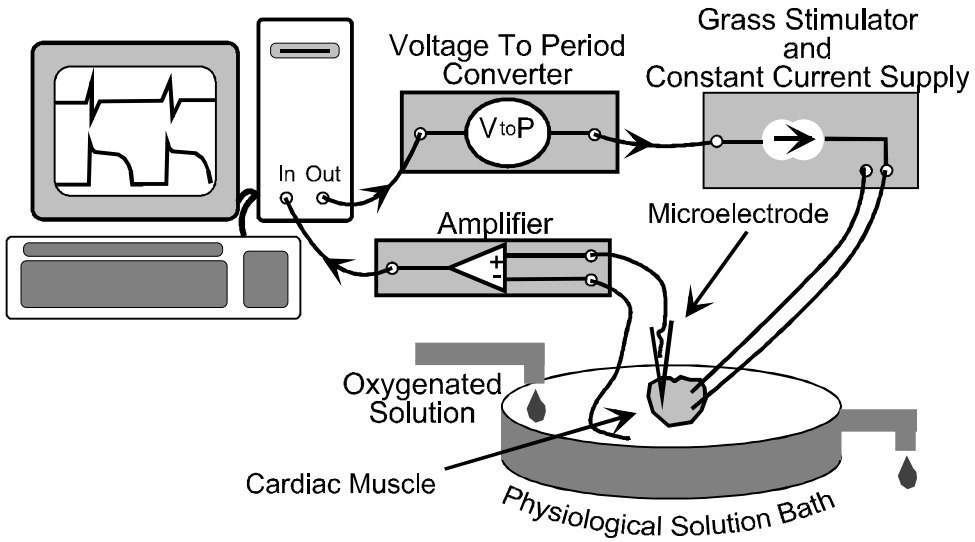

Figure 5.1: The experimental setup for inducing transitions between bistable states. Physically, this setup is the same as the characterization experiments in Chapter 3. The computer generates a voltage that is converted into a pacing period. In addition the computer records the response of the tissue. The extra stimuli are added to the periodic pulse train by the computer momentarily changing its output voltage to a level to produce an extra pulse with the proper timing. The computer then changes again to create a make-up pulse, and finally returns to the original pacing period.

increase the PP (closed triangles). The tissue returns to the 2:1 branch as the PP upsweep begins, and continues to exhibit 2:1 behavior until PP=765 ms, when it undergoes a transition to a 1:1 state (right vertical arrow). The tissue exhibits bistability between PP values of 660 and 765 ms in that it can exist on either the 1:1 or 2:1 branch, depending on the initial conditions.

After the range of pacing intervals that yield both 1:1 or 2:1 behavior is determined, I pace the tissue at a PP within this window. The tissue can be biased onto the 1:1 or 2:1 branch within the bistable regime by sweeping the PP down and up until the tissue responds with the desired behavior. Once the tissue is in the 1:1 or 2:1 state, I inject an extra stimulus at an interval T after the preceding normal

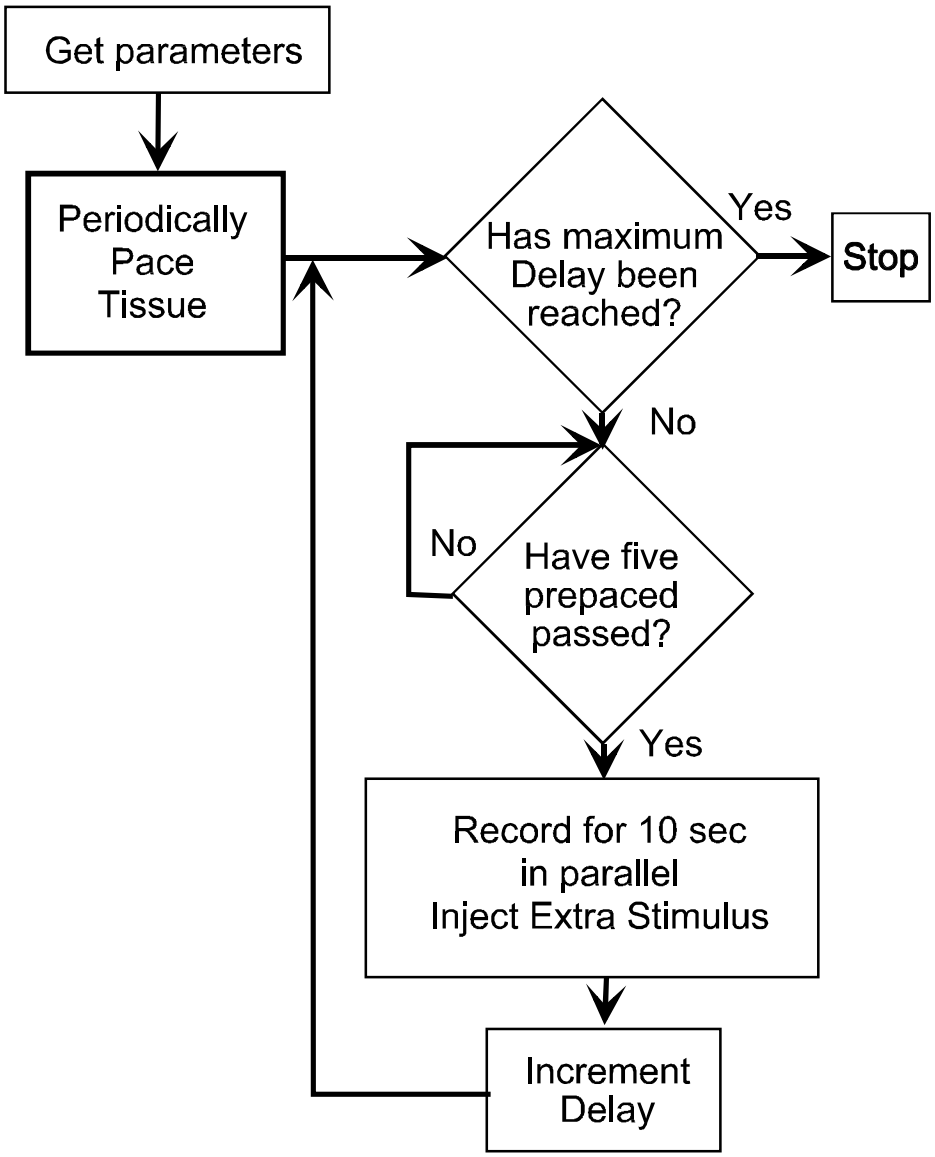

Figure 5.2: The flow chart for the LabView program that controls the injected stimulus experiment. The pacing period is selected manually. After pacing is initiated the computer counts 5 prepaces and injects an extra stimulus with some delay into the periodic pulse train. The response is recorded by the computer. At the same pacing period the process is repeated with a longer delay between a regular stimulus and the extra stimulus.

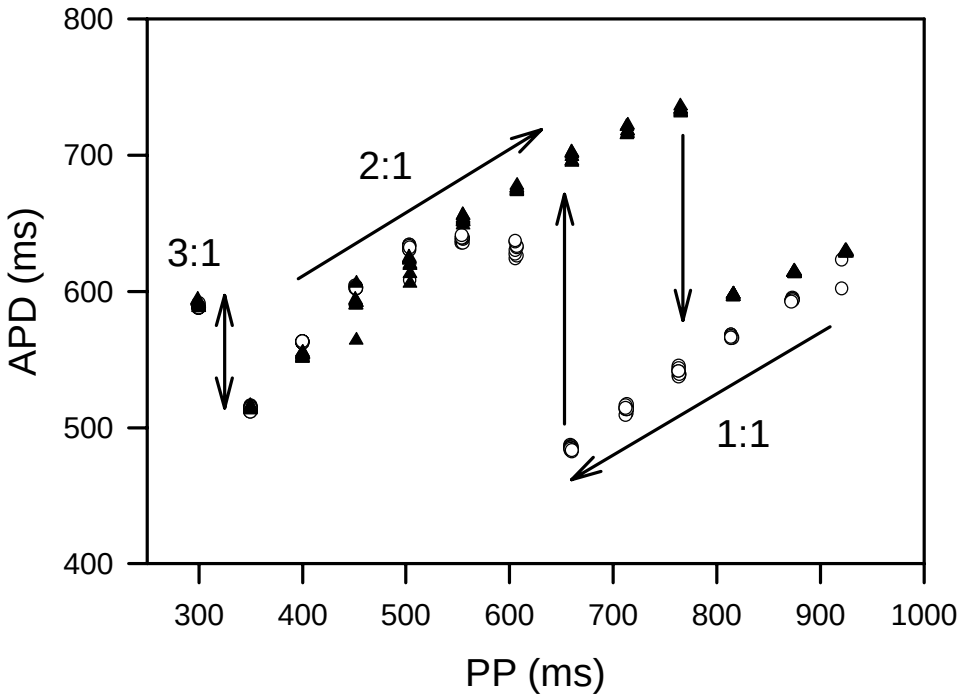

Figure 5.3: Action potential duration as a function of basic cycle length. Data is obtained by sweeping PP from 920 to 300 ms in decrements of ∼50-55 ms (open circles), and then from 300 to 920 ms in ∼50-55 ms increments (closed triangles). Arrows indicating sweep direction are added as a guide to the eye. Transitions between states are indicated by vertical arrows; bistability between N=1 and N=2 states occurs between 660 and 765 ms.

stimulus. The next normal stimulus is applied at an interval $PP - T$ following the extra pulse, marking the resumption of the normal stimulus train. I observe whether or not a transition takes place. This procedure is repeated for various PP values and T values in order to map the domain in the (PP, T) plane over which transitions can be induced. The interval T is varied from 50 ms to $PP - 50$ ms in 50 ms increments. After each attempt to induce a transition, the tissue is allowed to recover by driving it at the normal PP for at least 20 stimuli.

There are several limitations to the success of this experiment. First, the tis-

sue must be paced in the bistable window and on the appropriate branch of the dynamics. Finding the pacing period where the tissue dynamics is bistable takes several minutes of very rapid pacing. In addition, biasing of the tissue on the correct branch of the dynamics (2:1 or 1:1) takes a minute or two. The dynamics of the cardiac tissue can drift over this amount of time. Second, if a transition is successfully induced by an injected stimulus, the experiment has to be manually reset and re-biased on the correct branch unless there is a transition induced by the next injected stimulus in the opposite transition, which is unlikely.

5.2 Results

I observe that it is possible to induce experimentally four (maybe three) different types of transitions between bistable states. There seems to be two types of 1:1→2:1 transitions. One elicited by extra stimuli early in the pacing period and one elicited by stimuli arriving late in the pacing period. However, it is not clear if the mechanisms are different. Both of these transitions involve pacing the tissue before the end of an action potential. In addition, there are two 2:1→1:1 transitions (Type I and Type II). The types are differentiated by the transient behavior of the tissue after the transition is induced.

Of 12 animals in which extra-stimulus induced transitions were investigated, 9 exhibited bistable behavior. Experiments from two of these nine animals showed evidence of ectopic pacemaking cells and thus data from these experiments was discarded. In five of the remaining seven animals that exhibited bistability the addition of an extra stimulus induced transitions between bistable states. Three animals exhibited 1:1→2:1 transitions, and all five exhibited 2:1→1:1 transitions.

5.2.1 1:1→2:1 transitions

In three of seven animals I found that it was possible to elicit transitions from 1:1 dynamics to 2:1 dynamics. The injected stimuli that cause these transitions all occur during an action potential. The transitions divide into two different categories. The transitions from these categories, while not well resolved, are called Type A and Type B based on the cardiac tissues transient behavior after the injected stimulus. The different types of 1:1→2:1 transitions are illustrated in Fig. 5.4 and Fig. 5.5.

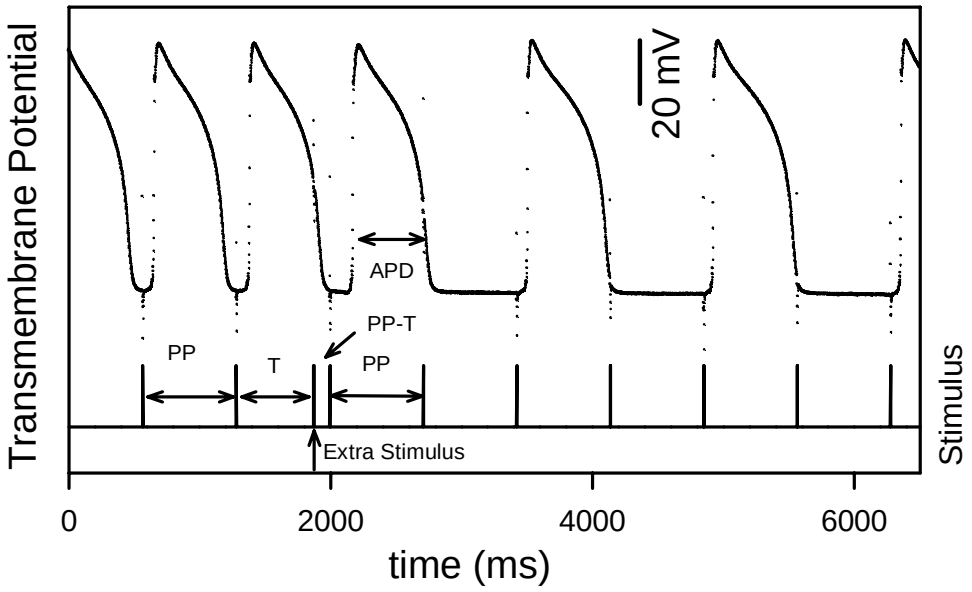

Figure 5.4: Temporal evolution of the transmembrane potential showing a Type A 1:1→2:1 transition. The stimulus train is shown at the bottom of the figure and the extra stimulus is marked with an arrow.

Figure 5.4 shows a Type A 1:1→2:1 transition. Initially, the tissue responds in a 1:1 pattern for a PP of 700 ms (within the bistable window). After the 2^{nd} normal stimulus shown in the figure, I apply an extra stimulus at T=595 ms as indicated by the arrow. The stimulus does not seem to effect the tissue at all. However, the action potential subsequent to the injected stimulus occurs later than normal. This

causes the following regular beat to be skipped and the tissue falls into a 2:1 pattern from that point. The injected stimulus comes so late in the action potential that it could actually be eliciting the response. If the measurement electrode had been in a cell under the stimulating electrode it might have been possible to distinguish which stimulus caused the action potential.

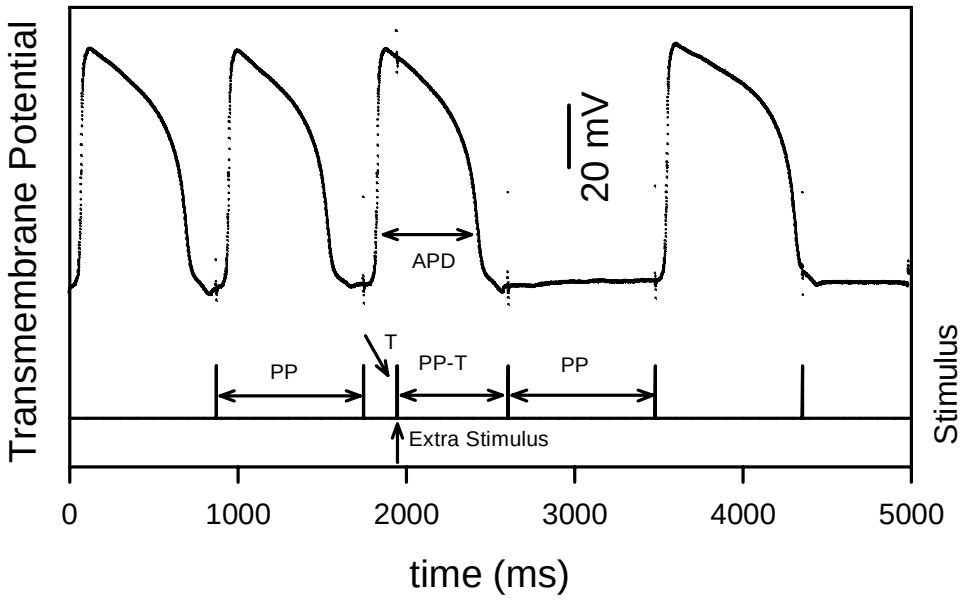

Figure 5.5: Temporal evolution of the transmembrane potential showing a Type B 1:1→2:1 transitions. The stimulus train is shown at the bottom of each figure and the extra stimulus is marked with an arrow.

Figure 5.5 shows a Type B 1:1→2:1 transition from a different animal. The extra stimulus (marked with an arrow) is applied early during the action potential. The injected stimulus comes early enough in the action potential so that it is apparent that it did not cause the next action potential. Therefore it must have affected the tissue dynamics in another manner. This injected stimulus may have extended the action potential's refractory period long enough to cause the next regular stimulus to be ineffective, giving the tissue a time interval equal to $2PP - T$ over which to

recover. Resulting in a 2:1 pattern.

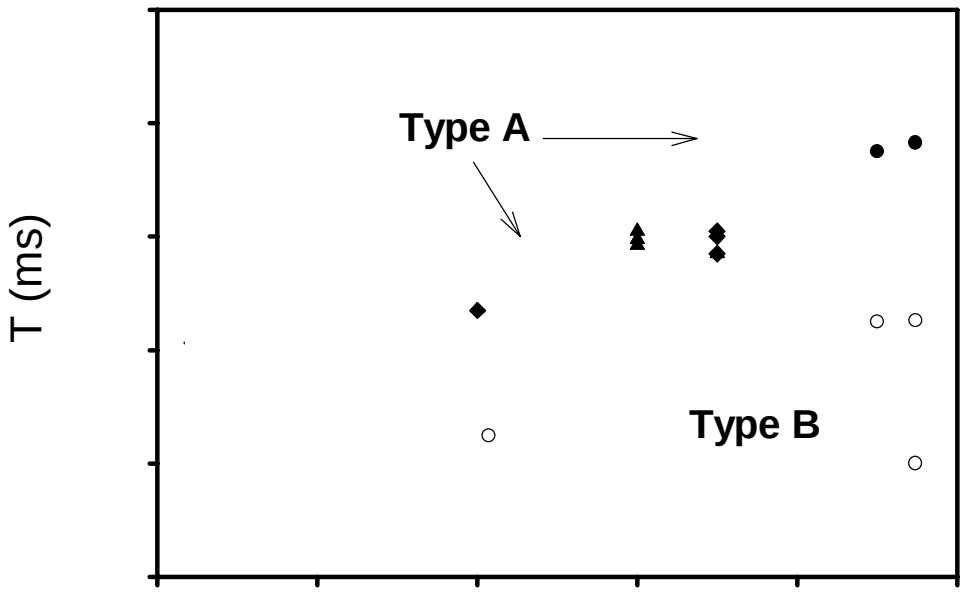

Figure 5.6: Observed timings of injected stimuli that cause 1:1→2:1 transitions as a function of the pacing period. Each shape corresponds to a different animal and the shading indicates the type of transititon. The filled shapes are Type A transitions and the open shapes are Type B transitions. The attempted transition times were swept from 50 ms to PP-50 ms in steps of 10 ms, typically 50 ms to 600 ms.

Figure 5.6 shows (PP, T) values from multiple animals resulting in 1:1→2:1 transitions. The filled shapes are the measured data points for Type A transitions. Different symbol shapes denote data from different animals. Open data points indicate type B transitions, which tend to be elicited by an extra stimuli delivered at small T, and lie in the lower half of the (PP, T) plane. Notice that the Type B transitions are elicited at shorter T than the Type A transitions. This could be because the criterion for categorizing them is based on rather or not they could possible elicit the next action potential and only stimuli injected late in the pacing

period qualify. It could also be possible be that the frog in which all the Type B transitions were found in was in some way more prone to transitions if the pacing was disturbed.

The injected stimuli that cause the Type A 1:1→2:1 transitions all occur during an action potential. This observation, regardless of how the Type B transitions are categorized, is contrary to the simple rule that cardiac tissue ignores stimulation applied during the refractory period. This observation may be prove to useful to the modify dynamics in whole heart during complex spatio-temporal behavior.

5.2.2 2:1→1:1 transitions

In five of seven animals I found that it was possible to elicit transitions from 2:1 dynamics to 1:1 dynamics. I observe that it is possible to induce two distinct types of 2:1→1:1 transition, which are shown in Fig. 5.7 and Fig. 5.8. Both types involve causing an action potential before the regular periodic pace can excite the tissue.

A Type I 2:1→1:1 transition is illustrated in Fig. 5.7. The tissue is driven at a PP of 650 ms and responds initially in a 2:1 pattern. The S_2 stimulus (marked with an arrow) is delivered after the 5^{th} normal stimulus, at T=100 ms. When the extra stimulus is applied, the tissue has just recovered sufficiently from its previous excitation so that the extra stimulus can elicit an action potential. However, the extra stimulus is applied early enough in the interstimulus interval that the resulting action potential ends before the next regular stimulus, giving rise to a 1:1 pattern.

Figure 5.8 illustrates a Type II 2:1→1:1 transition. The tissue begins in a 2:1 pattern, where it is driven at a PP of 700 ms, within the bistable window. In this case, the S_2 stimulus is delivered at T=590 ms. This results in an action potential that occurs slightly earlier than usual. The next regular stimulus is consequently skipped because it is delivered when the tissue is in its refractory period, and has

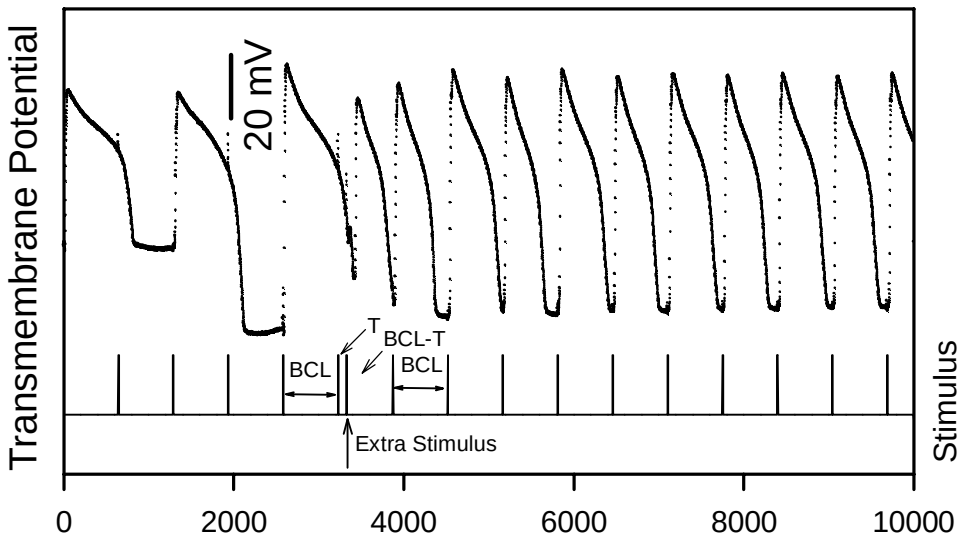

Figure 5.7: Temporal evolution of the transmembrane potential showing a Type I 2:1→1:1 transitions. The stimulus train is shown at the bottom of each time series. Extra stimuli are indicated with arrows. The shift in baseline during the measurement of the first two action potentials is due to microelectrode movement.

not yet repolarized following the previous action potential. The following stimulus that would normally be skipped in the 2:1 pattern now elicits a shortened action potential, and the tissue settles into a 1:1 pattern at PP=700 ms.

Figure 5.9 shows (PP, T) values from multiple animals resulting in 1:1→2:1 transitions. The filled shapes are the measured data points for Type A transitions. Different symbol shapes denote data from different animals. Open data points indicate type B transitions, which tend to be elicited by S_2 stimuli delivered at small T, and lie in the lower half of the (PP, T) plane.

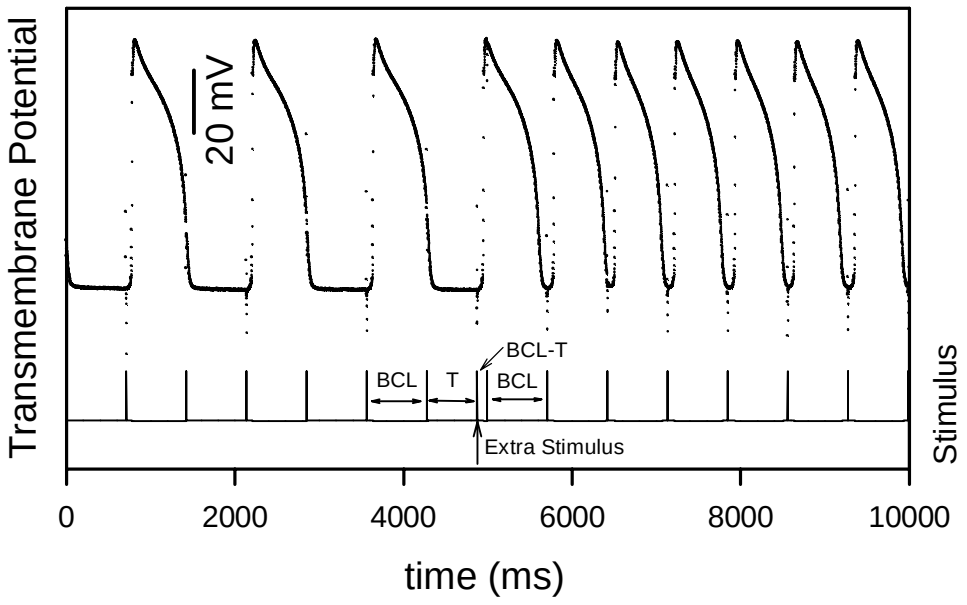

Figure 5.8: Temporal evolution of the transmembrane potential showing a Type II 2:1→1:1 transitions. The stimulus train is shown at the bottom of each time series. Extra stimuli are indicated with arrows.

5.3 Model Analysis

In this section I describe how the simple model discussed in Chapters 2 and 3 can be used to derive boundaries on the timing of injected stimuli that can elicit 2:1→1:1 transitions. These boundaries are a result of the parameters used in the restitution curve function. However, the simple treatment given here cannot describe the 1:1→2:1 transitions because mappings from APD_n to APD_{n+1} assume implicitly that every stimulus either elicits an action potential or is ignored. This deficiency is similar to the problem encountered when trying to describe both the N=1 and N=2 branches of behavior with a mapping as illustrated in Sec. 3.3.

The range of premature stimulus timings T that induce 2:1→1:1 transitions can be predicted qualitatively using the simple mathematical model of cardiac dynamics

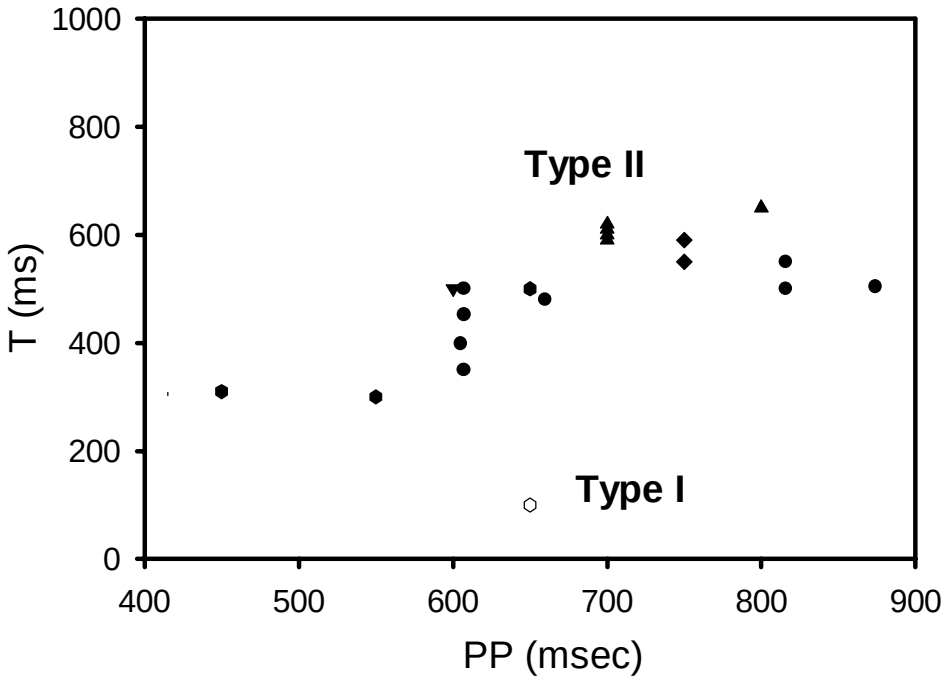

Figure 5.9: Observed timings of injected stimuli that cause 2:1→1:1 transitions as a function of the pacing period. Each shape corresponds to a different animal and the shading indicates the type of transititon. The filled shapes are Type I transitions and the open shapes are Type II transitions. The attempted transition times were swept from 50 ms to PP-50 ms in steps of 10 ms, typically 50 ms to 600 ms.

used in Chapter 2. Recall that the model consists of an iterative procedure (mapping) expressing the next action potential duration APD_{n+1} as a function of the current action potential duration APD_n [71, 63]. This function is constructed based on the pacing relation $APD_n + DI_n = N * PP$, where N is the smallest integer such that $N * PP - APD_n > \theta$, and θ is the shortest diastolic interval the tissue can sustain, and also on the assumption that APD can be described as a function of DI given by

$$APD_{n+1} = f(DI_n).$$

Solving for DI_n from the pacing relation and substituting in (1), I find

$$APD_{n+1} = f(N * PP - APD_n). \tag{5.1}$$

When N=1, every stimulus elicits a response, giving rise to patterns such as 1:1 or 2:2 (alternans) depending on the slope of the function f. When N=2, every other stimulus elicits a response (2:1 pattern) and the sum of the action potential duration and the diastolic interval equals the time between two stimuli.

Experimentally measured values of APD_{n+1} versus DI_n can be approximated by the function

$$f(DI) = APD_{\max} - A\exp(-DI/\tau). \tag{5.2}$$

Taken together, (5.1)-(5.2) define a mapping that takes APD_n into APD_{n+1}. The parameters in this model are found by a least squares fit to measured APD and DI values. When $APD_{\max}$, A and τ are all positive, APD decreases as DI decreases.

This map has a discontinuity when DI=θ, and each side of this discontinuity corresponds to a different value of N. Fixed points of the map occur when APD^*=APD_n=APD_{n+1}. The fixed point stability is governed by the slope of $f(APD^*)$ at a given PP. For some PP, there exist two stable fixed points APD_1^* and APD_2^*, which lie on the N=1 and N=2 branches respectively. This gives rise to bistability: two stable solutions coexist for the same parameter values. Note that no unstable state lies between the two stable steady states due to the discontinuity of the map.

There are two separate routes from the 2:1 to the 1:1 regime. For a Type I transition, the extra stimulus must occur after the periodically skipped pace, thereby giving the relation

$$T > \theta + APD_2^* - BCL, \tag{5.3}$$

where APD_2^* is the steady state APD on the N=2 branch. If the normal stimulus

immediately following the premature stimulus elicits a response, the condition

$$T < BCL - \theta - APD_2', \tag{5.4}$$

applies, where $APD_2' = f(BCL+T-APD_2^*)$ is the width of the first action potential following the S_2 stimulus.

For a Type II transition, similar arguments require that

$$T > BCL - \theta - APD_2' \tag{5.5}$$

holds in place of (5.3). For both Type I and Type II transitions, the conditions

$$T < 2 * BCL - \theta - APD_2', \tag{5.6}$$

$$BCL > \theta + APD_2'', \tag{5.7}$$

apply, where $APD_2'' = f(2 * BCL - T - APD_2')$. Conditions (5.3), (5.4), (5.6), and (5.7), enclose the lower region indicated in Fig. 5.10, where Type I 2:1→1:1 transitions occur. Conditions (5.5)-(5.7) enclose the upper region in Fig. 5.10, where Type II 2:1→1:1 transitions occur.

Figure 5.10 shows (PP, T) values resulting in 2:1→1:1 transitions. Only one frog, represented by the open hexagon, shows a Type I 2:1→1:1 transition (time series shown in Fig. 3a). The closed shapes show Type II 2:1→1:1 transitions. The data from different animals is indicated by different symbols. The larger proportion of Type II 2:1→1:1 transitions is indicative of our finding that Type II transitions are easier to induce than Type I. In Fig. 5.10, both shaded regions are generated by the same map parameters (fit to data from the frog whose transitions are indicated by diamonds). The horizontally striped region shows the model predictions for Type I transitions and the vertically striped region shows Type II transitions. The predicted transition regions for 2:1→1:1 transitions do not seem to be sensitive to

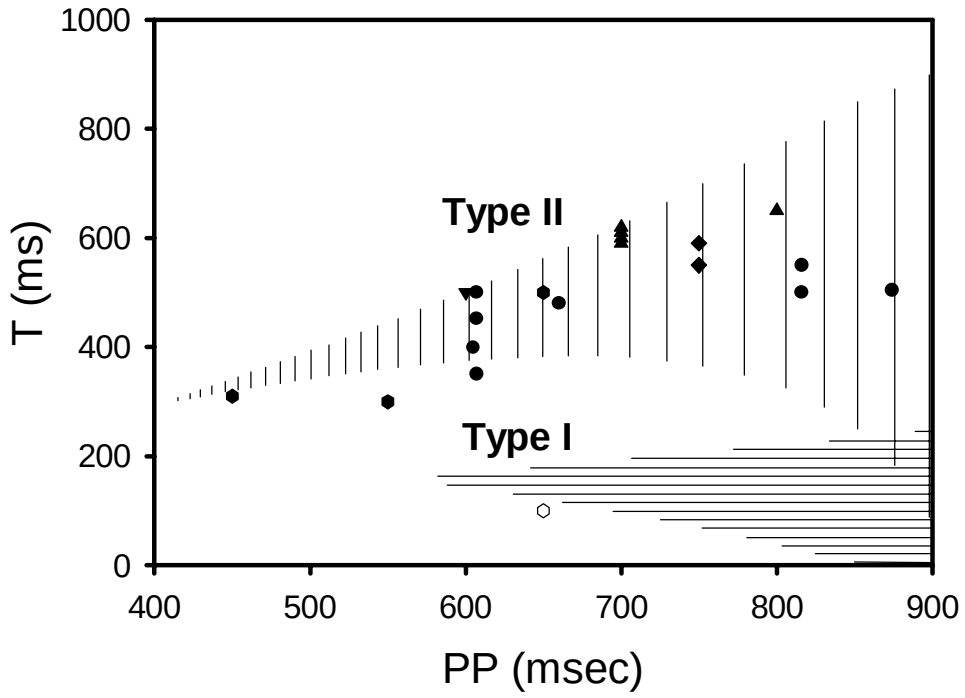

Figure 5.10: The regions of extra stimulus timings T that elicit various types of transitions are shown as a function of PP. Closed symbols indicate experimentally observed transitions. The upper (lower) shaded area encloses the region where Type II (Type I) 2:1→1:1 transitions occur. The open hexagon corresponds to the observed Type I transition illustrated in Fig. 3a. Parameters for both Type I and Type II regions are obtained from a fit to data from the same frog.

animal-to-animal parameter variations. For example, the predicted regions shown in Fig. 5.10, generated from parameters fit to data from a single frog, cover transitions observed in multiple animals.

5.4 Discussion and Conclusions

In clinical situations, it may be useful to modulate local cardiac dynamics that correlate with the onset of arrhythmic behaviors in the whole heart. In this Chapter, I show that a single premature stimulus injected into the train of periodic paces can induce transitions between bistable states in small pieces of bullfrog myocardial

tissue.

I find that the timing of injected stimuli that cause the 2:1→1:1 transitions can be described by a simple map based theory. Discrepancies arise between the measured and predicted timing regions for two reasons. One reason is that the one-dimensional model represents an approximation to the behavior. A shortcoming of the model is the assumption that stimuli encountered before the end of an action potential cannot generate a response. This assumption is clearly violated in the 1:1→2:1 transitions.

A second reason for the discrepancies is that the parameters used in Eq. (5.2) to generate each of the regions shown in Fig. 5.10 are obtained from a fit to data from a single animal, whereas the data points represent experiments from multiple animals. The parameters in Eq. (5.2) vary significantly from one animal to another. Therefore, it is important to design control protocols with sufficient flexibility to account for animal-to-animal parameter variations, as well as for different dynamical behaviors.

The method by which these transitions are induced make this technique particularly suited for clinical application. In the whole heart of a living animal, the sino-atrial node sets the upper limit on the period of stimuli delivered to the atrium. Additional stimuli can be applied by the clinician, but individual SA node impulses cannot be easily removed. The modulation of cardiac dynamics by injected stimuli is of great interest [33], since it may be more directly applicable to clinical settings than techniques that require the variation of the interstimulus interval as a control parameter [39, 40, 3, 70]. The induction of dynamical transitions by premature stimuli may, in combination with nonlinear control techniques [39, 40] and other standard medical procedures, be of great use as part of the clinical "toolkit" of low-energy cardioversion.

Chapter 6

Applying Closed-Loop Feedback to Atrial Fibrillation

The goal of this research is to develop control techniques to suppress the complex spatio-temporal dynamics that occur during fibrillation. It is believed by some research groups that control schemes originally designed for controlling *temporal* complexity can suppress spatio-temporal disorganization [23, 46, 8, 47]. While some early experiments have yielded promising results [23, 44] there is still a need for further experimentation.

Preliminary research by Ditto and collaborators [23] suggests that it is possible to capture at least a portion of a fibrillating human atria *in vivo* using a feedback controller. The location of the unstable steady state to be controlled was derived from observing the uncontrolled dynamics, similar to the OGY [29] scheme. In this experiment the heart dynamics were recorded and control stimuli were delivered by a quadrupolar electrode catheter inserted into the right atrium through the femoral vein. It was observed that the wide variation of the inter-beat interval could be suppressed using their control technique. However, due to the limited number of sensors, it could not be determined whether the entire atrium was controlled. In addition, atrial fibrillation was terminated only rarely using this method.

The purpose of the study presented in this chapter is to attempt to control sheep atrial fibrillation (AF) *in vivo* using a single feedback controller that measures the dynamics of the atria and applies control perturbations at a single spatial location. This study allows investigation of control of cardiac dynamics in a preparation that is physiologically close to an *in vivo* human heart. Both the temporal and spatial

response of the fibrillating sheep atria are measured using a multi-channel electronic recording system [97]. To suppress fibrillation, I implement a TDAS-like controller, which does not require *a priori* knowledge of the state of the tissue I wish to stabilize. This controller attempts to stabilize an unstable period-one behavior embedded in the fibrillation that may or may not be the normal sinus rhythm.

This was a difficult project to get working. While I directed the experiment, I required the assistance of several people. The experiments were performed in the Duke Cardiac Electro-Physiology Laboratory in the Biomedical Engineering department. Ms. Ellen Dixon-Tulloch prepared the sheep for the experiments by completing the required surgery and maintained the animal's health throughout the experiment. Dr. Patrick Wolf provided expertise on the mapping system and on sheep dynamics during the actual experiment. Mr. Robert Oliver played a fundamental role in all phases of the experiment. He sewed the plaque onto the heart; he managed the recording system; and he help design and build the plaque electrodes. Dr. Sonya Bahar assisted in the construction of the plaque as well. Dr. Joshua Socolar and his student Mr. Pavan Cheruvu performed a preliminary theoretical analysis that indicated the controller could at least control a 1-D unstable mapping. Finally, Dr. Daniel Gauthier helped to monitor the sheep, analyze the data, and design the controller.

In the first section of this chapter, I present the experimental setup for exploring the spatio-temporal dynamics *in vivo*. Then I discuss the plaque of extracellular electrodes and mapping system used to measure both temporal and spatial response of the tissue to control during fibrillation. In addition, I describe the typical types of dynamics that are observed. In the next section, I introduce the TDAS-like controller used to attempt control of fibrillation. Finally, I discuss the results.

6.1 Atrial Fibrillation in Sheep

The mammalian heart is a complex and nonlinear mechanical system, designed to pump blood. It has four chambers, divided left and right, atria and ventricle. The right two chambers take blood returning from the body and pump it to the lungs. Subsequently, the left two chambers pump the blood coming from the lungs out to the body. The atria act as priming pumps to the ventricles (the main pumping chambers). The pumping action of the heart is accomplished by the muscle tissue that makes up the walls of the various chambers. Its mechanical contractions are mediated by waves of electro-chemical excitation that sweep through specialized conduction systems and the muscle of the heart. These waves normally originate in the sinus node (the main pace-maker of the heart). Under normal and healthy conditions, these waves of excitation cause a coordinated contraction of the muscle. In some situations, this orderly procession of waves can devolve into a spatially complex dynamical state known as fibrillation [1], in which the waves of excitation and consequent contractions of the heart are not coordinated, causing a loss of blood pressure and death. While both the atria and ventricles can display fibrillation, atrial fibrillation is studied in my research because it can be sustained for some time without causing death, whereas ventricular fibrillation is often fatal [1].

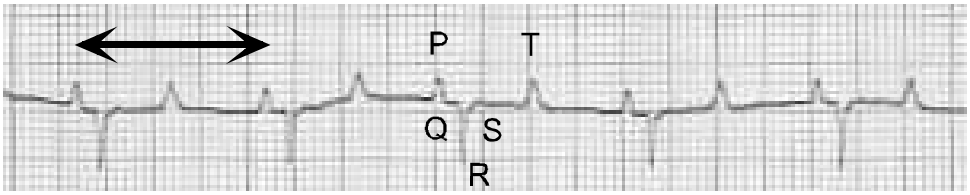

Figure 6.1: A Lead II electro-cardiogram of normal sinus rhythm. The deflection of the trace corresponds to the phases of a heart beat. The P complex corresponds to the depolarization of the atria. The QRS complex part of the signal corresponds to ventricular depolarization, and the T-wave is the repolarization of the ventricles.

Normal sinus rhythm (NSR) is a relatively regular process. Figure 6.1 shows a Lead II electro-cardiogram (ECG) time series [96] from a sheep during NSR. This signal is obtained by measuring the voltage differences between the left leg and right shoulder of the animal. It is important to note that this signal is a summation of the electrical activity of the whole heart, so it is not possible to distinguish the spatial patterning on the surface of the heart. The feature denoted P is associated with excitation of the atria and the QRS feature corresponds to excitation in the ventricles. The feature labeled T is associated with the repolarization of the ventricle. Notice that the separation between individual QRST shapes is about 1 second while the duration of the P-wave is less than 100 ms. This implies the atria has about 900 ms to recover between beats (see Table A.9).

The spatio-temporal electrical activity on the surface of the atria during can be observed with the plaque electrodes and mapping system (described in Sec. 6.3). The temporal pattern of activation during NSR is show in the series of panels in Fig. 6.2. Each panel corresponds to a 4.5 ms time slice of a single time series. The gray and black dots in each panel represent the spatial location of the electrodes. The black dots illustrate at which electrodes an activation was observed during that time slice. Arrows have been added to guide the eye through the time course of the wave. The wave of excitation shown in this figure corresponds to the P-wave part of the ECG and repeats approximately once a second. The total propagation time across the plaque (33 mm) is about 31 ms.

Atria fibrillation is very different from the orderly and periodic NSR. Figure 6.3 shows a Lead II electro-cardiogram (ECG) time series from a sheep experiencing atria fibrillation. There is no longer a clear P-wave and the QRS complex comes at what seems to be random intervals. In addition, notice that there is no time when activity ceases on the heart.

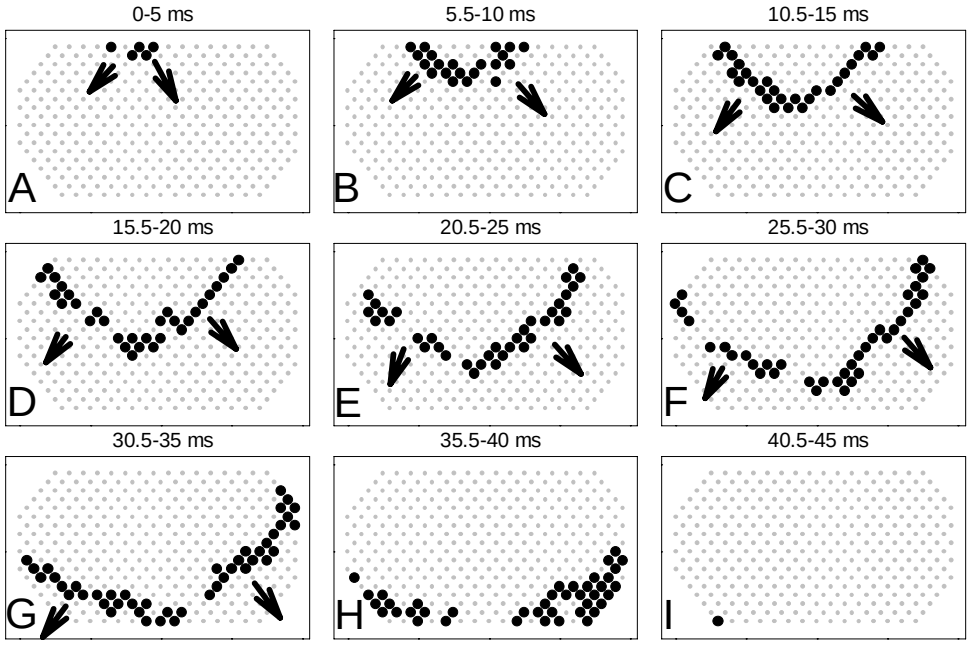

Figure 6.2: Normal sinus rhythm in a sheep stria measured with a plaque of electrodes. The panels A-E show the temporal evolution of a normal heart beat on the right atria of a sheep heart. The wave originates in the sinus node (off plaque in the upper left) and propagates across the atria. Each of the panels represents 4.5 ms of time. The black dots show where the leading edge of activation was during that time slice. The plaque is approximately 7.0 cm $\times$ 3.2 cm and the wave of excitation travels across it in 31 ms. Each NSR wave is separated in time by about 1 second from the next.

The spatio-temporal evolution of atrial fibrillation from the same sheep that produced this ECG chart is shown in the series of panels in Fig. 6.4. These panels are similar to the ones shown in Fig. 6.2, except that each panel corresponds to a 9.5 ms time slice of a single time series. A longer width of the time slice was used to generate these plots than in Fig. 6.2, because the waves propagate more slowly. During atrial fibrillation, it seems that there is no point of origin for the waves of excitation and that the observed activity is self-sustaining.

During atrial fibrillation, the shape of the wave is uneven and its speed varies widely from location to location, while during normal sinus rhythm the shape of

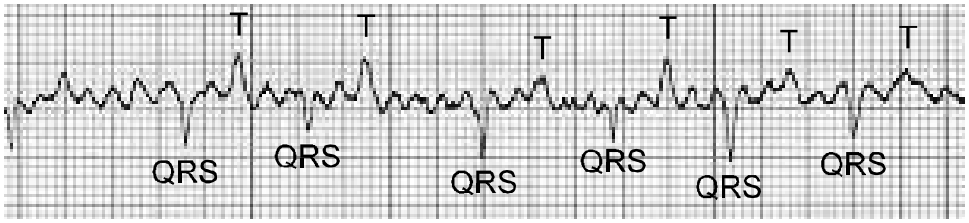

Figure 6.3: A Lead II electro-cardiogram during atrial fibrillation or flutter. There is no longer a clear PQRST shape. The atria is observed to be generating a seemingly random signal. The ventricle is firing at a more normal and slower rate. The AV node, which is an electrical connection between the atria and ventricle protects the ventricle by only allowing wave of excitations to pass with a low frequency.

the wave of electrical excitation is very simple. The ultimate goal of this research is to develop methods to convert the fibrillation state into the NSR state. In this experiment, however, I only attempt to stabilize a periodic state of the fibrillating tissue, which may or may not correspond to NSR.

6.2 Experimental Setup (system)

The experimental system is an *in vivo* sheep atria preparation. This system allows the investigation of fibrillation in a preparation that is similar to a human hearts. I use the atria because the animals can sustain atrial fibrillation for many minutes or hours without dying, whereas ventricular fibrillation is fatal in a very few minutes [1].

In these experiments, all actions taken on the animals are in accordance with a protocol approved by the Duke University Institutional Animal Care and Use Committee and conform to the Research Animal Use Guidelines of the American Heart Association. After recording the heart rate the sheep is anesthetized with ketamine hydrochloride (15-22 mg/kg IM). Once anesthesia is achieved, the animal is intubated with a cuffed endotracheal tube and ventilated with a North American Drager

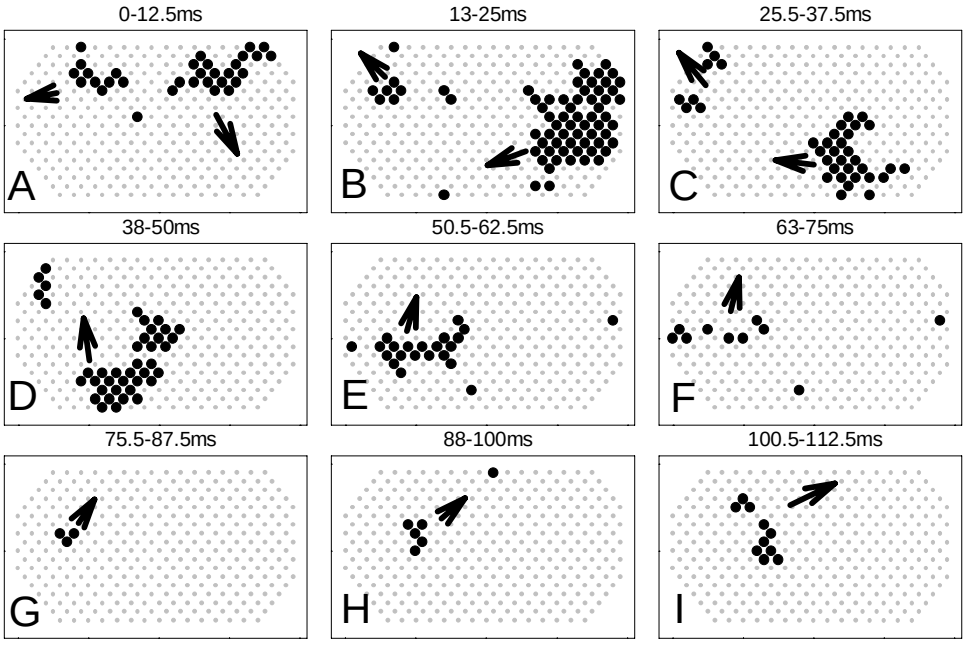

Figure 6.4: The panels A-I show the temporal evolution of a reentry circuit during fibrillation on the right atria of a sheep heart. The wave circulates around the surface of the atria. Each of the panels reprensents 9.5 ms of time. The black dots show where the leading edge of activation was during that time slice.

mode SAV ventilator. Isoflurane gas (1-5 percent) is administered continuously to maintain adequate anesthesia. A nasogastric tube is passed into the stomach to prevent rumen aspiration. Femoral arterial blood pressure and the lead II electrocardiogram are continuously displayed and monitored. Blood is withdrawn every 30-60 minutes to determine pH, P_{O_2}, P_{CO_2}, total CO_2, base excess and the concentrations of Ca^{2+}, K^+, Na^+, and HCO_3^-. Normal physiological levels of the above are maintained by adjusting the ventilator and by IV injection of electrolytes.

In order to observe directly the dynamics of the atria, it is necessary to attach the plaque of electrodes to the surface of the atria. To accomplish this, the chest is opened through a median sternotomy and the heart is suspended in a pericardial cradle. Two plaques described in Sec. 6.3 are affixed to the epicardium of the right

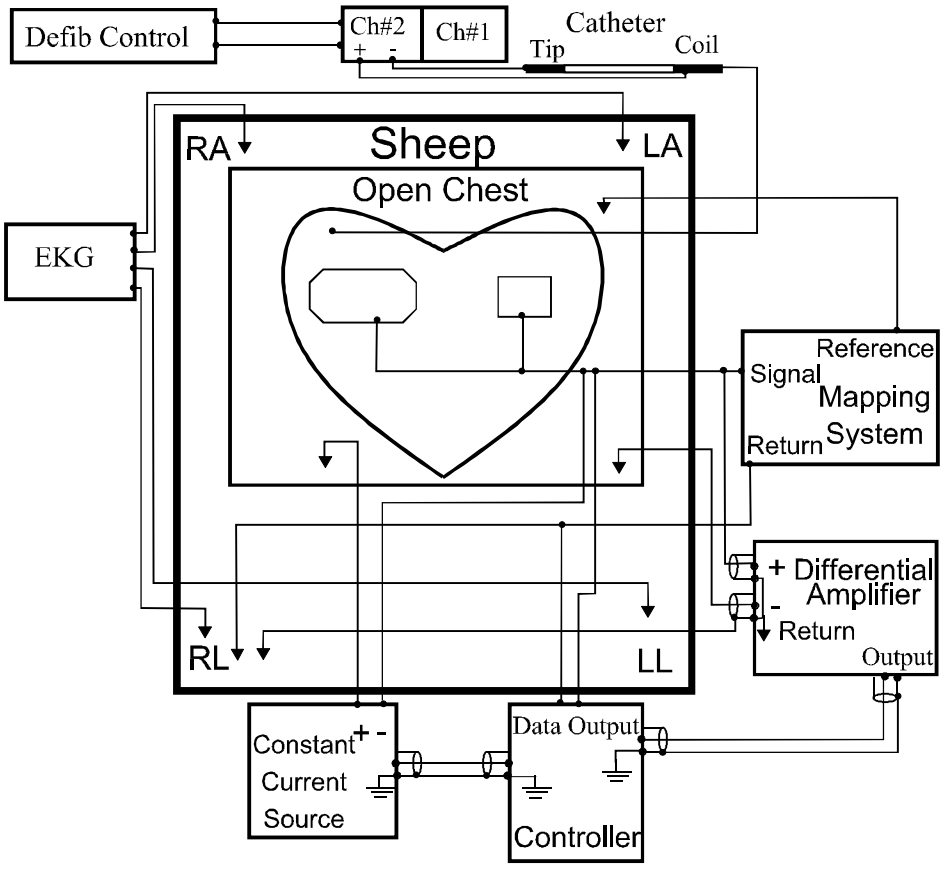

Figure 6.5: Wiring diagram for measuring and pacing sheep cardiac tissue *in vivo*. Starting on the far left and working clock wise, the equipment attacted to the sheep is: an EKG monitor, a defibrillation catheter, the multi-channel mapping system, a differential amplifier (20×), Projective TDAS controller, and a constant current source.

and left atrial free wall with sutures to the pericardial cradle and the fatty tissue in the atrioventricular (AV) groove. In all animals a Ventritex defibrillation and pacing catheter is placed in the right ventricle to help terminate an inadvertently induced ventricular fibrillation. All the electrical equipment connections made to the sheep are found in Fig. 6.5. Once the animal is fully prepared and all equipment is installed and activated, a normal sinus rhythm is recorded and analyzed to assess if the right atrium is behaving physiologically, i.e., whether a wave front moves across the plaque from the top near the sinoatrial node to the bottom toward the AV groove.

To identify the threshold current to use during pacing, I use two different protocols. The first protocol identifies the current threshold needed to elicit a wave of activation. The second protocol identifies the current level that produces consistent dynamics. Initially, the atria is periodically paced from an electrode in the middle of the left plaque with 4 ms pulses at a period of 400-500 ms with a current amplitude that is too low to stimulate the tissue. The current of the pacing pulses is slowly increased until the periodic train of pulses captures the dynamics of the whole atria. This current level is then used as the base current level for the second protocol.

The second threshold protocol identifies the minimum pacing current where no further changes in the window of bistability. This protocol was developed as a result of my research on the prevalence of bistability and hysterisis in bullfrog cardiac muscle described in Chapter 3. As the pacing period is decreased the behavior transitions to 2:1 locking with the periodic pacing. It was found during preliminary studies [65] that the pacing periods at which the 1:1-to-2:1 and 2:1-to-1:1 transitions occur decrease with increasing current strength. The tissue is periodically paced with a sequence of decreasing periods and then with a sequence of increasing periods. At each pacing current it is observed at which periods the 1:1-to-2:1 and 2:1-to-1:1

transitions take place. In most trials, this preliminary pacing protocol is run with progressively larger current until the transition pacing periods does not change. The resulting current is the pacing current that is used during the control experiments. In all experiments, stimulus current is at least twice the level that captured the dynamics with a pacing period of 400-500 ms.

I used three techniques to establish fibrillation in the sheep atria. The first technique is to repeat the slowly decreasing and increasing pacing period protocol described above. This pacing protocol starts pacing the atria at a slow rate of approximately 250 ms and progressively decreases the period by 10 ms to a minimum of 50 ms. At each pacing rate the tissue is paced for at least 8 seconds. Once the minimum pacing period was achieved the pacing period was increased. In preliminary studies [65], this pacing process was observed to cause entrant activity. If this technique was unsuccessful, the tissue was paced with a period selected to be the fastest rate at which 1:1 behavior was observed (typically 130 ms). This pacing rate was maintained for several minutes. The goal was to change the excitability of the atria, perhaps inducing spatial variations in refractoriness. Finally, if neither of these techniques establish fibrillation, the tissue was subjected to burst pacing. In burst pacing the tissue is periodically paced with a period of 50 ms for several seconds.

In the experiments on seven female 63 ± 5 kg sheep, one of these three pacing protocols were successful in inducing sustained complex dynamics (either fibrillation or flutter) in four out of seven animals. The difference between fibrillation and flutter is largely a matter of degree. Both dynamics are self-sustaining; however, flutter involves more organization and macro reentry circuit, while fibrillation show less correlation in time and space. I observed what I consider fibrillation in 2 of the animals and possibly a third.

6.3 The Plaque Electrode (the transducer)

The spatio-temporal dynamics of the atria is measured using a multi-channel electronic mapping system, developed by Wolf *et al.* [97]. This system simultaneously records the voltage from each of the individual electrodes in the plaque and streams this data to disk for later analysis. The feedback controller monitors in real time the dynamics from a single electrode in the center of the plaque.

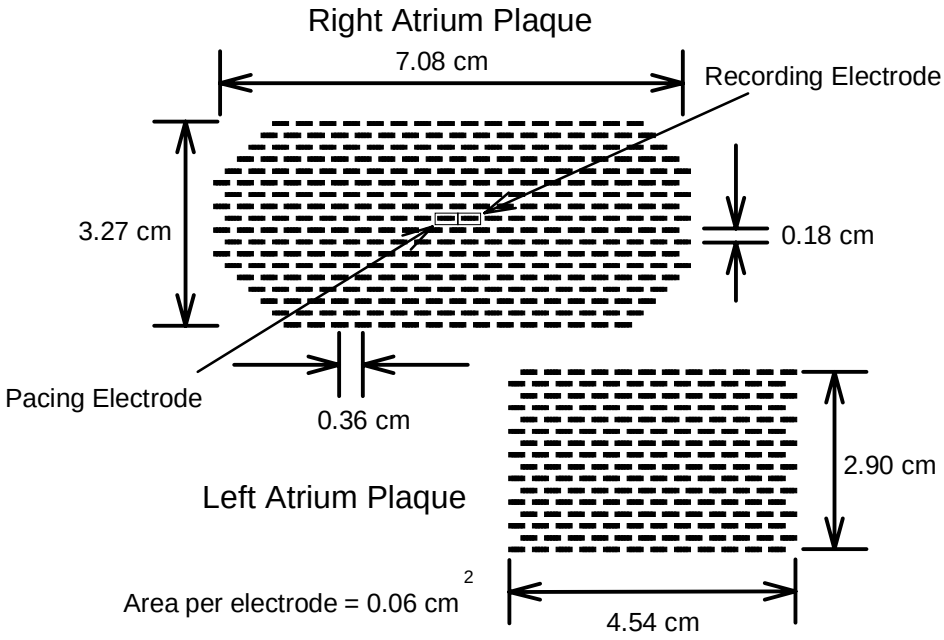

Figure 6.6: A diagram of the electrode layout of the plaque electrode. The plaque electrode consists of two pieces. One piece is attached to the left atria and the other to the right atria. The individual silver electrodes are set in a staggered pattern that is equivalent to a square lattice with side spacing of 40 mm rotated by 45°.

The recording system works in conjunction with a plaque placed on the atria with 528 individual extracellular electrodes. The two plaques measure the spatio-temporal dynamics on both the right and left atria. The left atrium was monitored to compare with the dynamics of the right atrium and observe large scale reentrant

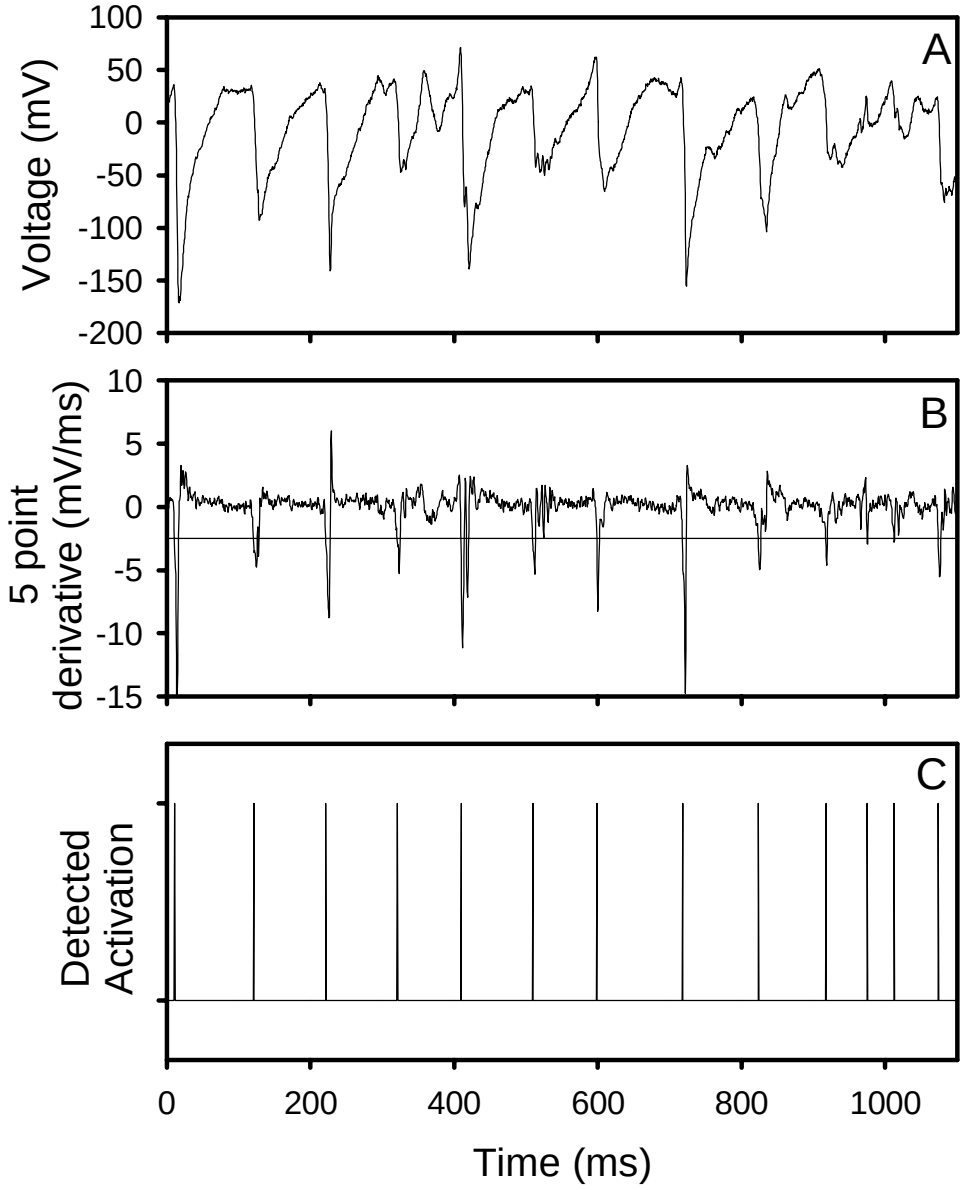

Figure 6.7: A set of time series showing the voltage from a single plaque electrode (A), the five point derivative (B), and detected activations (C). The top figure is the voltage measurement over 1100 ms from an electrode very near the center of the plaque on fibrillating sheep atria. The derivative signal is tested for threshold crossings to determine activations.

circuits. A diagram of the plaques is shown in Fig. 6.6. The individual electrodes are 0.01 in. diameter silver wires. The electrodes are set in a square grid with a 40 mm spacing. The electrodes are chloridized before each use to minimize the noise they generate [54].

Extracellular electrograms were recorded from the tips of each electrode in the plaque with respect to the return electrode placed in the aortic root. The electrograms were band-pass filtered from 0.5 to 500 Hz, sampled at 2 kHz, and saved to disk. The controller monitors only the electrode marked 'recording electrode' in the figure. The pacing stimulus is a cathodal stimulus current of duration 4 ms and strength (chosen by the procedure to find the threshold described in Sec. 6.2) in the range of 0.1-3.5 mA was applied at the pacing electrode. The return electrode for this current was attached to a chest retractor that remained in place during the studies. The stimulus current was generated by a constant-current source whose timing controlled by the control circuit described in Sec. 6.5.

The control circuit is attached to the plaque so that the controller can pace the tissue from the center-most electrode on the right atrial plaque and monitor the tissue dynamics from a neighboring electrode (approximately 3.6 mm away). The pacing and recording electrodes are different because the constant current pulse for pacing the tissue causes the stimulus electrode to become temporarily polarized. This charge saturates the amplifiers and make observing the temporal dynamics at this electrode impossible.

To analyze the electrograms, the signal from each electrode were differentiated using a five-point algorithm and then displayed on a computer as an array of elements corresponding to the geometry of the mapping plaque. A computer program using a level crossing routine determines activation times at all plaque electrodes

An illustration of the activation detection process is shown in Fig. 6.7. First, an

extracellular electrogram (Fig. 6.7a) from an electrode is differentiated (Fig. 6.7b). The differentiated signal is compared with a threshold value (the solid horizontal line in Fig. 6.7b). An activation is considered a threshold crossing. The observed detected activations are shown as pulses in Fig. 6.7c.

6.4 Observed behaviors

Under normal conditions, the dynamics of the atria are completely governed by the driving period of the sinus node. This intrinsic pacemaker causes a wave of excitation to be generated at the top of the atria. The wave sweeps across the atrial muscle (as shown in Fig. 6.8) and collides with the boundary at the bottom of the atria. After the passage of a wave of activation the atria muscle remains unexcited until the sinus node once again causes an activation wave. The pattern of activity is very regular and each location experiences essentially the same inter-activation interval. Figure 6.9 shows a histogram (normalized to unit area) of the inter-activation intervals from a 100 electrodes from the center of the right atrial plaque during NSR. Notice that the inter-activation intervals from all 100 electrodes fall inside a single 10 ms bin centered at 880 ms.

In experiments where I establish reentrant waves, several complicated spatio-temporal patterns of activity are observed. While every run was different and the tissue dynamics never repeated, the observed re-entry dynamics can be broadly categorized into two classes: flutter and fibrillation. Flutter is a macroscopic re-entry pattern of activity that involves most of the atria and is quite periodic. Fibrillation typically has little or no discernible structure, and appears to be the result of many small re-entrant circuits.

An example of atria flutter is illustrated in Fig. 6.10. In this figure, a well organized wave pattern is observed crossing the surface of the atria. This wave structure

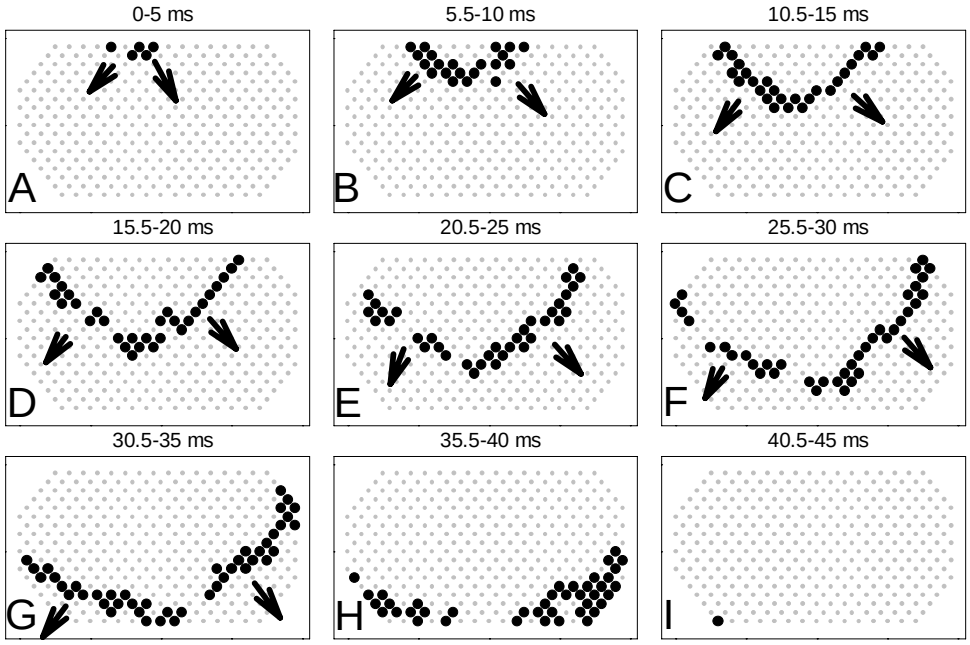

Figure 6.8: The time evolution of a wave of avtivation from NSR. During NSR the progress of activations is orderly and periodic. The sinus node is near the top center of the plaque. The arrows are added to guide the eye.

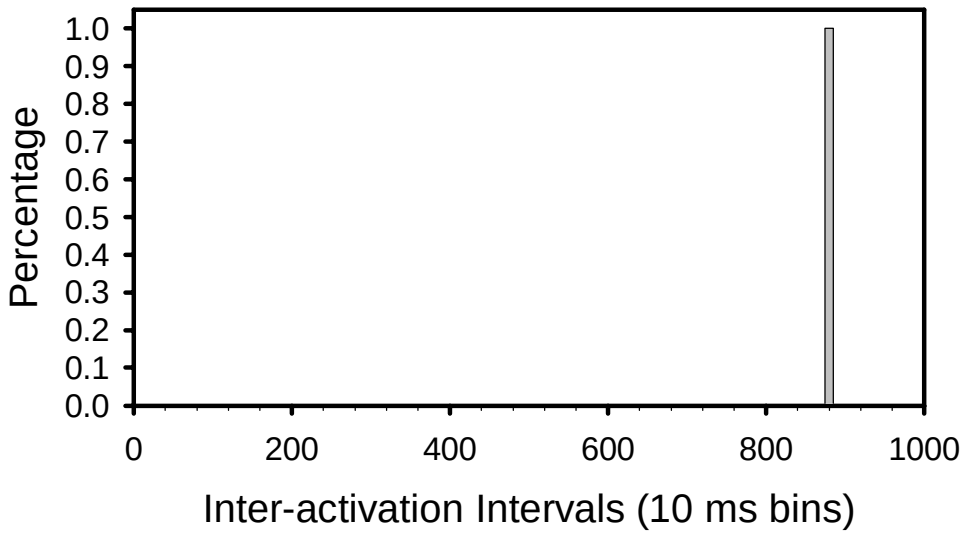

Figure 6.9: Histogram of inter-activation interval during NSR of 100 electrodes from the right atria. The bin sizes are 10 ms. There were 3 activations observed during the 2 seconds recorded here giving only 2 inter-activation intervals per electrode. Notice, that while the histogram is from inter-activation observed at many different locations on the atria. All the points fall in the bin centered at 880 ms.

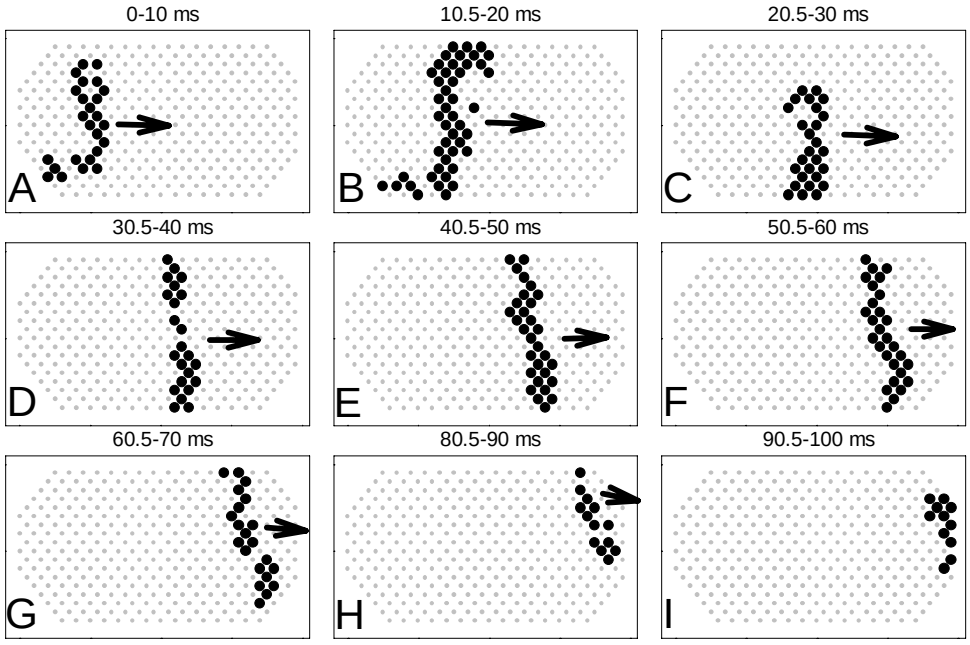

Figure 6.10: A series of panels showing the temporal evolution of atria flutter. An organized wave of excitation travels around the atria in a large reentrant circuit.

usually recurs in some form with a period of a few hundred milliseconds. Note that while the wave seem just as organized as in NSR, it does not originate from the sinus node and the propagation pattern varies with each recurrence. This orderly wave structure occasionally breaks up into more complicated spatio-temporal patterns. Figure 6.11 shows a histogram of the inter-activation intervals from both a single electrode (stripes) and 100 electrodes (solid grey) on the right atrial plaque during a sheep experiment where I observed flutter. In both the single point and multi-point histograms most of the inter-activation intervals cluster around 110 ms and show approximately the same spread in timing. This indicates similar dynamics take place everywhere on the atria and that this activity can vary in timing by more that 20%. Notice that the average inter-activation interval is much shorter than the NSR.

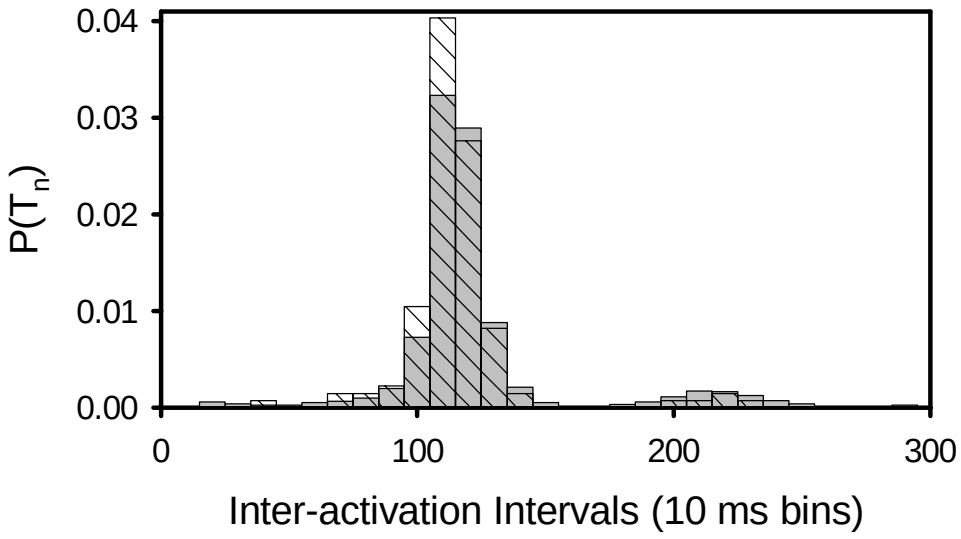

Figure 6.11: A histogram of inter-activation intervals observed during atria flutter. The solid gray bars are a histogram from the 100 midle electrodes. The diagonal line bars are the histogram of just the very middle two electrodes. Notice that the spread in the timing is about the same for both cases.

Atrial fibrillation is illustrated in Fig. 6.12. The activation of the atria does not seem to follow any clear pattern. At several points (panels A and H), waves break up into two waves. At other times two waves (not shown) can be observed to collide an annihilate each other. The single and multi-point histograms (see Fig. 6.13) of this behavior show about the same average timing as flutter but a larger variation in the inter-activation intervals.

From these observations, there is a clear difference between NSR and reentry patterns. However, the difference between atrial fibrillation and flutter is hard to specify exactly. Often, an atria that is displaying fibrillation-like dynamics with small reentry patterns will shift into flutter-like macroscopic patterns and then shift back to small patterns.

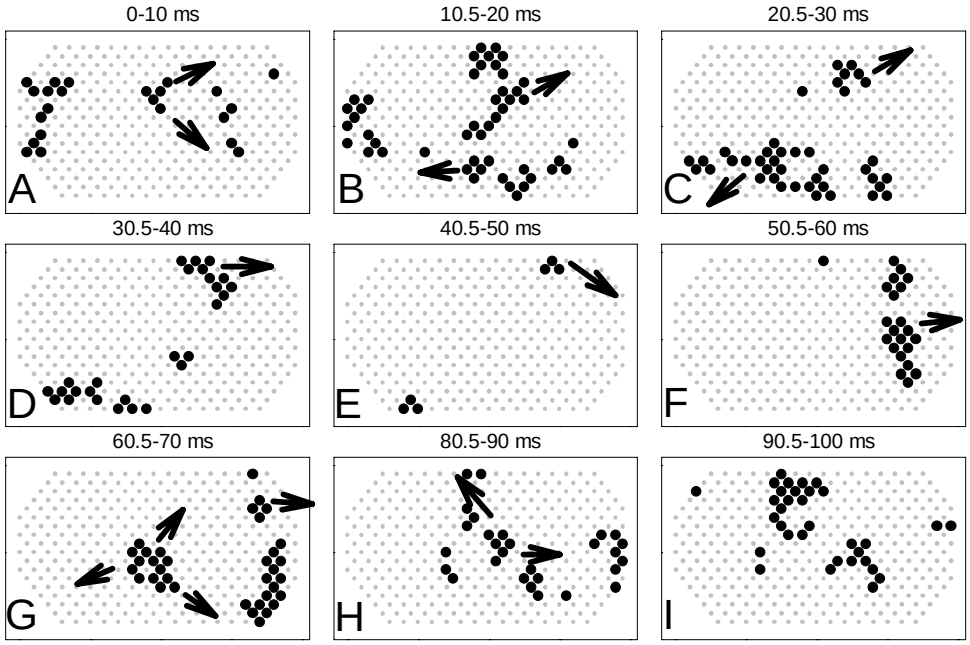

Figure 6.12: A series of panels showing the temporal evolution of atria fibrillation. With little or no organization wavelets circulate around the atria, sometimes colliding, other times breaking in two. Notice that in panel G a wave seems to appear from no where. It is likely the wave came from the interior structure of the atria wall.

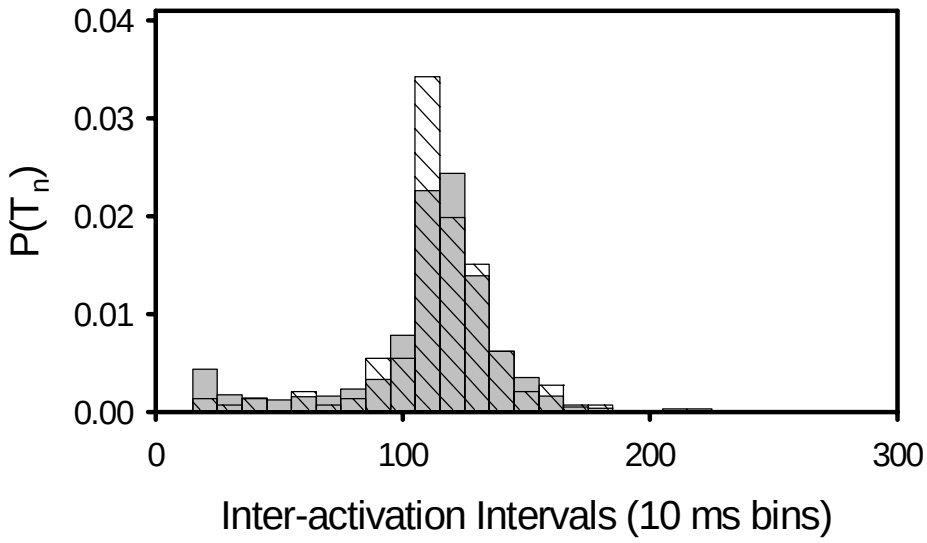

Figure 6.13: A histogram of inter-activation intervals observed during atria flibrillation. The solid gray bars are a histogram from the 100 middle electrodes. The diagonal line bars are the histogram of just the very middle two electrodes. Notice that there are more short period inter-activation intervals than in flutter.

6.5 Control and Actuation

The goal of this controller is to reduce the variation observed in the inter-activation intervals during atria fibrillation or flutter. This is accomplished by occasionally pacing the atria according to a control algorithm. The control algorithm computes the timing of a control pulse that is necessary to suppress variation in the dynamics. If an activation does not occur with the timing calculated by the controller, the controller paces the tissue to cause an activation. If a natural activation occurs at the correct time (or earlier), the controller does nothing. The control algorithm I used in this experiment is a TDAS-like scheme that I call Projective-TDAS (PTDAS) because it projects when the next activation should arrive.

To understand the action of the PTDAS controller, it is useful to assume that the dynamics of the atria can be described by a vector (T_n, Q_n). The inter-activation

time T_n is observed at a single location on the heart. The inter-activation times at every other location and any other information required to completely specify the state of the atria is represented by Q_n. This state vector will evolve in time and generate a new inter-activation time T_{n+1} at the observation point. The new inter-activation time is given by

$$T_n = F(T_n, Q_n) \tag{6.1}$$

where F an unknown function that propagates the state of the tissue forward in time.

Recall that TDAS compares consecutive action potential durations to develop an error signal, as described in Chapter 4. Unfortunately, the extracellular measurement technique that I use can only measure the activation timing (see Sec. 6.3), not the action potential duration. The PTDAS controller compares consecutive inter-activation intervals to generate an error signal. The error signal is given by

$$\varepsilon_n = -\gamma(T_n - T_{n-1}), \tag{6.2}$$

where γ is the gain of the controller.

To complete the feedback control loop as described in Chapter 2 it is necessary to modify some parameter of the system by an amount ε_n. However, the controller can not modify the pacing period as in Chapter 4 because the fibrillating atrium is not being driven by periodic pacing. Instead, the controller must generate an extra pace designed to cause the dynamics of the atria become periodic. It does this by projecting the arrival time of the next activation and adjusts that timing by an amount equal to the error signal. The controller uses the last inter-activation interval as an estimate of the next inter-activation interval. The controller paces the tissue if no activation is detected before this projected time. Combining this

estimate and the error signal gives

$$T'_{n+1} = T_n - \gamma(T_n - T_{n-1}) \tag{6.3}$$

as the time that the controller will initiate a pace to stabilize a period one behavior of the atria. However, it could be that the system produces an activation before the controller is able to cause an activation. If this happens the controller resets. Therefore the dynamics of the system plus control is given by the minimum of equations (6.1) and (6.3), this can be expressed by

$$T_n = \min[F(T_n, Q_n), T_n - \gamma(T_n - T_{n-1})] \ . \tag{6.4}$$

To understand the action of this controller it is useful to consider the dynamics of the system as a simple unstable fixed point. That is equation (6.1) becomes

$$T_n = -\alpha * T_n,$$

where $\alpha > 1$. This simple model of the dynamics allows the effect of the controller to be understood theoretically. Mr. Pavan Cheruvu and Dr. Joshua Socolar [98] developed a closed form expression for the stability boundary of this simple system.

Unfortunately, this controller assumes that a stimulus always elicits an immediate activation. In addition, because the controller only shortens inter-activation intervals it will tend to generate shorter and shorter pacing intervals. In fact, this shortening bias would lead eventually to the controller 'latching-up' at the fastest pacing rate it can assuming any amount of noise in the detection process. One solution to this problem is to require the controller to turn off occasionally and let the system evolve naturally [98]. This requirement is met by preventing the controller from pacing the tissue two times in a row, so at least every other time the system evolves according to equation (6.1).

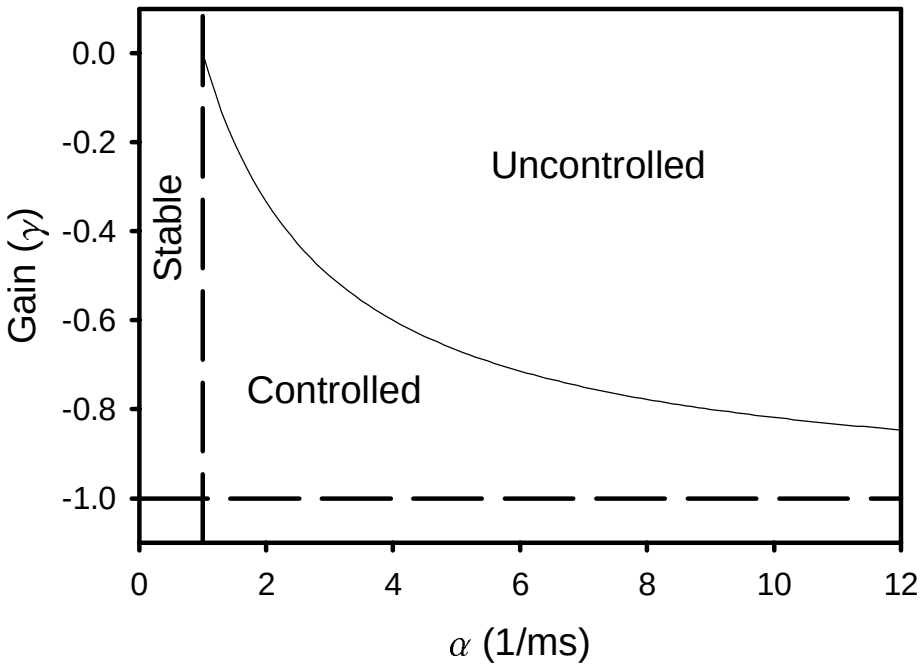

Figure 6.14: Domain of control for the projective TDAS algorithm. The stability of the system is represented by the α and the gain by γ. To the right of the vertical dashed line the system is unstable, however, under the solid line the control algorithm is able to stabilize the dynamics of the simple system.

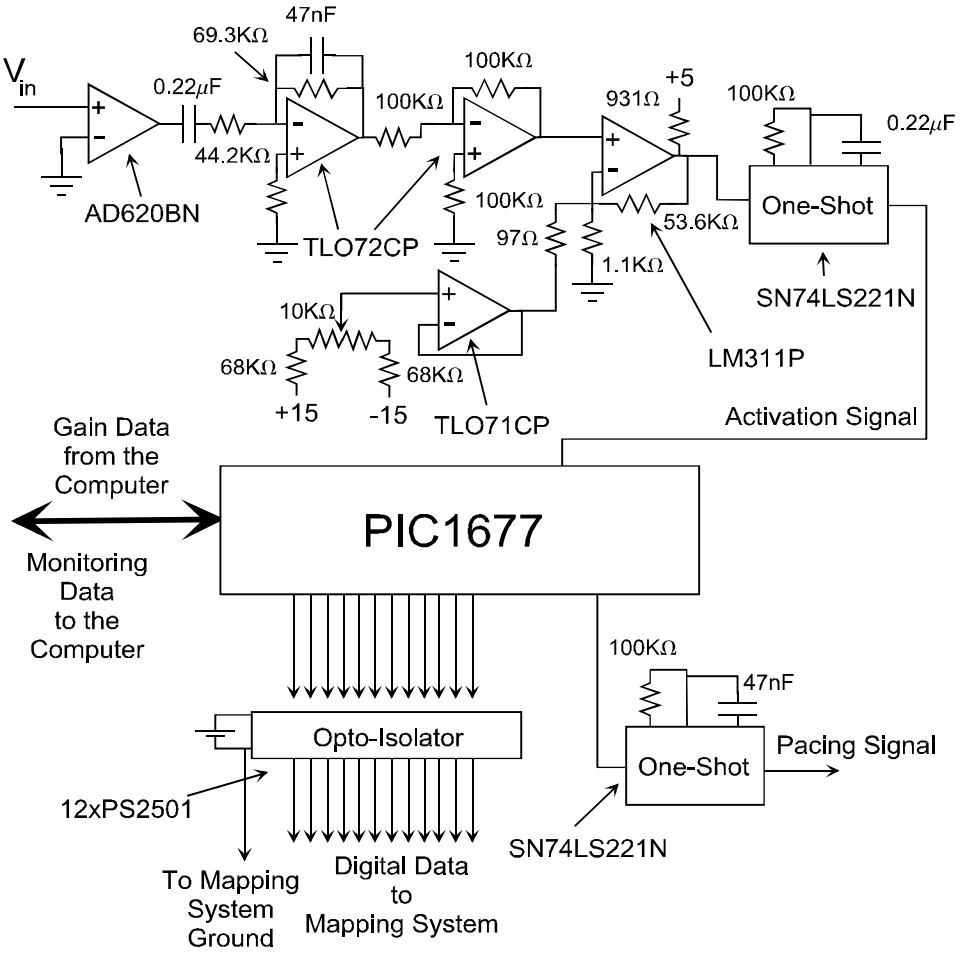

Figure 6.15: A schematic of the PIC1677 based Projective TDAS controller. The signal from one of the electrode on the surface of the atria is differentiated. A negative threshold detector is employed to detect activations. A threshold crossing causes a pulse to be sent to the microcontroller. This microcontroller in software implements the PTDAS algorithm and output diagnostic data the a computer as well as sending a pulse to a constant current source to cause an activation.

The PTDAS scheme is implemented using an analog circuit to detect activations and a microcontroller to calculate the timing of the control pulse. A schematic of the control circuit is shown in Fig. 6.15. The voltage from a single electrode is band passed filtered. The lower 'knee' of the filter is set at approximately 20 Hz so that the filter acts as a differentiator at low frequencies. The upper 'knee' of the filter is set at 50 Hz to help attenuate 60 Hz noise. The filtered signal is compared to a manually set threshold. A threshold crossing causes a pulse to be sent to the microcontroller.

A PIC1677 microcontroller from MicroChip generates the pulses to pace the atria based on the algorithm in (6.3). A simple flow chart of the microcontroller code is shown in Fig. 6.16. The time between activations is calculated with a timer built into the microcontroller. This time is stored on a stack for use in calculating the timing of the output pulse. The gain for the control algorithm is supplied by a personal computer. The microcontroller generates a control pulse that is sent to the constant current source to pace the tissue. The actual PIC1677 assembly code can be found in Appendix F.

6.6 Results

The results of experiments attempting to control sheep atria fibrillation (or flutter) *in vivo* with PTDAS have been inconclusive. The controller is designed to stabilize some period-1 behavior. The best possible outcome would be that the controller would cause the entire atria to start producing perfectly periodic behavior. Another possible outcome is that the controller would locally force the dynamics of the atria to regularize at a small localized region in a neighborhood of the stimulus and sensing electrode. Neither outcome was observed.

Figure 6.17 and Fig. 6.18 illustrate the type of dynamics I observed. In each

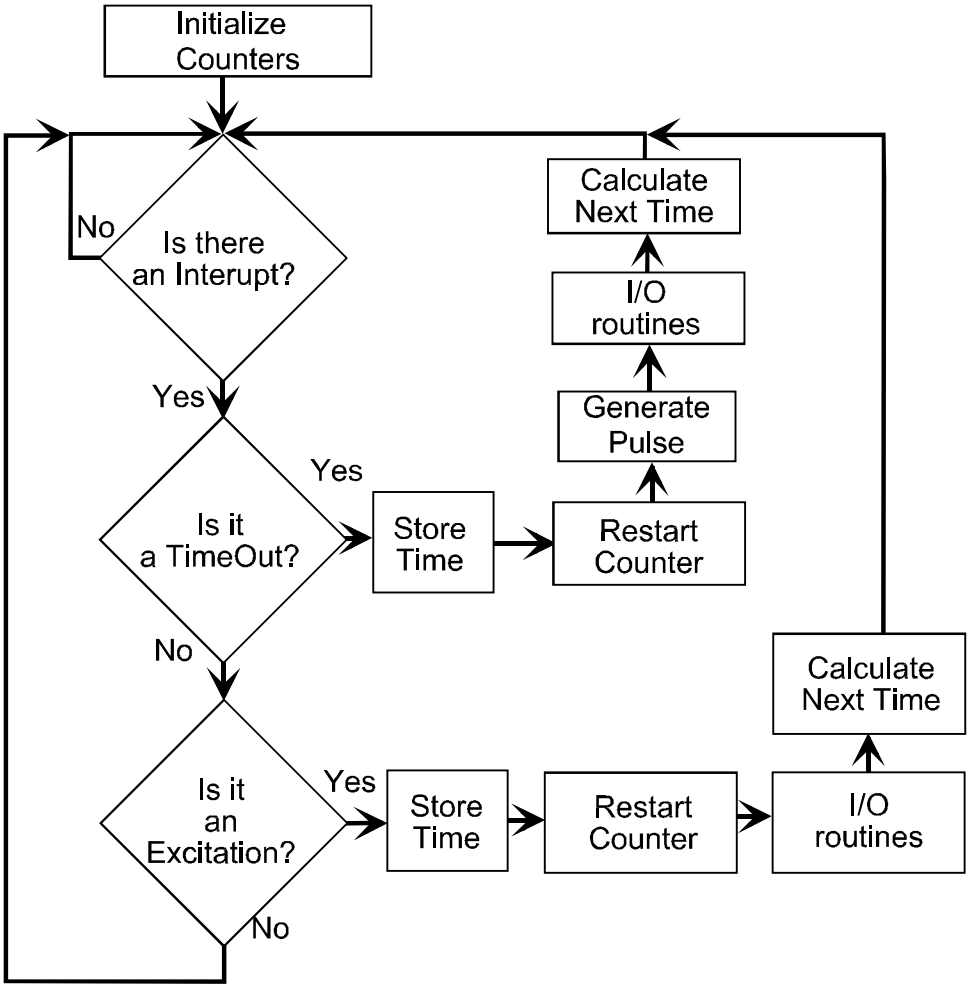

Figure 6.16: A flowchart of the PTDAS implimentation by the microcontroller. An activation or a timer over flow causes an interupt. The type of interupt is determined. If it is an activation the next control time is computed. If it is a timer overflow the tissue is paced an then the next control time is computed.

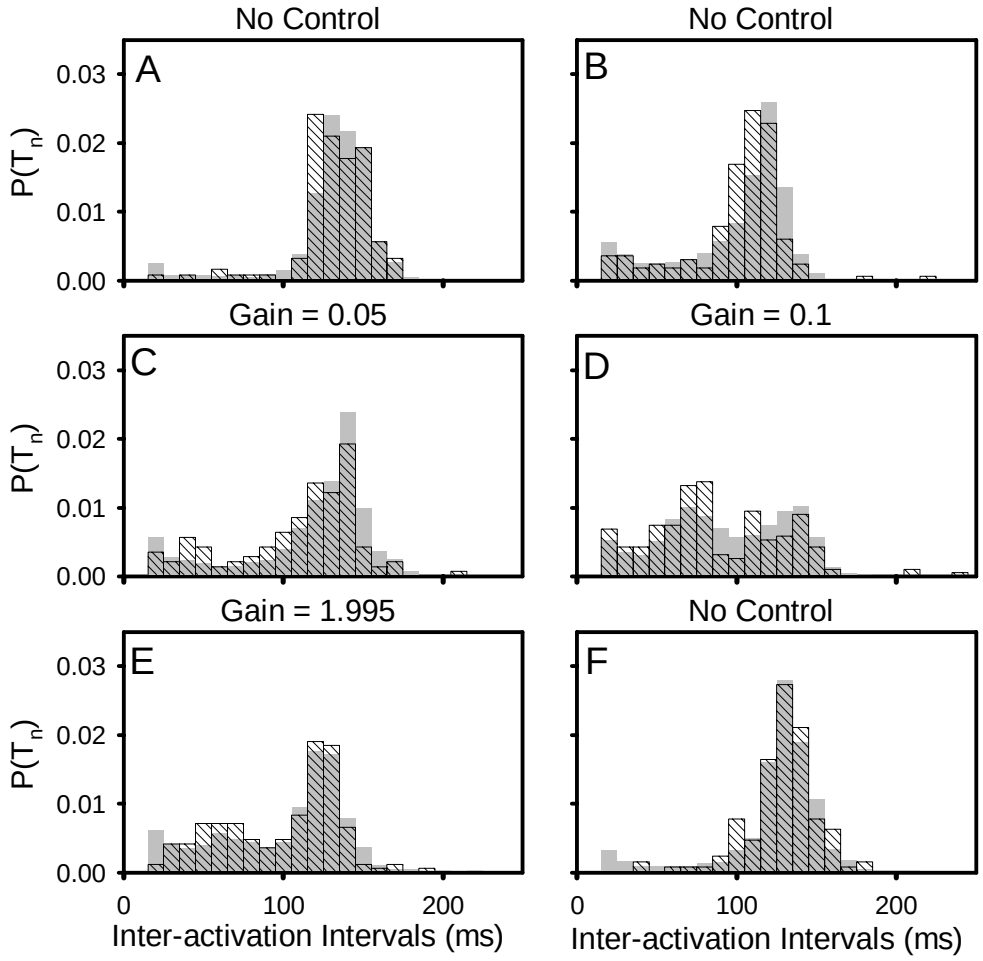

Figure 6.17: Histograms from positive gain PTDAS control experiments on fibrillating sheep atria *in vivo*. The grey bars are from the middle 100 electrode from the plaque. The striped regions are from the electrode the controller uses to observe the dynamics and a neighboring electrode.

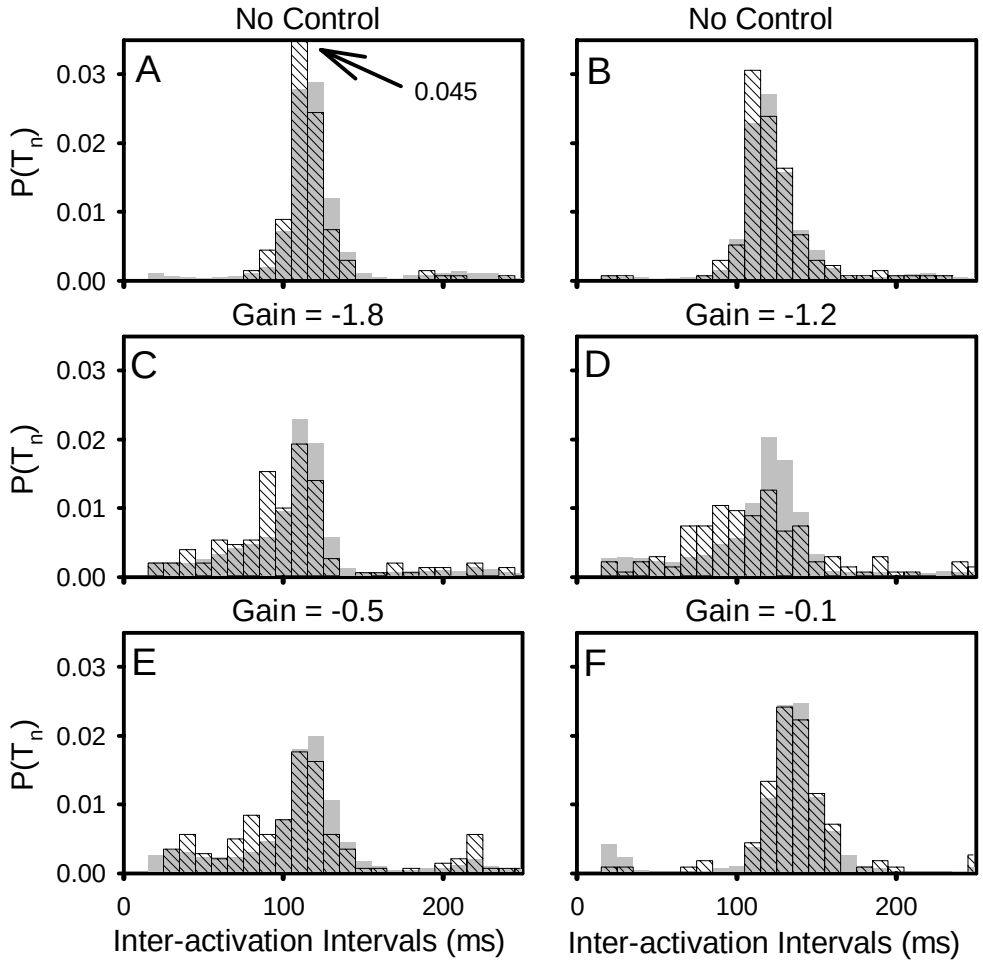

Figure 6.18: Histograms from negative gain PTDAS control experiments on fibrillating sheep atria *in vivo*. The grey bars are from the middle 100 electrode from the plaque. The striped regions are from the electrode the controller uses to observe the dynamics and a neighboring electrode.

figure are six panels showing a set of histograms (normalized to unit area) for a set of PTDAS experiments with several different gains. These experiments cover both positive (Fig. 6.17) and negative (Fig. 6.18) gains values. The grey bars in each histogram are for 100 electrodes from the center of the plaque. The diagonal stripped lines are from the controller's observation electrode and one neighboring electrode, both are very near the center of the plaque. In all panels from both figures except Fig. 6.17D, I observe that regardless of the gain the histograms for the observation electrode mirror the dynamics seen in the broader 100 point measure of atrial activity. In addition, it seems that for all gains except γ=-0.1 (Fig. 6.18F) control increases the observed variation observed in the inter-activation interval activations. Figure 6.18F is interesting because only its distribution is shifted towards longer inter-activation intervals when compared with the no control case. It is unclear why this happened.

6.7 Discussion

There are several possible reasons why this controller seems to be ineffective. Implicitly I have assumed that the atria are two dimensional sheets of muscle tissue. However, the structure of the atria is complicated by the existence of pectinate muscles on the endocardium (inside wall of the atria). These large cable like structures are excitable and could provide a path for reentry. This might also explain why my results differ from those of Ditto *et al.* [23], because their experiments were conducted on the interior surface of the right atrium. In addition, the lack of success in this experiment may be a result of the fact that the range of gains explored was not exhaustive and it is possible that the domain of control is very narrow. In addition, because the pacing and recording sites were slightly different (3.6 mm) it could be the control pulses were mis-timed. The most likely explanation of the apparent

failure of control is that the algorithm implicitly assumes that every pacing pulse elicits an activation.

Figure 6.19 illustrates that not every pacing pulse elicits an activation. The time series shown in Fig. 6.19a was taken from an electrode neighboring the pacing electrode. The stimulus at ~170 ms into the time series does not cause an activation of the tissue under this electrode. The derivative signal Fig. 6.19b shows that there is no threshold crossing for more than 20 ms after the stimulus. A possible explanation for why some paces are ignored is that the stimulus occurs while the tissue is still refractory from the last action potential. If this explanation is true then the control algorithm would have to be modified to account for this effect.

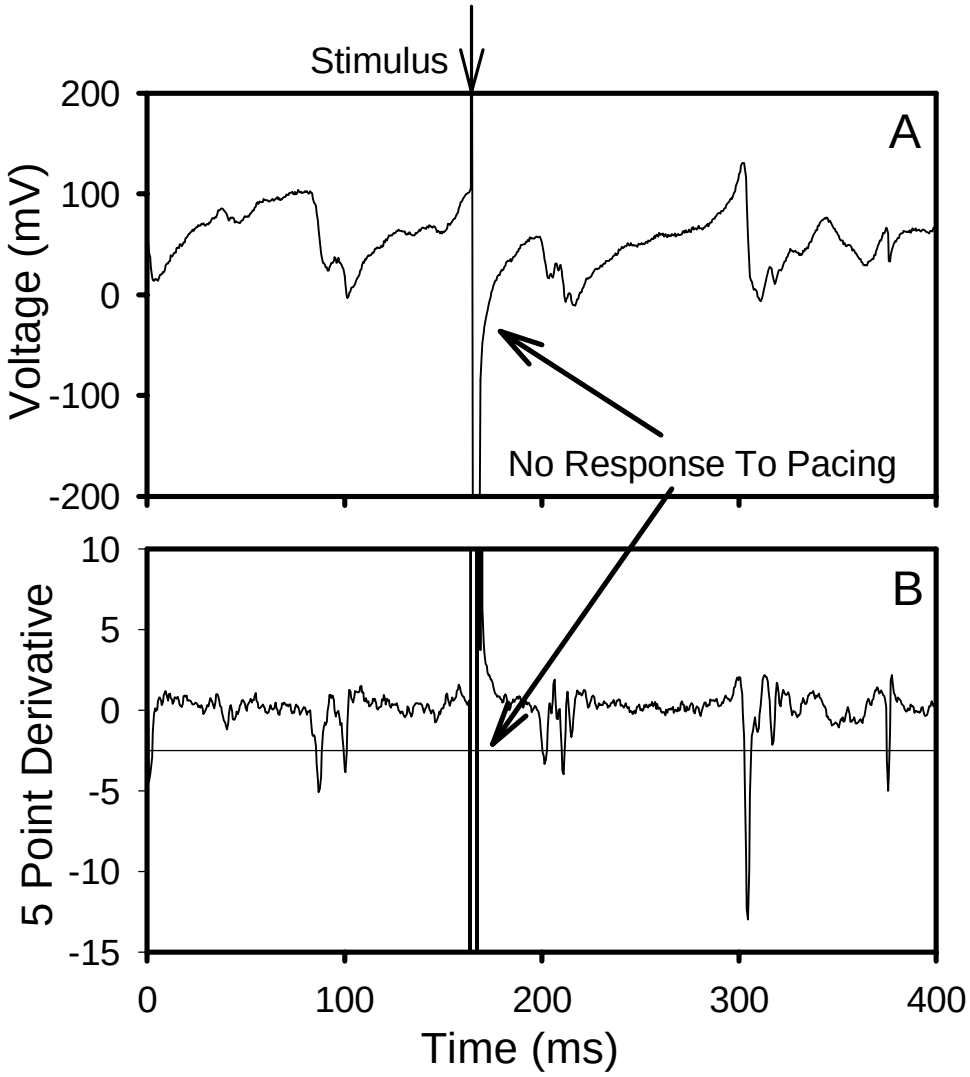

Figure 6.19: A time series showing that some pacing pulses are ignored by the tissue. The stimulus is marked with an arrow. The time series from the control observation electrode (A) does not show any active response to the stimulus. This can also be seen in the derivative signal (B).

Chapter 7

Conclusion

Many times a system's performance is degraded by the occurrence of complex behavior. In the case of cardiac tissue, since the presence of complex behavior either degrades the heart's performance or indicates disease, it is valuable from a fundamental as well as a clinical standpoint to investigate both the behaviors that contribute to the complex dynamics and how to control them.

In the main part of this dissertation, I use small pieces of periodically paced cardiac tissue as a test bed to study the behavior of local muscle tissue and demonstrate how to control the observed dynamics. Using small pieces of cardiac tissue allows the study of muscle dynamics exclusively without the complications of spatially complex dynamics or internal cells that stimulate the tissue. This work on small pieces of tissue has implications for controlling the whole heart, since the initiation of complex spatio-temporal dynamics is believed to originate with local tissue instabilities [24].

In Chapter 3, I investigated *in vitro* the response of small pieces of bullfrog (*Rana catesbeiana*) cardiac muscle to periodic electrical stimulation to determine the prevalence of different rate-dependent behaviors. I concentrate on rate-dependent behaviors in cardiac muscle because of the wide range of excitation rates that occur in both healthy and pathological cardiac tissue (See Table A.6). I observe that alternans occurs in 41% of frog ventricles and bistability occurs in 75% of frogs ventricles. In addition, I observe that while the pacing periods where the bifurcations between behaviors and the duration of action potentials depend sensitively on animal-to-animal and run-to-run variations, the types of dynamics do not. This

information is important because control protocols need to be designed to deal with commonly encountered behaviors.

The conventional wisdom is that spatio-temporal complexity is initiated via a local tissue bifurcation to alternans [19, 24, 63]. This alternating state is believed to cause a spatial variation in the excitability of the cardiac muscle tissue which in turn causes the wave of excitation to break up into fibrillation. Therefore, in Chapter 4, I investigate the control of alternans with a closed loop controller.

I use the Time Delay Autosynchronization (TDAS) protocol, which does not require that the desired state to be stabilized be known *a priori*. Instead, TDAS compares the current state of the system to a past state, in effect using the past state as a surrogate for the reference state. In addition, I demonstrate control using a version of TDAS restricted to only allow a shortening of paces.

I have observed during experiments with collaborators in Biomedical Engineering a correlation between the edges of windows of bistability and the genesis of spatially complex waves in sheep atria *in vivo*, [65]. In addition, I have found in my experimental investigations that small pieces of cardiac muscle display bistability much more often than alternans. The observation of the prevalence of bistability along with the observation that the occurrence of complex spatio-temporal behavior is correlated with windows of bistability suggest that perhaps local transitions between bistable states in muscle tissue dynamics are the cause of spatial complexity.

In Chapter 5, I explore modulation of the cardiac muscle dynamics during bistability by injecting extra stimuli into the periodic pulse train. Experimentally I find it is possible to induce transitions between bistable states. I find injecting a stimulus into the periodic pulse train can cause transitions in both from 1:1 to 2:1 dynamics and from 2:1 to 1:1 dynamics. In addition, I also observe that there are multiple types of transitions. This modulation is different from control; it causes transitions

between two stable states; it does not stabilize unstable steady states. I observe that during 2:1 behavior it is possible to initiate a new action potential indicating that there is a window of excitability. Surprisingly, I also find during 1:1 dynamics that it is possible to modify the dynamics of the tissue even if it is in the refractory period.

In the last part of this dissertation I discuss a preliminary study of control of spatio-temporal disorganization *in vivo*. This study, using fibrillating sheep atria and a multi-channel mapping system, allows the observation of the spatial dynamics during control experiments. The nonlinear dynamics community hypothesizes that feedback methods designed for controlling complex *temporal* dynamics using small perturbations can be used to control complex spatio-temporal dynamics [23, 46, 8, 47]. I attempted to verify early promising results in controlling spatio-temporal complexity with simple feedback controllers. While I was unable to demonstrate conclusive control over any region, at least one or two data sets indicated that the controller had some effect. This area of research is exciting both because of it possible application to general problems of controlling spatio-temporal complex dynamics and because of the impact this work could have on many peoples lives.

My contribution to the goal of controlling complex spatio-temporal dynamics in cardiac muscle tissue is in developing an understanding of how to control local tissue behaviors observed in cardiac muscle tissue, and attempting to make an initial connection to controlling spatially extended complex behavior. To accomplish this goal I explore an animal model test-bed for analyzing local electro-dynamics using cardiac muscle consisting of small pieces of periodically stimulated bullfrog (*Rana catesbeiana*) cardiac muscle. Because the breakup of relatively simple dynamics into full spatio-temporal complexity has been related to local tissue instabilities to rapid stimulation [24, 25, 26, 27], I use rapid periodic pacing to approximate conditions

experienced *in vivo*. An experiment *in vivo* on sheep hearts is presented to explore a simple adaptation of small tissue control procedures to spatially extended cardiac tissue.

7.1 Future Directions

In pursuit of the goal of controlling spatio-temporal complexity, I believe that it is crucial to develop a quantitative understanding of how control stimuli interact with cardiac muscle during activation. I am especially interested in the situation where the stimulus is applied during the tissue's refractory period since pulses applied during this interval seem to have an significant effect on the subsequent tissue dynamics [43]. In addition, there have been several indications in this dissertation that pacing cardiac muscle during an action potential affects the dynamics of the tissue.

It is important to continue to study small pieces of cardiac muscle to understand how stimuli interact with cardiac muscle during activation. Experimental observations need to be compared quantitatively to ionic-based cardiac mathematical models in order to extend theoretical understanding of real tissue. An analysis of ionic-based model will in turn allow us to determine the bifurcation structure of the tissue and predict the behavior better than the simple mapping models used in Chapters 2 and 3 and will guide the development of robust control methods for stabilizing the various dynamical states.

In addition, I believe that it is important to refine and expand the experiments on whole sheep atria. One possible avenue is to modify the PTDAS algorithm to account for the possibility of skipped paces. An alternative approach is to attempt proportional control where the reference state is calculated from an average of past inter-beat intervals. It may also be necessary to observe the action potential dura-

tion and not just the activations for a controller to be effective. This suggests that new measurement techniques, such as voltage sensitive dyes, should be pursued.

Appendix A

Quick Reference

The purpose of this appendix is to provide a location where all relavent numbers could be quickly accessed.

Physical Properties	**Value**	**Reference**
Membrane thickness:	Approx. 7.5 nm	[49] p 33
Hydrophobic Lipid		
Layer Thickness:	Approx. 3.0 nm	[49] p 34
Cell Size (Frog Ventrical):	131μm (length)$\times$17.5μm(radius)	[49] p 209
Cell Size (Frog Atria):	0.0025nl	[51]
Cell Size (Human Ventrical):	100μm$\times$15μm (radius)	[49] p 207
Cell Size (Guinea Pig):	100μm (length)$\times$11μm(radius)	[90]
Cell Size (Frog Pacemaker):	200μm (length)$\times$5μm(radius)	[52]

Table A.1: Physical Membrane Properties

Electrical Properties	**Value**	**Reference**
Resting Potential (Frog Ventrical):	-62 mV	[54] p 224
Membrane Resistance (Frog Atria):	250 MΩ	[51]
Membrane Capacitance (Frog Atria):	100 pF	[51]
Membrane Capacitance (Guinea Pig):	1 μF/cm^2	[90]
Typical Capacitance of membrane	0.9 μF/cm^2	[49] p 35

Table A.2: Electrical Membrane Properties

Reactions	**Potential** (25°C)	**Temp. Coeff.**	**Reference**
$Ag = Ag^+ + e^-$	+0.7991 V	-0.129 mV/°C	[54] p 6
$Ag + Cl^- = AgCl + e^-$	+0.2225 V	+0.213 mV/°C	[54] p 6
$Fe = Fe^{2+} + 2e^-$	-0.4402 V	+0.923 mV/°C	[54] p 6

Table A.3: Electrode Half-Cells Potentials

Metal	Δ Potential	Reference
Stainless Steel	10 mV	[54] p 7
Silver (Ag)	94 mV	[54] p 7
Silver/Silver Chloride (Ag/AgCl)	2.5 mV	[54] p 7

Table A.4: Fluctuation in Potential between Electrodes in Saline

Solution	Resistance	Reference
0.9% Saline	70 Ω-cm	[54] p 54
Internal Resistance (Guinea Pig):	200 Ω-cm	[90]
Frog Ventricle Internal Resistance	$R_i = 588\ \Omega$	[49] p 209

Table A.5: Solution Resistances

Name	Rates	Reference
Normal Sinus Rythim (Human):	60 bpm $<$ X	[91] p 3
Atrial Fibrillation (Human):	350 bpm $<$ X $<$ 600 bpm	[91] p 35
Atrial Flutter (Human):	250 bpm $<$ X $<$ 350 bpm	[91] p 41

Table A.6: Rates of selected dynamics

Name	Value	Reference
Frog Ventricle Length Scale (passive)	$\lambda = 0.328$ mm	[49] p 209
Frog Ventricle Time Scale (passive)	$\tau = 4.15$ ms	[49] p 209

Table A.7: Selected Length and Time Scales

Name	Value	Reference
Frog Ventricle	300-900 ms	Chapter 3

Table A.8: Action Potential Durations

Name	Value	Reference
P-R	100-200 ms	[1] p 486
QRS	60-100 ms	[1] p 486
Q-T	300-400 ms	[1] p 486

Table A.9: Human ECG Timings

Appendix B

Glossary

B.1 Nonlinear Dynamics Terms

Chaos - Highly erratic, unpredictable, noise-like temporal behavior characterized by a broad power-spectrum and extreme sensitivity to small perturbations.

Dynamical Behavior - The temporal evolution of a system.

Eigenvalue - The action of a matrix can be reduced to multiplication by a scaler in certain (eigenvector) direction. In each of these directions the scalar value that is equivalent to the action of the matrix is the eigenvalue.

Excitable Medium - An excitable media is a system that is stable to infinitesimal perturbations. However, if the system is perturbed with a stimulus greater than some small (but finite) threshold the system will display a large but transient response. During this response the system is unaffected by further stimulation.

Floquet Multiplier - The characteristic expansion or contraction rate of a linear mapping.

Forward (supercritical) Bifurcation - A bifurcation where the distance between two behaviors grows continuously as a function of the bifurcation parameter.

Length Scale - The typical length over which interesting physical effects can happen.

Nonlinear Dynamics - A field of research devoted to the study of the spatial and temporal evolution of systems whose response is governed by the nonlinear interaction among quantities (variables) that characterize their behavior.

Saddle Node Bifurcation - A bifurcation where at a specific parameter value

a pair of states, stable and unstable, appear. Below that parameter value neither solution exists.

Sensitivity to small perturbations - The long-term dynamical behavior of a system is completely different in the presence versus the absence of perturbations, no matter how small the perturbations. Our ability to predict the long-term behavior of such a system is lost because we cannot determine to sufficient accuracy the size of the perturbations (that could arise from random noise, for example).

Spatial-temporal Complexity - Nonlinear dynamical behavior that displays a loss of temporal as well as spatial correlations.

Unstable State - A dynamical state of a system that has become unstable due to changes in system parameters. The stability of the state can be determined by slightly perturbing the system. The state is stable if the system decays back to the state; it is unstable if the perturbations grow.

B.2 Cardiac Terms

Action Potential - The typical response to stimulation of excitable tissue, where the transmembrane potential initially in a negatively polarized state transiently become positively polarized.

Action Potential Duration (APD)- The temporal extent of an Action Potential.

Alternans (2:2) - A behavior where the tissue responds in an alternating fashion to stimulation.

Atria - The smaller pair of chambers in a four chambered heart such as in humans. Its purpose is to provide an input pressurization stage to the ventricle.

Auricles - A muscular region of the veins just outside of the single ventricle in a frog that serves the same purpose as an Atria in larger hearts.

Arrhythmia - Any abnormal heart rhythm.

Defibrillation - Restoring the normal rhythm of a fibrillating heart, for example, by delivering a strong electric shock.

Diastolic Interval (DI)- The period of time between the end of one Action Potential and the beginning of the next.

Ectopic Pacemakers - Sites in cardiac tissue other than the sinus node (normal pacemaker) that periodically stimulate the heart.

Extracellular Measurement- A measurement made exclusively outside of the cell referenced against a distant ground.

Fibrillation - The erratic and disorganized contraction of cardiac muscle, which can effect the atria or ventricle

Intracellular Measurement- A measurement across the cell wall.

Pacemaking Cells - Cells whose voltage oscillates and periodically stimulates the heart, usually in the sinus node.

Refractory Period - A time during which cardiac tissue apparently is unaffected by stimulation. This periods follows activation of the tissue.

Transmembrane Current - The current passing through the membrane of a cardiac cell.

Ventricles - The main pumping chambers of the heart.

B.3 Control Terms

Domain of Control - A region of gains where a controller will be successful for a given set of parameters.

Proportional Feedback - A control scheme whose feedback "strength" is proportional to the difference between some measured variable of the system and a

reference variable.

Restricted Time Delay AutoSynchronization (RTDAS) - A TDAS variant restricted to only negative valued feedback signals.

Time Delay AutoSynchronization (TDAS) - A control scheme that attempts to synchronize the current state of the system with its past states.

B.4 Experimental Terms

Extracellular Stimulation - Exciting cardiac tissue by delivering electrical current through electrodes located outside cardiac cells, that is, in the extracellular space.

Interbeat Interval - The duration between two consecutive action potentials in excitable media.

Mapping System - A system that is capable of measuring simultaneously the electrical activity of the heart at many locations, storing the information, processing it, and displaying it in a useful manner.

Microelectrode - A glass pipette that disrupts the cellular membrane to establish a salt bridge with the intracellular fluid.

Mono-Phasic Action Potential Electrodes (MAP) - One of several extracellular electrode configurations that measures an action potential as a positive deflection in voltage, similar to a transmembrane voltage measurement.

Stimulation Threshold - The minimum level of electrical stimulus delivered to the heart that results in excitation.

Appendix C

Membrane theory

The purpose of this chapter is to explore the underlying physics of excitable membranes and develop a useful model for predicting membrane dynamics. The physics of membranes can be understood through cable theory, which describes the membrane wall with nonlinear conductance and passive capacitive response. The cable theory analysis gives a length and time scale that sets the minimum scales over which any interesting dynamics can take place. I also present a heuristic estimate based on the bullfrog experiment of a dynamic length scale.

C.1 Core Conductor

Cardiac tissue is visualized as a cylindrical resistive core conductor in a resistive medium. The inside and the outside of the conductor is separated by a membrane with a nonlinear conductance per length (g_m) and capacitance per length (c_m). The following quantities are defined for the conductor, medium,

$$\begin{array}{lcl} I_i & \equiv & \text{interior current (A)} \\ I_e & \equiv & \text{exterior current (A)} \\ \Phi_i & \equiv & \text{interior potential (V)} \\ \Phi_e & \equiv & \text{exterior potential (V)} \\ r_i & \equiv & \text{interior resistance } (\Omega/\text{cm}) \\ r_e & \equiv & \text{exterior resistance } (\Omega/\text{cm}) \end{array}$$

The currents across the membrane per unit length are defined as,

$i_m \equiv$ membrane current (A/cm)	$i_p \equiv$ pacing current (A/cm).

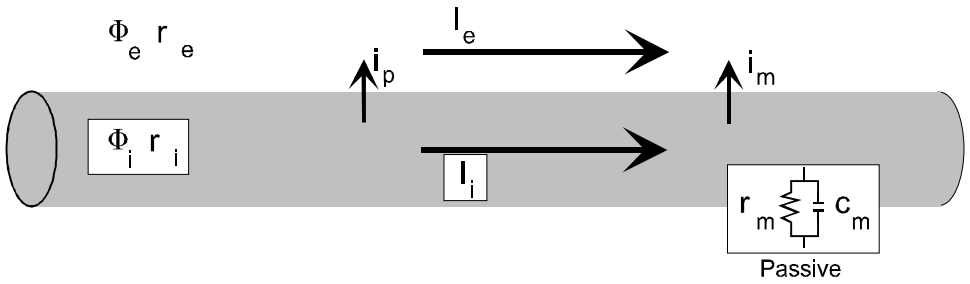

Figure C.1: A drawing of a core conductor along with the relevant the voltages and currents.

Using Ohm's Law to show how the voltage varies as current flows through a resistive media gives,

$$\begin{aligned} \frac{d\Phi_e}{dx} &= -\mathrm{I}_e \mathrm{r}_e \\ \frac{d\Phi_i}{dx} &= -\mathrm{I}_i \mathrm{r}_i. \end{aligned}$$

Kichoff's current laws insures current is conserved and gives,

$$\begin{aligned} \frac{d\mathrm{I}_e}{dx} &= \mathrm{i}_m + \mathrm{i}_p \\ \frac{d\mathrm{I}_i}{dx} &= -\mathrm{i}_m. \end{aligned}$$

Notice that the pacing current i_p is injected from outside this system and so it is not conserved. Let,

$$\begin{aligned} \mathrm{I} &= \mathrm{I}_i + \mathrm{I}_e \equiv \text{Total Current} \\ \mathrm{V_m} &= \Phi_i - \Phi_e \equiv \text{Transmembrane Membrane Voltage,} \end{aligned}$$

or

$$\begin{aligned} \mathrm{I}_e &= \mathrm{I} - \mathrm{I}_i \\ \Phi_i &= \mathrm{V_m} + \Phi_e. \end{aligned}$$

Using these definitions gives,

$$\begin{aligned}
\frac{d\Phi_e}{dx} &= -(\mathrm{I}_i - \mathrm{I})\mathrm{r}_e \\
\frac{d\mathrm{V}_m}{dx} &= -\mathrm{I}_i\mathrm{r}_i - \frac{d\Phi_e}{dx} \\
\frac{d\mathrm{I}}{dx} &= \mathrm{i}_p \\
\frac{d\mathrm{I}_i}{dx} &= -\mathrm{i}_m.
\end{aligned}$$

Differentiating gives,

$$\begin{aligned}
\frac{d^2\Phi_e}{dx^2} &= (\frac{d\mathrm{I}_i}{dx} - \frac{d\mathrm{I}}{dx})\mathrm{r}_e = -(\mathrm{i}_m + \mathrm{i}_p)\mathrm{r}_e \\
\frac{d^2\mathrm{V}_m}{dx^2} &= -\frac{d\mathrm{I}_i}{dx}(\mathrm{r}_e + \mathrm{r}_i) + \frac{d\mathrm{I}}{dx}\mathrm{r}_e = \mathrm{i}_m(\mathrm{r}_e + \mathrm{r}_i) + \mathrm{i}_p\mathrm{r}_e \\
\frac{d\mathrm{I}}{dx} &= \mathrm{i}_p \\
\frac{d\mathrm{I}_i}{dx} &= -\mathrm{i}_m.
\end{aligned}$$

This set of equations describe the core conductor. All that is needed is a description of how the membrane current i_m varies with voltage. This is were the complex ionic models are needed.

C.2 Length and Time Scales

C.2.1 Passive Length and Time Scales

To use the core conductor model to find a time and length scales assume that the tissue only reacts passively with properties,

$\mathrm{r}_m \equiv$membrane resistance (Ω*cm) $\quad c_m \equiv$membrane capacitance (μF/cm),

this gives,

$$\mathrm{i}_m = \frac{d\mathrm{V}_m}{dt}c_m + \frac{\mathrm{V}_m}{\mathrm{r}_m}.$$

This implies with no pacing that,

$$\frac{d^2\mathrm{V}_m}{dx^2} = \frac{d\mathrm{V}_m}{dt} c_m(\mathrm{r}_e + \mathrm{r}_i) + \mathrm{V}_m \frac{\mathrm{r}_e + \mathrm{r}_i}{\mathrm{r}_m}.$$

Assuming the system is in steady state, i.e.

$$\frac{d\mathrm{V}_m}{dt} = 0$$

then the solution has the form,

$$\begin{aligned} \mathrm{V}_m &= Ae^{-\lambda x} \\ \frac{d^2\mathrm{V}_m}{dx^2} &= \lambda^2 Ae^{-\lambda x}. \end{aligned}$$

This gives

$$\begin{aligned} \lambda^2 Ae^{-\lambda x} &= Ae^{-\lambda x} \frac{\mathrm{r}_e + \mathrm{r}_i}{\mathrm{r}_m} \\ \lambda^2 &= \frac{\mathrm{r}_e + \mathrm{r}_i}{\mathrm{r}_m}. \end{aligned}$$

So the passive length scale of the tissue is,

$$\lambda = \sqrt{\frac{\mathrm{r}_e + \mathrm{r}_i}{\mathrm{r}_m}}.$$

If instead of assuming the membrane is in steady state, I assume that the tissue is all acting synchronously (space clamped) then the PDE becomes,

$$0 = \frac{d\mathrm{V}_m}{dt} c_m(\mathrm{r}_e + \mathrm{r}_i) + \mathrm{V}_m \frac{\mathrm{r}_e + \mathrm{r}_i}{\mathrm{r}_m},$$

and the solution has the form

$$\begin{aligned} \mathrm{V}_m &= Ae^{-x/\tau} \\ \frac{d\mathrm{V}_m}{dt} &= \frac{1}{\tau} Ae^{-x/\tau}. \end{aligned}$$

This gives

$$\begin{aligned} 0 &= \frac{1}{\tau} Ae^{-x/\tau} c_m \mathrm{r}_m + Ae^{-x/\tau} \\ \tau &= \mathrm{r}_m c_m. \end{aligned}$$

So the passive time scale of the tissue is,

$$\tau = \mathrm{r}_m c_m.$$

C.2.2 Dynamics Length and Time Scales

The core conductor model suggests the minimum length and time scales based solely on the passive electrical properties of the membrane. A dynamics length scale is the minimum size of tissue that is required for more that simple dynamics to occur. The assumption is that if the tissue is only large enough to have one wave of excitation propagate across it at any time then it acts for most purposes as a single cell.

A quick estimate of the dynamic length scale of cardiac tissue can be found by considering exactly how a periodic pacing experiment is accomplished. The bullfrog tissue in Chapter 3 is paced approximately 1 mm away from the recording electrode. Looking at the microelectrode time series Fig. 2.4 the pacing artifact is approximately 10 ms earlier than the action potential depolarization. This indicates that waves of excitation travels at approximately 0.1 m/s. The duration of a frog action potential is at least 300 ms. Therefore, the minimum size it takes for one wave of excitation to fit on a small piece of tissue is approximately 3 cm.

Appendix D

Electrodes

This appendix is intended to give some guide in the design of, use and interpretation of signals from the different electrodes used in this dissertation. In each case there is an implied return electrode in the physiological solution bathing the tissue. In addition, the size of each electrode should be compared with a typical cell size of 100 μm$\times$15 (radius) μm.

D.1 Microelectrodes

A microelectrode is one of the best devices for measuring the internal state of a cardiac muscle cell. The microelectrode provides a direct electrical connection to the internal cellular solution [54]. The theory of operation for microelectrodes is quite simple. A microelectrode consists of a pipette with a tip sharp enough (approximately 1 μm in diameter) to puncture a single cardiac cell. After being punctured, the cell membrane often closes around the tip of the microelectrode, forming a good seal. Inside the microelectrode is a salt solution that provides a conductive salt bridge between the inside of the cell and the other end of the pipette where a silver electrode is placed. Figure D.1 shows a drawing of a microelectrode.

To manufacture a microelectrode a borosilicate glass pipettes is heated and pulled until the ends are only a few microns across (0.5-3μm). There is a machine specifically built for the purpose, called a 'microelectrode puller.' I used the puller that is in Dr. Somjen in the neurobiology. The settings are 840/255/150/90. It is unclear what these values mean but they work. The pipettes I use are 1 mm in

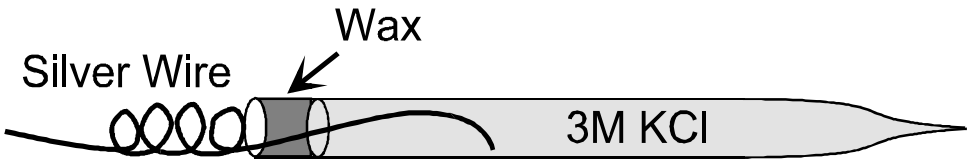

Figure D.1: A drawing of a microelectrode. A microelectrode is a glass pipette with a sharp tip (approximately 1μm in diameter). It is filled with a 3M KCl solution. The solution is contained and the silver wire is held in place by some wax placed in the end.

diameter. They can be thick-walled and thin-walled, and within these types there are 'with filament' and without. I have tried them all and have no recommendation.

The salt bridge between the tip and a silver wire is provided by the 3M KCL solution that fills the electrode. When filling a microelectrode the 3 KCL solution must go all the way to the tip. To fill a microelectrode requires a long flexible syringe sold by World Precision Instruments. If bubbles get into the tip of the electrode thumping on the side of the pipette while holding the tip down often dislodges them.

When manufactured correctly microelectrodes have a tip resistance of $\sim$ 15MΩ. This can be measured by using the Z-test feature on DAGAN 8100 amplifier. It injects a periodic train of 2 nA pulses into the microelectrode while measuring its voltage relative to a reference electrode. If the microelectrode tip is submerged in a salt bath and the reference electrode is in contact with the same bath then a periodic voltage appears across the two electrode. The height of the pulses indicate what the resistance of the microelectrode is.

Figure D.2 shows a recording of the transmembrane potential difference using a micro-electrode technique. The signal from the microelectrode and a signal from a wire in the physiological solution near the tissue were subtracted to reduce noise and amplified by the DAGAN 8100 10$\times$ differential amplifier. The signal was then

digitized at 2 KHz.

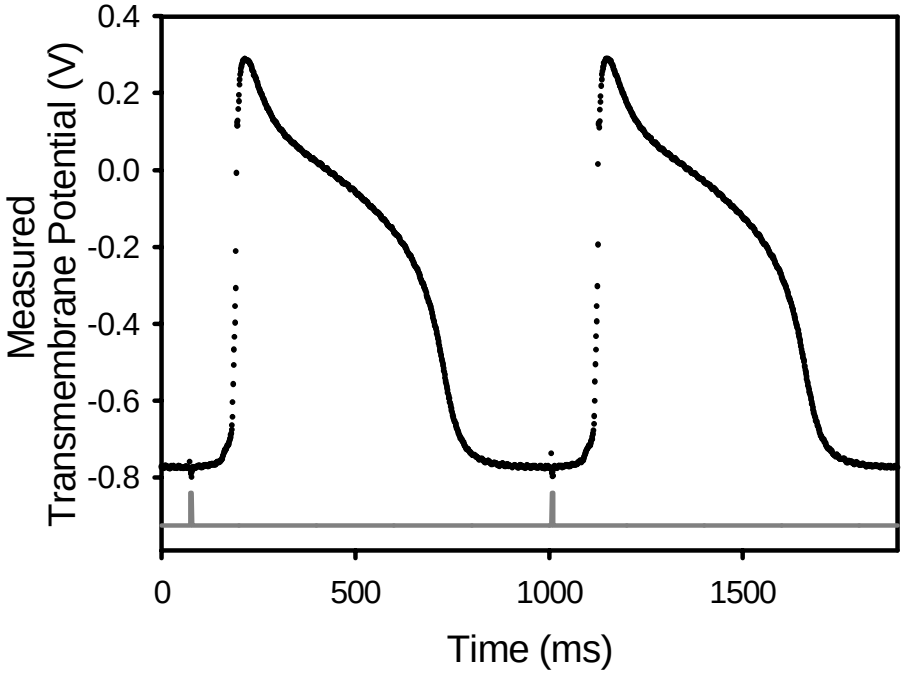

Figure D.2: Microelectrode signal. This signal is from a small peice of periodically paced bullfrog ventricle muscle that was pinned down. The pacing signal is shown at the bottom of the figure. The pacing period was 950 ms. The signal was amplified by a factor of ten by the differential amplifier and then digitized with 12-bit resolution over 2 to -2 volts range at 2000 samples/sec.

This operation sounds simple, but in practice it is not. Cardiac tissue is intended to pump blood and the displacements that individual cells experience during a contraction can be orders of magnitude larger than the approximately 1 μm tip of the micro-electrode. This results in the electrode pulling out of the cell or breaking off in the cell. Not all transmembrane measurements are as good as Fig. D.2. A relatively typical but non-ideal signal from a micro-electrode of a train of action potentials is shown in Fig. D.3.

There are several techniques that can be used to minimize the motion of the tis-

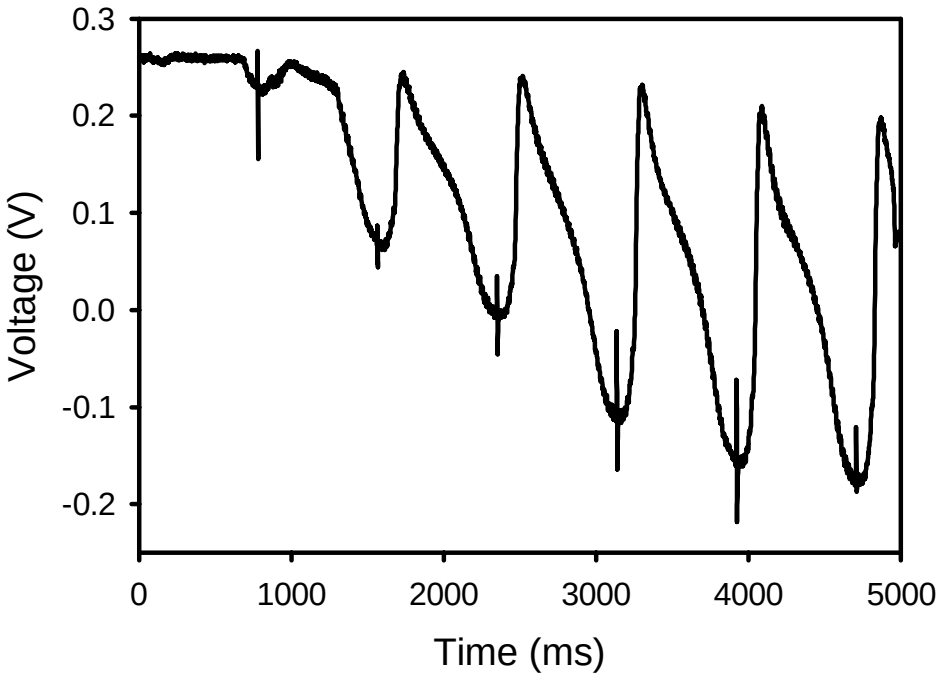

Figure D.3: An unstable microelectrode. The microelectrode is entering the cell. Notice that the size of the observed action potential varies. In addition the baseline of the signal changes as a microelectrode enters of leaves the cell.

sue or its effects on the micro-electrodes. A pharmacological agent, 2,3-Butanedione Monoxime (DAM), can be used to suppress contractions. I have used this agent with some success, however, it does not totally suppress contractions. In addition, Riccio *et al.* [89] have shown that the DAM alters the dynamics of the heart muscle, however, I have not ever observed any effects. Physical restraint of small pieces of tissue is also successful in allowing good micro-electrode recordings. Also a floating electrode technique where the micro-electrode is mounted so that it is free to move with the tissue is somewhat effective. I use this technique here with the wire acting as a spring.

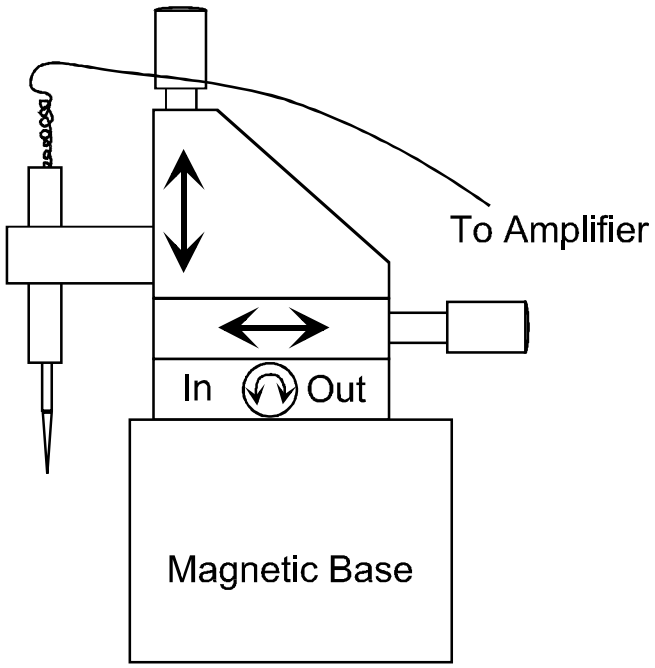

Figure D.4: A drawing of the microelectrode mount. The microelectrode is held in place by the tension in the silver wire. It is kept vertical by a large tube that allows free vertical movement.

D.2 Extracellular Electrodes

Extracellular electrodes consisting of 30 awg silver wire were implanted in the tissue, two for pacing and one for recording. The AP were recorded from the single recording electrode by a differential amplifier with one lead submerged in the physiological solution for noise cancellation reasons. The two tungsten wire electrodes are placed on the surface of the tissue with enough pressure to make contact but not enough pressure to damage the tissue.

It is much more difficult to obtain anything but timing information from this extracellular signal. In Fig. D.5 it is clear how to find the initiation and completion of the action potential. However this is not always true, if the downward sloping portion of the transmembrane signal were inflected more gently then the extracel-

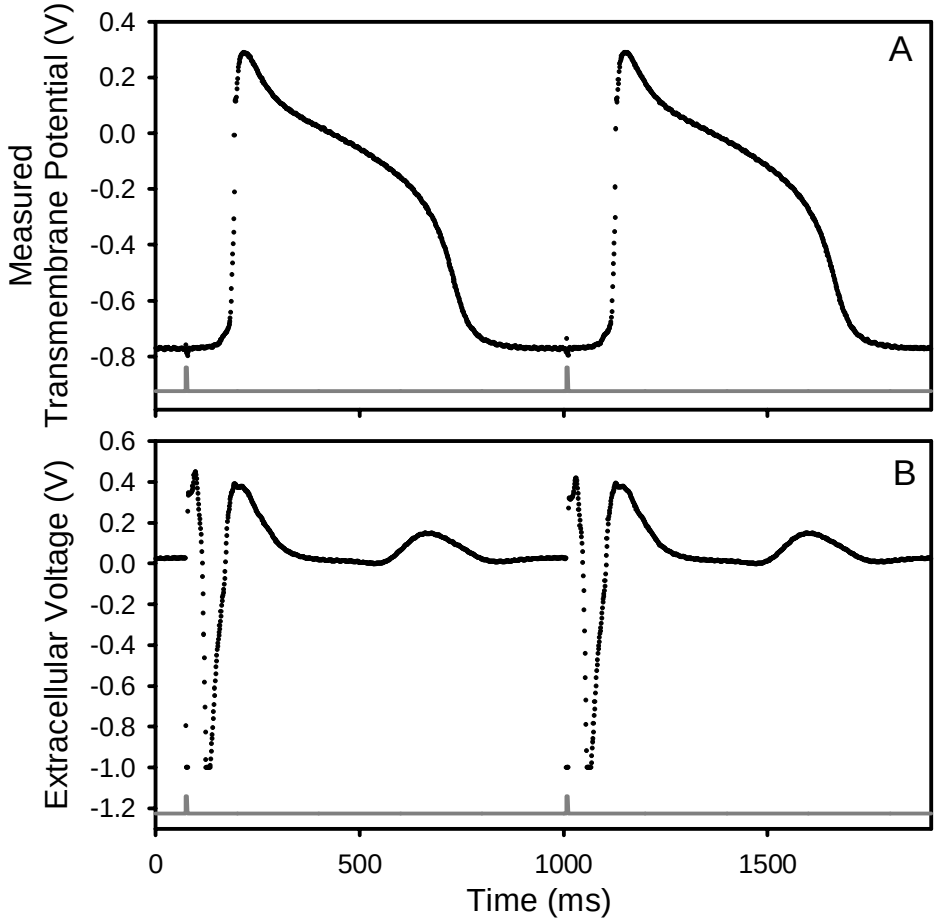

Figure D.5: Comparison between an transmembrane signal (A) and a extracellular signal (B).

lular signal for that portion of the signal would get lost in the noise. This is true for mammalian hearts like sheep and humans. Despite this problem this is the most practical means of measuring bio-electric events because it is minimally invasive and large arrays of those are readily available for use.

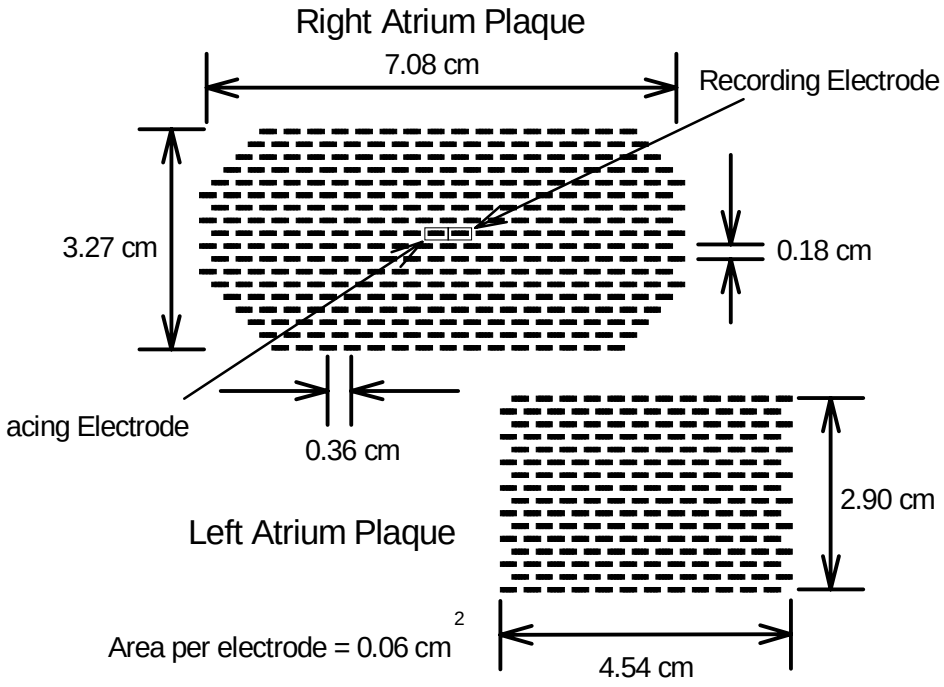

Figure D.6: A diagram of the electrode layout of the plaque electrode. The plaque electrode consists of two pieces. One piece is attached to the left atria and the other to the right atria. The individual silver electrodes are set in a staggered pattern that is equivalent to a square lattice with side spacing of 40 mm rotated by 45°.

D.3 MAP Electrodes

While the microelectrode gives a more accurate reproduction of the transmembrane signal, it is more sensitive to muscle movement than the suction MAP electrode.

There are two basic types of MAP electrodes: pressure and suction. Schematics of each are shown in Fig. D.7. The pressure MAP electrode damages the tissue by poking it. The particular type drawn here is a catheter that is inserted into the heart via an artery. The suction MAP electrode has two concentric hollow electrodes separated by an insulator. The suction is applied to the inner electrode

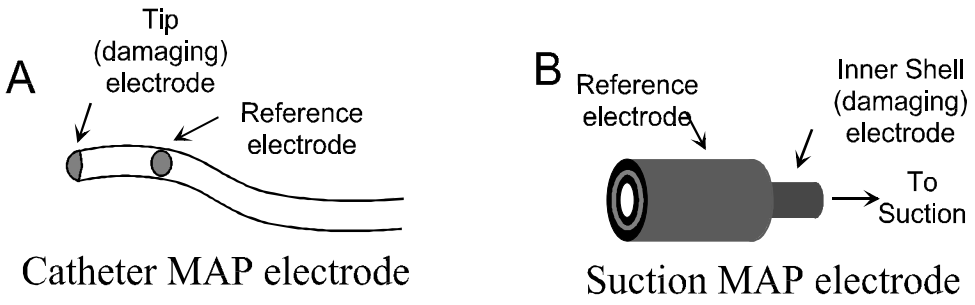

Figure D.7: MAP electrode. The catherter MAP electrode (A) is used to measure on the inside (endocardium) of the heart. The tip presses on the tissue to damage it and a differential measurement is made verses the reference elctrode on its side. The suction MAP electrode (B) is used to measure signals from the outside surface of the tissue (epicardium). The suction throught the inner electrode damages the tissue and the outer one is the reference.

and the differential measurement is made between them.

MAP electrodes have several useful properties. In most situations signals they measure are stable to tissue movement. Therefore, they can be used on both *in vivo* and the transmembrane measurements. It is possible to observe both the initiation and repolarization of the tissue. Unfortunately, MAP electrodes also have some drawbacks. By definition they damage the tissue. This is problematic for human use and could be detrimental in situations where this could form a physical block for excitation waves. The signals are not always available; variations in the surface of the heart may prevent acquisition of a signal.

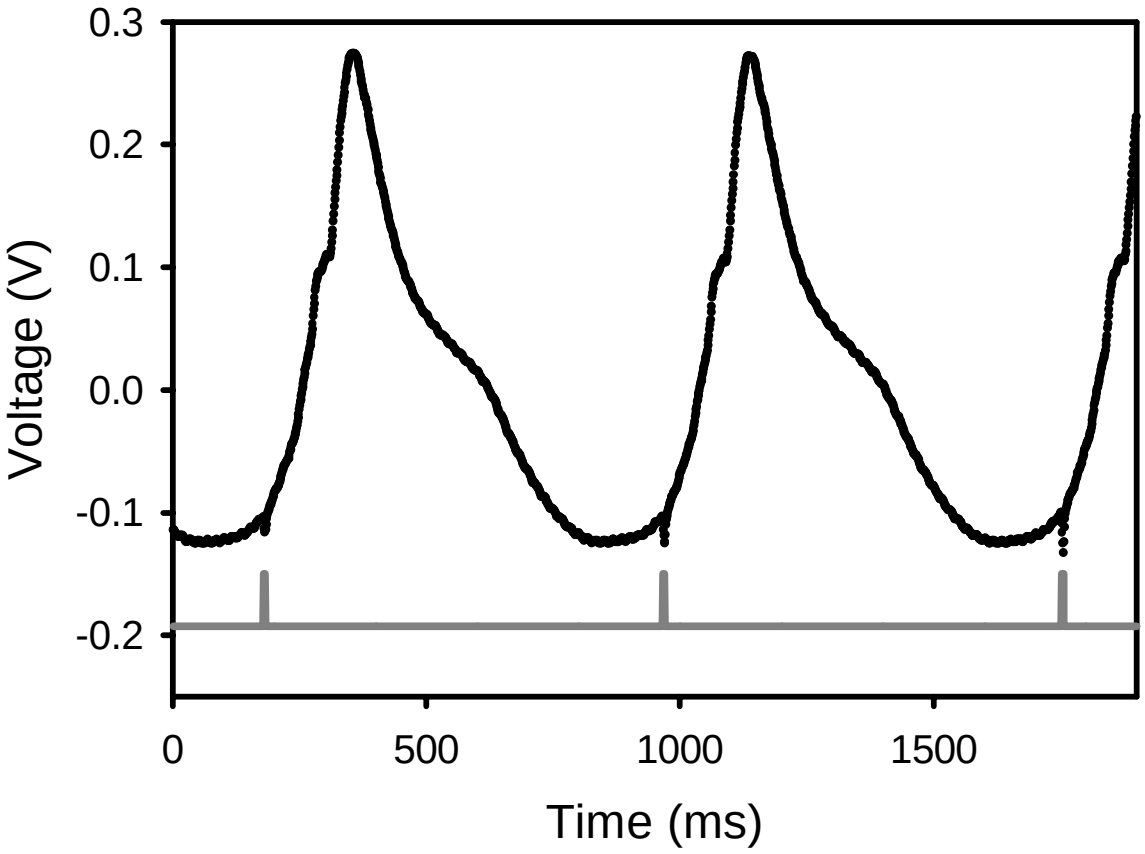

Figure D.8: Signal recorded from a MAP electrode

Appendix E

Physiological Solutions

This appendix contains a description of the physiological solutions I use and how they are designed. Initially, I describe the basic components of any solution. Then I illustrate how to calculate the pH of a buffering solution. Then I list the solutions I use for the small piece of cardiac frog experiments and *in vitro* pieces of sheep tissue.

E.1 Basic Solution

Three parts make up basic physiological solutions. They are the ion salts necessary for activations, glucose and oxygen needed for energy and the buffering system to stabilize the pH. The major ions that are required for proper tissue function (regardless of type) are Na^{+1}, K^{+1}, Ca^{+2}, and Cl^{-1}. Some relatively minor ions that are sometimes added are Mg^{+2} and PO_4^{+3}. Glucose is also universally added in at 5.6 mM. The possible buffering configurations is innumerable. However, there is a typical set of buffering components. The most important one is the carbonate buffering system that is employed by all living animals. Additionally, HEPES and phosphate are sometimes used.

E.2 Buffering

An important issue is the pH of the solution. According to Burton [69] any value between 7.2-7.6 is acceptable for frogs. I choose a pH of 7.4 as the target value, so I can determine the appropriate values of the buffering components. Carbonate

buffering is the most important biological buffering system. The balance of carbonate dissolved in blood is typically regulated by breathing. However, in the small piece of tissue experiments it is regulated by bubbling CO_2 into the superfusate.

Carbonate Buffering Reaction:

$$CO_2 + H_20 <=> H^+ + HCO_3^-$$

Disassociation Constant:

$$K = \frac{[H^+][HCO_3^-]}{[CO_2]}$$

$$pH = pK + Ln(\frac{[HCO_3^-]}{[CO_2]})$$

Henry's Law (Describes dissolution of Gas in Solution):

$$[CO_2] = S * P(CO_2),$$

where $P(CO_2)$ is the partial pressure of CO_2 in contact with the solution.

$$pH = (pK - Ln(S)) + Ln(\frac{[HCO_3^-]}{P(CO_2)})$$

Note that $(pK - Ln(S))$ depends on the ionic strength (in this case approximately 200mM) and temperature (see graph, page 44 ref. [69]).

Therefore

$$\begin{aligned} pH &= (\sim)7.4 + Ln(\frac{[HCO_3^-]}{P(CO_2)}) = 7.4, \\ &\Longrightarrow Ln(\frac{[HCO_3^-]}{P(CO_2)}) = 0 \\ &\Longrightarrow [HCO_3^-] = P(CO_2)\ (mM- > Torr) \\ &\Longrightarrow [HCO_3^-] = 5\% \text{ of } 760 \text{ Torr} = 38mM \end{aligned}$$

That is if the solution is at pH 7.4 then given enough time with 5% CO_2/95% O_2 bubbled through water, 38mM of HCO_3^- will be dissolved into the water, or

38 mM of HCO_3^- is in equilibrium with 5% CO_2 at a pH of 7.4. However, this is based on a somewhat questionable figure and I find that 20 mM of $NaHCO_3$ works with our bubbling system (which may not keep 5% CO_2) to give pH of 7.4. In addition to the carbonate buffer both a Phosphate and HEPES buffers are used. The phosphate is added to aid in conversion of sugar to energy, however, the dibasic form was chosen to aid the buffering. Burton [69] (p38) points out that it is difficult to dissolve both phosphates and calcium together. In fact he presents a rule of thumb, $[PO_3^-][Ca_2^-] \leq 25$*Ionic Strength(approx. 0.2). Therefore the highest level of phosphate allowed is 2.8mM which is in line with the literature. The HEPES was added to conform with advice from Witkowski [129] and for no other reason, however, this adds to the buffering capacity of the solution.

E.3 Frog Physiological Solution

E.3.1 Frog

The frog solution used was developed from several sources [69, 71, 122, 123, 124, 125, 126, 127, 128, 57]. The basic ingredients and their concentrations are:

Component	Concentration
NaCl	110 mM
KCl	2.7 mM
$CaCl_2$	1.8 mM
$MgCl_2$	1.5 mM
Glucose	5.6 mM
Na_2HPO_4	2.8 mM
HEPES	1.0 mM
$NaHCO_3$	25 mM

Table E.1: Frog Physiological Solution

The concentrations of the ions was developed from a survey of papers describing physiological solutions used on bullfrogs and from the relevant sections of Burton

[69]. The sodium concentration I use seems absolutely standard (110mM). The potassium concentration is the mean value of the solutions that were used or suggested in the various papers. Calcium is one of the most important ions, the almost universally agreed on value is 1.8mM. Magnesium seems to be optional, however, the discussion in Burton [69] and the fact that all 'modern' solutions contain it, caused me to include an average value in this solution (1.5mM). In some instances 5-20 mM 2-3-butanedione monoxime (DAM) is added to reduce the mechanical motion of the tissue due to contractions. The solution is kept at a pH of 7.4±0.1 and a temperature of 20±2 °C.

E.4 Sheep Physiological Solution

The Sheep Solution was copied directly from Gray *et al.* [58] with adjustments made to the sodium carbonate to achieve the correct pH without titration at 37°C.

Component	Concentration
NaCl	125 mM
KCl	5.4 mM
$CaCl_2$	1.8 mM
$MgCl_2$	1.0 mM
Glucose	5.6 mM
Na_2HPO_4	0.4 mM
$NaHCO_3$	28.8 mM

Table E.2: Sheep Physiological Solution

The sheep solution needs to be kept at 37°C for the health of the tissue.

Appendix F

MicroChip PIC1677 Code

This is the Assembly language code that the controller runs for experiment in Chapter 6. It flows the flow chart in Fig. F.1.

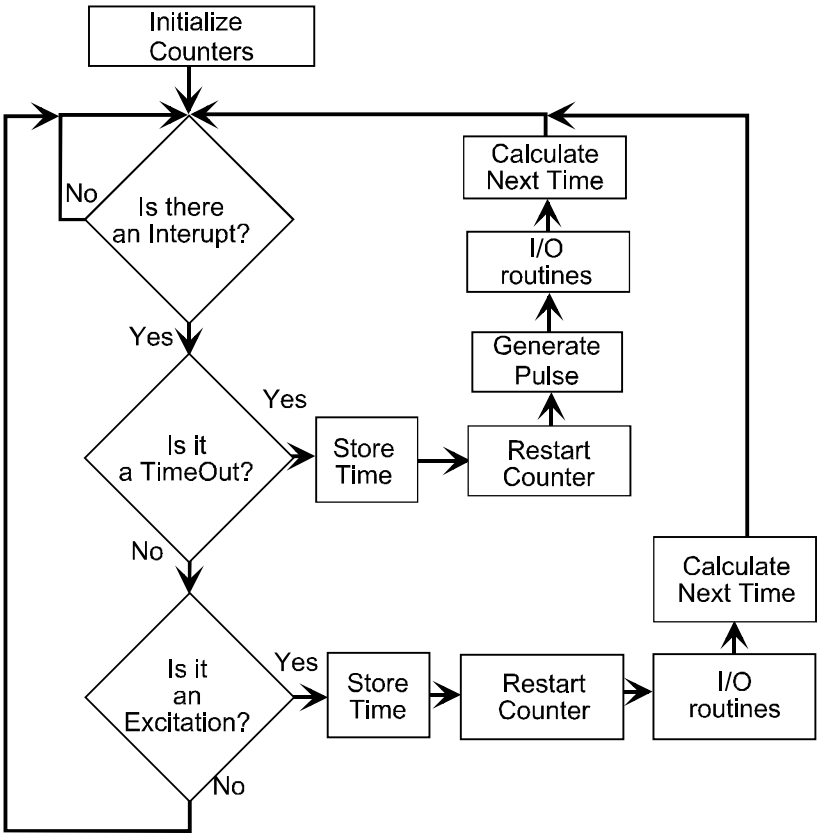

Figure F.1: A flowchart of the PTDAS implimentation by the microcontroller. An activation or a timer over flow causes an interupt. The type of interupt is determined. If it is an activation the next control time is computed. If it is a timer overflow the tissue is paced an then the next control time is computed.

```
;====Sheep Controller 1===scon1.asm====Version 1.0===July 99

; Written by G. Martin Hall
```

```
;
;-------Options-----------------
LIST P=PIC16C77, R=HEX ;Options
                                                    ;specifing
                                                    ;PIC16C77
; Chip and HEX
                                                    ;notation
INCLUDE "c:\progra~1\mplab\P16c77.inc" ;Standard Include
                                                    ;Files
;
;-------Registers---------------
_W equ 0x0020 ;Temp_W during Interupts
_STATUS equ 0x0021 ;Temp_STATUS during Interupts
_FSR equ 0x0022 ;Temp_FSR during Interupts
_PCLATH equ 0x0023 ;Temp_PCLATH during Interupts
; ---> Unused at the moment
;
ACCaLO  equ     0x0024 ; Used in Math Routines
ACCaHI  equ     0x0025
ACCbLO  equ     0x0026
ACCbHI  equ     0x0027
ACCcLO  equ     0x0028
ACCcHI  equ     0x0029
ACCdLO  equ     0x002A
ACCdHI  equ     0x002B
temp    equ     0x002C
```

```
sign    equ     0x002D
TRUE    equ     1
FALSE   equ     0
;
CountP1 equ 0x002E ;Counter for PAUSE1
CountP2A equ 0x002F ;Counter for PAUSE2
CountP2B equ 0x0030 ;Counter for PAUSE2
CountP3A equ 0x0031 ;Counter for PAUSE2
CountP3B equ 0x0032 ;Counter for PAUSE2
;
StackTpH equ 0x0033 ;4 Deep Stack Variables
StackTpL equ 0x0034
Stack1H equ 0x0035
Stack1L equ 0x0036
Stack2H equ 0x0037
Stack2L equ 0x0038
Stack3H equ 0x0039
Stack3L equ 0x003A
Stack4H equ 0x003B
Stack4L equ 0x003C
;
Max_CountH equ 0x003D ;Compare Values for CCP2
Max_CountL equ 0x003E
;
Min_CountH equ 0x003F ;Compare Values for CCP2
Min_CountL equ 0x0040
```

```
;
Skip_Flag equ 0x0041 ;Used to keep track of skip
                              ;conditions
;
GainHI equ 0x0042 ;Current Gain Value
GainLO equ 0x0043
;
ErrorHI equ 0x0044 ;Current Error Signal
ErrorLO equ 0x0045
;
Err_SIGN equ 0x0046 ;Sign For Error
;
Address equ 0x0047 ;Address For Mapping Sysstem Data
;
Time_Adjust equ 0x0048 ;Adjust for missing time
;
N_Count equ 0x0049
;
TempH equ 0x004A ;Temporary 16-bit Variable
TempL equ 0x004B
;
;-------Constants---------------
DEBUG equ FALSE ;Debug Flag
;
Control_Light equ 5 ;The high orange light
; indicating Control On
```

```
Data_Light equ 4 ;The middle orange light indicating
; Data Sent
Gain_Light equ 3 ;The low orange light indicating Gain
; information transfer
;
Excite_Light equ 2 ;Green light indicating Excitation
                              ;detected
Time_Light equ 1 ;Yellow light indicating Time Out
                         ;detected
Skip_Light equ 0 ;Red light indicating a skip condition
                         ;detected
;
Control_Switch equ 0 ;Manual Control on/off switch
;
;-------Configuartion Fuses-----
__CONFIG _XT_OSC & _WDT_OFF & _BODEN_OFF & _CP_OFF & _PWRTE_OFF
;
;-------Jump to Main Code-------
org 0x000
  goto Main
;
;-------Jump to Interupt Code---
org 0x004
goto Inter
;
;-------Interupt Code-----------
```

```
;  Each interupt handler should clear its own flag.
Inter call Store ;Save important Registers
;
; Sort Interupts
btfsc PIR2,CCP2IF ;Is there an excitation?
 call EXCITE
btfsc PIR1,CCP1IF ;Is there a timeout?
 call TIMEOUT
;
call ReStore ;Return important Registers
retfie
;------End Interupt Code--------
;
;-------Main Line Code----------
Main ;---Begin Main Code
;----Setup Variables-------------
movlw 0x06 ;Approx 16ms
movwf Min_CountH
movlw 0xF0 ;
movwf Min_CountL
;
    IF DEBUG
movlw 0x00 ;
movwf Max_CountH
movlw 0x7F ;
movwf Max_CountL
```

```
movlw 0x04
movwf Time_Adjust
    Else
movlw 0xFF ;
movwf Max_CountH
movlw 0xF0 ;
movwf Max_CountL
movlw 0x04
movwf Time_Adjust
    ENDIF
;
movf Max_CountH,W
movwf StackTpH
movwf Stack1H
movwf Stack2H
movf Max_CountL,W
movwf StackTpL
movwf Stack1L
movwf Stack2L
;
movlw 0x00
movwf GainHI
movlw 0xFF
movwf GainLO
;
movlw 0x01
```

```
movwf N_Count
;----End Setup Variables --------
;
;-Initialize PORTA to control lights-
movlw ADCON1 ;indirect addressing of ADCON1
movwf FSR
movlw 0xff ;Set PORTA to Digital I/O
movwf INDF
;
clrf PORTA ;Clear The Port
;
movlw TRISA ;indirect addressing of TRISA
movwf FSR
movlw 0x00 ;make all of PORTA output lines
movwf INDF
;----End Initialization of PORTA----
;
;-Initialize PORTB to output data --
clrf PORTB ;Clear The Port
;
movlw TRISB ;indirect addressing of TRISB
movwf FSR
movlw 0x00 ;make all of PORTB output lines
movwf INDF
movlw 0xFF
movwf PORTB
```

```
;----End Initialization of PORTB----
;
;-Initialize PORTD to send address data-
clrf PORTD
;
movlw TRISE
movwf FSR
bcf INDF,4
movlw TRISD ;indirect addressing of TRISD
movwf FSR
clrf INDF ;Pins 4-7 are address lines for Data
; to the Mapping System
clrf PORTD
movlw 0xFF
movwf PORTD
;----End Initialization of PORTD----
;
;-Initialize PORTE to send address data-
clrf PORTE
;
movlw TRISE ;indirect addressing of TRISE
movwf FSR
bsf INDF,0 ;Control on/off switch
;----End Initialization of PORTE----
;
;--------Begin USART Setup-------
```

```
bsf STATUS,5 ;Move to Bank 1
;
movlw b'11000000' ;Set PORTC for Serial
movwf TRISC ;I/O
;---Set Up Transmitting---
movlw b'00100110' ;CRSRC=(unused),TX9=0,TXEN=1
movwf TXSTA ;SYNC=0,Unused,BRGH=1,TRMT=1,TX9D=0
movlw b'00001100' ;Set baud rate to 9600
movwf SPBRG
;
bcf STATUS,5 ;Move to Bank 0
clrf PORTC ;Clear PORTC
;---Set Up Recieving---
movlw b'10010000' ;SPEN=1,RX9=0,SREN=(unused)
movwf RCSTA ;CREN=1,Unused,FERR=0,OERR=0,RX9D=0
;
bcf RCSTA,CREN ;Clear Out OERR
bsf RCSTA,CREN
movf RCREG,W ;Clear Out RCIF
movf RCREG,W
;----------End USART Setup---------
;
;----Setup CCP1 to Compare----------
;bits 7&6 are unused, 5&4 unused in Compare mode,
;3-0 are used to set CCP1 module to Compare mode
;with Tigger Special.
```

```
movlw b'00001011'
movwf CCP1CON
movlw TRISC ;Indirectly Address TRISC in Bank1
movwf FSR ;
bcf INDF,2 ;Set CCP1 pin as output
bcf PORTC,2 ;Set CCP1 to low
;----End Setup of CCP1-----------------
;
;----Setup CCP2 to Capture-------------
;bits 7&6 are unused, 5&4 unused in Capture mode,
;3-0 are used to set CCP2 module to Capture (rising) mode
;with Tigger Special.
movlw b'00000101'
movwf CCP2CON
movlw TRISC ;Indirectly Address TRISC in Bank1
movwf FSR ;
bsf INDF,1 ;Set CCP2 pin as input
;----End Setup of CCP2-----------------
;
;----Initialize Timer,CCP1&CCP2---------
; Timer
movlw 0x00 ;Zero Counter
movwf TMR1H ; High byte
movwf TMR1L ; Low byte
; CCP1
movf Max_CountH,w ;Set Max Count High Byte
```

```
movwf CCPR1H ;
movf Max_CountL,w ;Set Max Count Low Byte
movwf CCPR1L ;
; CCP2
movlw 0x00 ;Init Capture High Byte
movwf CCPR2H ;
movlw 0x00 ;Init Capture Low Byte
movwf CCPR2L ;
;----End Init Timer,CCP1&CCP2---------
;
;----------Begin Interupt Setup----------
bcf PIR1,2 ;Clear CCP1 interupt Flag
bcf PIR2,0 ;Clear CCP2 interupt Flag
movlw INTCON ;indirect addressing of INTCON
movwf FSR
movlw b'11000000' ;Allow Interupts (GIE&PEIE)
movwf INDF
;
movlw PIE1 ;indirect addressing of PIE1
movwf FSR
bsf INDF,CCP1IE ;Enable CCP1IE interupts
bcf INDF,RCIE ;Disable RECIEVE interupts
bcf INDF,TXIE ;Disable TRANSMIT interupts
;
movlw PIE2 ;indirect addressing of PIE2
movwf FSR
```

```
bsf INDF,CCP2IE ;Enable CCP2IE interupts
;-----------End Interupt Setup-----------
;
;----Setup Timer1-----------------------
;bits 7&6 are unused, 5&4 sets prescaler,
;3&2 are used in timer mode,
;bit 0 starts the clock.
    IF DEBUG
movlw b'00110001' ;Wait until first stim to start clock
    Else
movlw b'00110001' ;Wait until first stim to start clock
    ENDIF
movwf T1CON
;----End Setup of Timer1----------------
;
;----End Initialization of All----------
;
goto $ ;Wait until Something Happens
;
;---------------End Main Line Code--------------
;
;
;
;--------Subroutines--------
;---Interupt Over Head---
```

```
Store movwf _W ;Copy W to _W
swapf STATUS,W ;Swap STATUS into w
movwf _STATUS ;Copy W to _STATUS
movf FSR,W ;Copy FSR into W
movwf _FSR ;Copy W to _FSR
clrf STATUS ;Sets to bank 0 &
; Clears IRP,RP1,RP0 ??????
return
;
ReStore movf _FSR,W
movwf FSR
swapf _STATUS,W
swapf _W,f
swapf _W,W
return
;
;******Compare two 16-bit numbers********
; The STATUS register has the Z, and C bit set just as if
; the subwf command had been used with ACCa being W and ACCb
; being F.
; STATUS Bits C,Z reflects sign of ACCb - ACCa
COMPARE movf ACCaHI,W
subwf ACCbHI,W
btfss STATUS,Z
 return
movf ACCaLO,W
```

```
subwf ACCbLO,W
return
;
;**********32-bit Right Shift***********
; This is used with Multiply. This is effectively
;a 32 bit divide by 2
; ACCbHI->ACCbLO->ACCcHI->ACCcLO
TTBRR bcf STATUS,C
bcf ACCcLO,0
rrf ACCcLO,F
rrf ACCcHI,F
btfsc STATUS,C
 bsf ACCcLO,7
bcf STATUS,C
rrf ACCbLO,F
btfsc STATUS,C
 bsf ACCcHI,7
bcf STATUS,C
rrf ACCbHI,F
btfsc STATUS,C
 bsf ACCbLO,7
return
;
;*****Find Most Significant Bit*********
; The highest bit (zero indexed) of ACCa that is set is
; returned in W
```

```
FindMSB movlw 0x0F
btfsc ACCaHI,7 ;High Byte
 goto MSB_end
movlw 0x0E
btfsc ACCaHI,6
 goto MSB_end
movlw 0x0D
btfsc ACCaHI,5
 goto MSB_end
movlw 0x0C
btfsc ACCaHI,4
 goto MSB_end
movlw 0x0B
btfsc ACCaHI,3
 goto MSB_end
movlw 0x0A
btfsc ACCaHI,2
 goto MSB_end
movlw 0x09
btfsc ACCaHI,1
 goto MSB_end
movlw 0x08
btfsc ACCaHI,0
 goto MSB_end
movlw 0x07
btfsc ACCaLO,7 ;Low Byte
```

```
 goto MSB_end
movlw 0x06
btfsc ACCaLO,6
 goto MSB_end
movlw 0x05
btfsc ACCaLO,5
 goto MSB_end
movlw 0x04
btfsc ACCaLO,4
 goto MSB_end
movlw 0x03
btfsc ACCaLO,3
 goto MSB_end
movlw 0x02
btfsc ACCaLO,2
 goto MSB_end
movlw 0x01
btfsc ACCaLO,1
 goto MSB_end
movlw 0x00
MSB_end return
;
;*************************************************************
;                          Math Routines
;*************************************************************
;                          Shared Subroutines
```

```
;*************************************************************
SIGNED  equ     FALSE ; Set This To 'TRUE' if the routines
;                     ; for Multiplication & Division needs
;                     ; to be assembled as Signed Integer
;                     ; Routines. If 'FALSE' the above two
;                     ; routines ( D_mpy & D_div ) use
;                     ; unsigned arithmetic.
     IF    SIGNED
S_SIGN  movf    ACCaHI,W
xorwf   ACCbHI,W
movwf   sign
btfss   ACCbHI,MSB      ; if MSB set go & negate ACCb
goto    chek_A
;
comf    ACCbLO          ; negate ACCb
incf    ACCbLO
btfsc   STATUS,Z
decf    ACCbHI
comf    ACCbHI
;
chek_A  btfss   ACCaHI,MSB    ; if MSB set go & negate ACCa
retlw   0
goto    neg_A
     ENDIF
;
setup   movlw   .16           ; for 16 shifts
```

```
movwf   temp
movf    ACCbHI,W          ;move ACCb to ACCd
movwf   ACCdHI
movf    ACCbLO,W
movwf   ACCdLO
clrf    ACCbHI
clrf    ACCbLO
retlw   0
;
neg_A   comf    ACCaLO, F       ; negate ACCa (-ACCa -> ACCa)
incf    ACCaLO, F
btfsc   STATUS,Z
decf    ACCaHI, F
comf    ACCaHI, F
retlw   0
;
;************************************************************
;                 Double Precision Addition & Subtraction
;************************************************************;
;   Addition :  ACCb(16 bits) + ACCa(16 bits) -> ACCb(16 bits)
;    (a) Load the 1st operand in location
; ACCaLO & ACCaHI ( 16 bits )
;    (b) Load the 2nd operand in location
; ACCbLO & ACCbHI ( 16 bits )
;    (c) CALL D_add
;    (d) The result is in location ACCbLO & ACCbHI (16 bits)
```

```
;   Performance : Program Memory  :       07
;                 Clock Cycles    :       08
;************************************************************;
;   Subtraction : ACCb(16 bits) - ACCa(16 bits) -> ACCb(16 bits)
;    (a) Load the 1st operand in location ACCaLO & ACCaHI (16 bits)
;    (b) Load the 2nd operand in location ACCbLO & ACCbHI (16 bits)
;    (c) CALL D_sub
;    (d) The result is in location ACCbLO & ACCbHI (16 bits)
;   Performance : Program Memory  :       14
;                 Clock Cycles    :       17
;     Program: DBL_ADD.ASM
;     Revision Date: 1-13-97 Compatibility with MPASMWIN 1.40
;************************************************************
;         Double Precision Subtraction ( ACCb - ACCa -> ACCb )
;
D_sub   call    neg_A           ; At first negate ACCa; Then add
;************************************************************
;       Double Precision  Addition ( ACCb + ACCa -> ACCb )
;
D_add   movf    ACCaLO,W
addwf   ACCbLO, F       ;add lsb
btfsc   STATUS,C        ;add in carry
incf    ACCbHI, F
movf    ACCaHI,W
addwf   ACCbHI, F       ;add msb
retlw   0
```

```
;*****************************************************************
;                        Double Precision Multiplication
;                ( Optimized for Speed : straight Line Code )
;*****************************************************************;
; Multiplication : ACCb(16 bits) * ACCa(16 bits) -> ACCb,ACCc (32
;                                                          bits)
; (a) Load the 1st operand in location ACCaLO & ACCaHI (16 bits)
; (b) Load the 2nd operand in location ACCbLO & ACCbHI (16 bits)
; (c) CALL D_mpy
; (d) The 32 bit result is in location
;              (ACCbHI,ACCbLO,ACCcHI,ACCcLO )
;   Performance :
;                Program Memory  :  240
;                Clock Cycles    :  233
;Note : The above timing is the worst case timing, when the
;      register ACCb = FFFF. The speed may be improved if
;      the register ACCb contains a number ( out of the two
;      numbers ) with less number of 1s.
;      The performance specs are for Unsigned arithmetic ( i.e,
;      with "SIGNED equ  FALSE ").
;   Program:        DBL_MPYF.ASM
;   Revision Date:  1-13-97      Compatibility with MPASMWIN 1.40
;*****************************************************************;
;       multiplication macro
;
mulMac  MACRO
```

```
LOCAL   NO_ADD
rrf     ACCdHI, F       ;rotate d right
rrf     ACCdLO, F
btfss   STATUS,C    ;need to add?
goto    NO_ADD          ; no addition necessary
movf    ACCaLO,W        ; Addition ( ACCb + ACCa -> ACCb )
addwf   ACCbLO, F       ;add lsb
btfsc   STATUS,C    ;add in carry
incf    ACCbHI, F
movf    ACCaHI,W
addwf   ACCbHI, F       ;add msb
NO_ADD  rrf     ACCbHI, F
rrf     ACCbLO, F
rrf     ACCcHI, F
rrf     ACCcLO, F
ENDM
;*************************************************************
;        Double Precision Multiply ( 16x16 -> 32 )
;   ( ACCb*ACCa -> ACCb,ACCc ) : 32 bit output with high word
; in ACCb ( ACCbHI,ACCbLO ) and low word
; in ACCc ( ACCcHI,ACCcLO ).
;*************************************************************
;
D_mpyF          ;results in ACCb(16 msb's) and ACCc(16 lsb's)
     IF   SIGNED
     CALL    S_SIGN
```

```
    ENDIF
call    setup
mulMac ; use the mulMac macro 16 times
mulMac
mulMac
mulMac
mulMac
mulMac
mulMac
mulMac
mulMac
mulMac
mulMac
mulMac
mulMac
mulMac
mulMac
mulMac
mulMac
    IF    SIGNED
btfss   sign,MSB
retlw   0
comf    ACCcLO          ; negate ACCa ( -ACCa -> ACCa )
incf    ACCcLO
btfsc   STATUS,Z
decf    ACCcHI
comf    ACCcHI
```

```
btfsc   STATUS,Z
neg_B   comf    ACCbLO          ; negate ACCb
incf    ACCbLO
btfsc   STATUS,Z
decf    ACCbHI
comf    ACCbHI
retlw   0
    ELSE
retlw   0
    ENDIF
;****************END MATH ROUTINES***************
;
;++++++++++++If the time reaches CCPR1H & CPPR1L++++++++++++
TIMEOUT bsf PORTA,Time_Light ;From CCP1 set in Compare mode
movf CCPR1H,W ;Store Time High Byte
movwf StackTpH
movf CCPR1L,W ;Store Time Low Byte
movwf StackTpL
call PUSH
;
bcf T1CON,0 ;Stop Counter
movf Time_Adjust,W ;Reset Counter To Adjusted Value
movwf TMR1L ; Low byte
clrf TMR1H ; High byte
    IF DEBUG
movlw b'00110001'
```

```
    Else
movlw b'00110001'
    ENDIF
movwf T1CON ;Reset prescaler and Start Counter
;
movf Max_CountH,W ;Set Time Out to minimum
movwf CCPR1H
movf Max_CountL,W
movwf CCPR1L
;
bcf PORTA,Control_Light
btfss PORTE,Control_Switch ;Check and see if control is on
 goto TIME2 ; If not skip pacing
bsf PORTA,Control_Light ;Set Control Light
;
bsf PORTC,2 ;Toggle CCP1-Pin
call PAUSE1 ;Pause for 4ms
call PAUSE1
call PAUSE1
call PAUSE1
bcf PORTC,2
;
bcf PORTA,Skip_Light
incf Skip_Flag,F ;Increment Skip Flag if Pulse sent
movf Skip_Flag,W ;Find out if next time is a skip time
subwf N_Count,W
```

```
btfsc STATUS,Z ;If so light light
 bsf PORTA,Skip_Light
;
TIME2 bcf PORTA,Gain_Light
btfsc PIR1,RCIF ;Check if Recieved Data Present
 call RECEIVE ;Handle it
;
call CONTROL ;Compute next Pulse
;
call SEND ;Send Computer and Mapping System Data
;
bcf PIR2,CCP2IF ;Clear Flag
bcf PIR1,CCP1IF ;Clear Flag
bcf PORTA,Time_Light ;Clear Time Out Light
return
;
;+++++++++++++++If the CCP2 Pin is set+++++++++++++++
EXCITE bsf PORTA,Excite_Light;From CCP2 set in Capture mode
movf CCPR2H,W ;Store Time High Byte
movwf StackTpH
movf CCPR2L,W ;Store Time Low Byte
movwf StackTpL
call PUSH
;
bcf T1CON,0 ;Stop Counter
movf Time_Adjust,W ;Reset Counter To Adjusted Value
```

```
movwf TMR1L ; Low byte
clrf TMR1H ; High byte
    IF DEBUG
movlw b'00110001'
    Else
movlw b'00110001'
    ENDIF
movwf T1CON ;Reset prescaler and Start Counter
;
movf Max_CountH,W ;Set Time Out to minimum
movwf CCPR1H
movf Max_CountL,W
movwf CCPR1L
;
bcf PORTA,Control_Light
btfss PORTE,Control_Switch ;Check and see if control is on
 goto EXCITE2 ; If not skip pacing
bsf PORTA,Control_Light ;Set Control Light
;
EXCITE2 bcf PORTA,Skip_Light
clrf Skip_Flag ;Reset Skip_Flag
;
bcf PORTA,Gain_Light
btfsc PIR1,RCIF ;Check if Recieved Data Present
 call RECEIVE ;Handle it
;
```

```
call CONTROL ;Compute next Pulse
;
call SEND ;Send Computer and Mapping System Data
;
bcf PIR1,CCP1IF ;Clear Flag
bcf PIR2,CCP2IF ;Clear Flag
bcf PORTA,Excite_Light ;Clear Excite Light
return
;
;+++++++++If Called the routine trys to get a new Gain++++++++
RECEIVE bsf PORTA,Gain_Light
;
btfsc RCSTA,OERR ;If Overflow detected throw error
 goto ERROR1
;
movf RCREG,W ;Read First Value
movwf TempH
btfss PIR1,RCIF ;Is there waiting Data?
 call PAUSE1 ; If not wait one 1ms > 1byte @9600
btfss PIR1,RCIF ;Now is there more data?
 goto ERROR2 ; If not throw error
movf RCREG,W ;Read Second Value
movwf TempL
;
movf TempH,W
movwf GainHI
```

```
movf TempL,W
movwf GainLO
;
bcf RCSTA,CREN ;Clear out OERR
bsf RCSTA,CREN
movf RCREG,W ;Clear out RCIF
movf RCREG,W
;
RetE1 return
;
;++++++++++++++++++OUTPUT INTERNAL CURRENT DATA++++++++++++
SEND bsf PORTA,Data_Light
clrf PORTB ;Set Adress Lines to Low
clrf PORTD
clrf Address
call PAUSE1
call PAUSE1
;
movlw TXSTA ;indirect addressing of TXSTA
movwf FSR
;
btfss PORTA,Control_Light ;Test if Control is On?
 goto SEND1
;----Status-----
movlw 0xFF ;Status - High Byte - Control On
btfss INDF,TRMT
```

```
 goto $-1
movwf TXREG
movlw 0xF2 ;Status - Low Byte
movwf TXREG
 goto SEND2
;
SEND1 movlw 0xFF ;Status - High Byte - Control Off
btfss INDF,TRMT
 goto $-1
movwf TXREG
movlw 0xF1 ;Status - Low Byte
movwf TXREG
;----Gain-----
SEND2 movf GainHI,W ;Gain - High Byte
movwf PORTB
incf Address,F
swapf Address,W
movwf PORTD
call PAUSE1
call PAUSE1
clrf PORTD
clrf PORTB
call PAUSE1
call PAUSE1

movf GainLO,W ;Gain - Low Byte
```

```
movwf PORTB
incf Address,F
swapf Address,W
movwf PORTD
call PAUSE1
call PAUSE1
clrf PORTD
clrf PORTB
call PAUSE1
call PAUSE1
;
movf GainHI,W ;Gain - High Byte
btfss INDF,TRMT
 goto $-1
movwf TXREG
movf GainLO,W ;Gain - Low Byte
movwf TXREG
;----Tn-----
call READ1
movf StackTpH,W ;Tn - High Byte
movwf PORTB
incf Address,F
swapf Address,W
movwf PORTD
call PAUSE1
call PAUSE1
```

```
clrf PORTD
clrf PORTB
call PAUSE1
call PAUSE1

movf StackTpL,W ;Tn - Low Byte
movwf PORTB
incf Address,F
swapf Address,W
movwf PORTD
call PAUSE1
call PAUSE1
clrf PORTD
clrf PORTB
call PAUSE1
call PAUSE1
;
movf StackTpH,W ;Tn - High Byte
btfss INDF,TRMT
 goto $-1
movwf TXREG
movf StackTpL,W ;Tn - Low Byte
movwf TXREG
;----Error-----

movf ErrorHI,W ;Error - High Byte
```

```
movwf PORTB
incf Address,F
swapf Address,W
movwf PORTD
call PAUSE1
call PAUSE1
clrf PORTD
clrf PORTB
call PAUSE1
call PAUSE1

movf ErrorLO,W ;Error - Low Byte
movwf PORTB
incf Address,F
swapf Address,W
movwf PORTD
call PAUSE1
call PAUSE1
clrf PORTD
clrf PORTB
call PAUSE1
call PAUSE1
;
movf ErrorHI,W ;Error - High Byte
btfss INDF,TRMT
 goto $-1
```

```
movwf TXREG
movf ErrorLO,W ;Error - Low Byte
movwf TXREG
;
call PAUSE1
call PAUSE1
movlw 0xFF
movwf PORTD
movwf PORTB
bcf PORTA,Data_Light
return
;
;+++++++++++++++++Generate next Control Time++++++++++++
CONTROL clrf Err_SIGN
;
call READ1 ; Tn   -> ACCb
movf StackTpH,W
movwf ACCbHI
movf StackTpL,W
movwf ACCbLO
call READ2 ; Tn-1 -> ACCa
movf StackTpH,W
movwf ACCaHI
movf StackTpL,W
movwf ACCaLO
call COMPARE ;Compare the two Times (b-a)
```

```
btfsc STATUS,C ; If negative goto Con1
 goto Con2 ; Else goto Con2
;
Con1 bsf Err_SIGN,0 ;Switch ACCa and ACCb and save sign
movf ACCaHI,W ;Move ACCa -> ACCb
movwf ACCbHI ;   Tn-1 -> ACCb
movf ACCaLO,W
movwf ACCbLO
call READ1 ;   Tn   -> ACCa
movf StackTpH,W
movwf ACCaHI
movf StackTpL,W
movwf ACCaLO
;
Con2 call D_sub ;Calculate Error -> ACCb
;
movf ACCbHI,W ;Store Error
movwf ErrorHI
movf ACCbLO,W
movwf ErrorLO
;
btfss PORTA,Control_Light;Check and see if control is on
 goto CONTR2  ; If so jump to CONTR2
;
movf Skip_Flag,W ;Find out if this is a skip time
subwf N_Count,W
```

```
btfsc STATUS,Z ;If so jump to CONTR2
 goto CONTR2
;
movf GainHI,W ;Load Gain -> ACCb
movwf ACCbHI
movf GainLO,W
movwf ACCbLO
;
movf ErrorHI,W ;Load Error -> ACCa
movwf ACCaHI
movf ErrorLO,W
movwf ACCaLO
;
call FindMSB ;Find MSB of ACCa
sublw 0x0E
btfss STATUS,C ; If it is not to big continue
 goto ERROR3 ; else throw error3
call D_mpyF ;Calculate Epsilon -> ACCc
movf ACCcHI,W ;Shift 8 to the right
movwf ACCcLO
movf ACCbLO,W
movwf ACCcHI
movf ACCbHI,W
movwf ACCbLO
clrf ACCbHI
call TTBRR ;Shift 3 more
```

```
call TTBRR
call TTBRR
;
movf ACCcHI,W ; Move Epsilon into ACCa
movwf ACCaHI
movf ACCcLO,W
movwf ACCaLO
;
call READ1 ; Tn -> ACCb
movf StackTpH,W
movwf ACCbHI
movf StackTpL,W
movwf ACCbLO
;
btfss Err_SIGN,0 ;If Epsilon>=0 then Tn + ||Epsilon||
 goto N_CON ;Else               Tn - ||Epsilon||
;
P_CON call D_add ;Tn + ||Epsilon|| -> ACCb
 goto CON_Ret
N_CON call D_sub ;Tn - ||Epsilon|| -> ACCb
;
CON_Ret movf Min_CountH,W
movwf ACCaHI
movf Min_CountL,W
movwf ACCaLO
call COMPARE ;Compare the two Times (b-a)
```

```
btfss STATUS,C ; If positive Continue
 goto CONTR3 ; Else goto CONTR3
;
movf ACCbHI,W ;Load up Time Out registers
movwf CCPR1H
movf ACCbLO,W
movwf CCPR1L
return
;
CONTR2 movf Max_CountH,W ;Set Time Out to maximum
movwf CCPR1H
movf Max_CountL,W
movwf CCPR1L
clrf Skip_Flag
return
;
CONTR3 movf Min_CountH,W ;Set Time Out to minimum
movwf CCPR1H
movf Min_CountL,W
movwf CCPR1L
clrf Skip_Flag
return
;
;+++++++++++++++++Error Routines++++++++++++
;+++++Note that these are not call able ++++
ERROR1 ;FFFE = overflow error -> resend valid data
```

```
bcf RCSTA,CREN ;Clear out OERR
bsf RCSTA,CREN
movf RCREG,W ;Clear out RCIF
movf RCREG,W
movlw 0xFF ;Send Error Signal
movwf TXREG
movlw 0xFE
movwf TXREG
call PAUSE1
call PAUSE1
goto RetE1
;
ERROR2;FFFF = one byte recieved -> resend valid data
bcf RCSTA,CREN ;Clear out OERR
bsf RCSTA,CREN
movf RCREG,W ;Clear out RCIF
movf RCREG,W
movlw 0xFF ;Send Error Signal
movwf TXREG
movlw 0xFF
movwf TXREG
call PAUSE1
call PAUSE1
goto RetE1
;
ERROR3 ;FFFD OverFlow in Error Signal For that gain
```

```
movlw TXSTA ;indirect addressing of TXSTA
movwf FSR
btfss INDF,TRMT
 goto $-1
movlw 0xFF ;Send Error Signal
movwf TXREG
movlw 0xFD
movwf TXREG
call PAUSE1
call PAUSE1
goto CONTR2
;
;---General Routines---
    IF DEBUG
PAUSE1 return
;PAUSE2 return
;PAUSE3 return
    ELSE
PAUSE1 movlw 0xA4 ;Pause for 500 Cycles -> 1ms
movwf CountP1
P1Entry decfsz CountP1,F
 goto P1Entry
return
;
    ENDIF
;
```

```
PUSH movf Stack1H,W ;Move 1->2
movwf Stack2H
movf Stack1L,W
movwf Stack2L
movf StackTpH,W ;Move Top->1
movwf Stack1H
movf StackTpL,W
movwf Stack1L
return
;
READ1 movf Stack1H,W ;Move 1->Top
movwf StackTpH
movf Stack1L,W
movwf StackTpL
return
;
READ2 movf Stack2H,W ;Move 2->Top
movwf StackTpH
movf Stack2L,W
movwf StackTpL
return
;
 end
```

Bibliography

[1] A.M. Katz, in *Physiology of the Heart, 2nd edition,* (Raven Press, New York, 1992)

[2] American Heart Association, *1999 Heart and Stroke Statistical Update*, Dallas TX, Amer. Heart Assoc. 1998.

[3] G.R. Mines, 'On dynamic equilibrium in the heart,' *J. Physiol (London)* **46**, 349-383 (1913)

[4] G.R. Mines, 'On circulating excitation on heart muscles and their possible relation to tachycardia and fibrillation,' *Trans. R. Soc. Can.* **4**, 43 (1914).

[5] A.L. Hodgkin and A.F. Huxley, 'A quantiative description of membrane current and its application to conduction and excitation in nerve,' *J. Physio.* 117 (1952), pp 500-544.

[6] R. Fitzhugh, 'Impulse and physiological states in theoretical models of nerve membrane,' *Biophy. J.* 1 (1961), pp 445-466.

[7] J. Nagumo, S.A. Rimoto, and S. Yoshizowa, 'An active pulse transmission line simulating nerve axon,' *Proceedings of the IRE*, April 26 1962, pp 2061-2070.

[8] R.O. Grigoriev, M.C. Cross, and H.G. Schuster, 'Pinning Control of spatiotemporal chaos,' *Phys. Rev. Lett.* **79**, 15 (1997).

[9] N. Parekh, V.R. Kumar and B.D. Kulkarni, 'Synchronization and control of spatiotemporal chaos using time-series data from local regions,' *Chaos* **8,** 1 (1998).

[10] I. Aranson, H. Levine, and L. Tsimring, 'Controlling spatio-temporal chaos,' *Phys. Rev. Lett.* **72**, 2561 (1995).

[11] W. Lu, D. Yu, and R.G. Harrison, 'Control of patterns in spatiotemporal chaos in optics,' *Phys. Rev. Lett.* **76**, 18 (1996).

[12] R. Martin, A.J. Scroggie, G.-L. Oppo, and W.J. Firth 'Stabilization, Selection, and Tracking of Unstable Patterns by Fourier Space Techniques,' *Phys. Rev. Lett.* **77**, 19 (1996).

[13] V. Petrov, M.F. Crowley, and K. Showalter, 'Stabilizing staedy and periodic behavior in propagating flame fronts,' *Physica D* **84** (1995).

[14] R.J. Wiener, D.C. Dolby, G.C. Gibbs, and B. Squires, 'Control of chaotic pattern dynamics in Taylor vortex flow,' *Phys. Rev. Lett.* **83** 12 (1999).

[15] J.J. Gallagher, J.H. Kasell, J.L. Cox, W.M. Smith, R.E. Ideker, and W.M. Smith, 'Techniques of intraoperative electrophysiologic mapping,' Am. J. Cardiol. **49**, 221 (1982).

[16] F.X. Witkowski and P.B. Corr, 'An automated simultaneous transmural cardiac mapping system,' Am. J. Physiol. **247**, H661 (1984).

[17] R.E. Ideker, W.M. Smith, P.D. Wolf, N.D. Danieley, and F.R. Bartram, 'Simultaneous multichannel cardiac mapping systems,' PACE **10**, 281 (1987).

[18] *Cardiac Mapping*, M. Shenasa, M. Borggrefe, and G. Breithardt, eds., (Futura Publishing Company, Inc., Mount Kisco, New York, 1993).

[19] J. Jalife, J.M. Davidenko, and D.C. Michaels, 'A new perspective on the mechanisms of arrhythmias and sudden cardiac death: Spiral waves of excitation in heart muscle,' *J. Cardiovasc. Electrophysiol.* **2**, S133 (1991).

[20] J.M. Davidenko, 'Spiral wave activity: A possible common mechanism for polymorphic and monomorphic ventricular tachycardias,' *J. Cardiovasc. Electrophysiol.* **4**, 730 (1993).

[21] P.V. Bayly, E.E. Johnson, P.D. Wolf, H.S. Greenside, W.M. Smith, and R.E. Ideker, 'A quantitative measurement of spatial order in ventricular fibrillation,' *J. Cardiovasc. Electrophysiol.* **4**, 533 (1993).

[22] F.X. Witkowski, K.M. Kavanagh, P.A. Penkoske, R. Plonsey, M.L. Spano, W.L. Ditto, and D.T. Kaplan, 'Evidence for determinism in ventricular fibrillation,' *Phys. Rev. Lett.* **75**, 1230 (1995).

[23] W. L. Ditto and M. L. Spano, 'Electromagnetic Fields and Biological Tissues: From Nonlinear Response to Chaos Control,' to appear in *Self-Organized Biological Dynamics and Nonlinear Control by External Stimuli*, Jan Walleczek, Ed., (Cambridge University Press, London, 1999).

[24] A. Karma, 'Spiral breakup in model equations of action potential propagation in cardiac tissue,' *Phys. Rev. Lett.* **71**, 7 (1993)

[25] M. Courtemanche, 'Complex spiral wave dynamics in a spatially distributed ionic model of cardiac electrical activity,' *Chaos* **6**, 4 (1996).

[26] A.V. Panfilov, P. Hogeweg, 'Scroll breakup in three-dimensional excitable medium,' Phy. Rev. E **53**, 2 (1996).

[27] A.F.M. Marée, A.V. Panfilov, 'Spiral Breakup in excitable tissue due to lateral instability,' Phy. Rev. Lett. **78**, 9 (1997).

[28] M.C. Cross and P.C. Hohenburg, 'Pattern formation outside of equilibrium,' *Reviews of Modern Physics*, **65**, 3, Part II (1993).

[29] E. Ott, C. Grebogi, and J.A. Yorke, 'Controlling Chaos,' *Phys. Rev. Lett.* **64**, 1196 (1990).

[30] H.M. Hastings, S.J. Evans, W. Quan, M.L. Chong, and O. Nwasokwa, 'Nonlinear dynamics in ventricular fibrillation,' *Proc. Nat. Acad. Sci.* **93** (1996), pp. 10495-10499.

[31] Z. Qu, J.N. Weiss, and A. Garfinkle, 'Spatiotemporal chaos in a simulated ring of cardiac cells,' *Phy. Rev. Lett.* **78**, 7 (1997).

[32] D.J. Christini and J.J. Collins, 'Controlling neuronal noise using chaos control,' *Phys. Rev. Lett.* **75**, 2782 (1995).

[33] P-S Chen, PD Wolf, EG Dixon, ND Danieley, DW Frazier, WM Smith, and RE Ideker, 'Mechanism of ventricular vulnerability to single premature stimuli in open-chest dogs,' *Circ Res* **62**:1191-1209 (1988).

[34] M. Allessie, C. Kirchhof, G.J. Scheffer, F. Chorro, and J. Brugada, 'Regional control of atrial fibrillation by rapid pacing in concious dogs,' *Circulation* **84**, 1689 (1991).

[35] C. Kirchhof, F. Chorro, G.J. Scheffer, J. Brugada, K. Konings, Z. Zetelaki, and M. Allessie, 'Regional entrainment of atrial fibrillation studied by high-resolution mapping in open-chest dogs,' *Circulation* **88**, 736 (1993).

[36] B.H. KenKnight, P.V. Bayly, R.J. Gerstle, D.L. Rollins, P.D. Wolf, W.M. Smith, and R.E. Ideker, 'Regional capture of fibrillating myocardium: Evidence of an excitable gap,' *Circ. Res.* **77**, 849 (1995).

[37] T. Shinbrot, C. Grebogi, E. Ott, and J.A. Yorke, 'Using small perturbations to control chaos,' *Nature* **363**, 411 (1993).

[38] T. Shinbrot, 'Chaos: Unpredictable yet controllable?,' *Nonlin. Sci. Today* **3**, 1 (1993).

[39] A. Garfinkel, M.L. Spano, W.L. Ditto, and J.L. Weiss, "Controlling cardiac chaos," *Science,* **257**, pp 1230-1235 (1992).

[40] K. Hall, D. J. Christini, M. Tremblay; J. J. Collins, L. Glass, and J. Billette, 'Dynamic control of cardiac alternans,' *Phys. Rev. Lett.* **78**, 4518 (1997).

[41] L. Glass and M. F. Josephson, 'Resetting and annihilation of reentrant abnormally rapid heartbeat' Phys. Rev. Lett. **75**, 2059 (1995).

[42] V. N. Biktashev and A. V. Holden, 'Control of re-entrant activity in a model of mammalian atrial tissue,' Proc. R. Soc. Lond. B **261**, 211 (1995).

[43] M. Watanabe and R. F. Gilmour, Jr, 'Strategy for control of complex low-dimensional dynamics in cardiac tissue,' *J. Math. Biol.* **35**, 73 (1996).

[44] W.J. Rappel, F. Fenton, and A. Karma, 'Spatiotemporal control of wave instabilities in cardiac tissue,' *Phys. Rev. Lett.* **83**, 2 (1999).

[45] D.J. Gauthier and J.E.S. Socolar, 'Comment on "Dynamic control of cardiac alternans",' *Phys. Rev. Lett.* **79**, 4938 (1997).

[46] S. J. Schiff, K. Jerger, D. H. Duong, T. Chang, M. L. Spano, and W. L. Ditto, 'Controlling chaos in the brain,' *Nature* (London) **370**, 615 (1994).

[47] D.A. Egolf and J.E.S. Socolar, 'Failure of linear control in noisy coupled map lattices,' *Phy. Rev. E* **57**, 5 (1998).

[48] M. Ciofini, A. Labate, R. Meucci, and M. Galanti, 'Stabilization of unstable fixed points in the dynamics of a laser with feedback,' *Phy. Rev. E* **60**, 1 (1999), pp 398-402.

[49] R. Plonsey, RC Barr, *Bioelectricity: a Quantitative Approach.* New York, NY, Plenum Press, 1991, p. 143.

[50] C.-H. Luo and Y. Rudy, 'A model of the ventricular cardiac action potential: Depolarization, repolarization, and their interaction,' *Circ. Res.* **68**, 1501 (1991).

[51] R.L. Rasmusson, J.W. Clark, W.R. Giles, E.F. Shibata, and D.L. Campbell, 'A mathematical model of electrical activity in the bullfrog atrial cell,' *Am. J. Physiol.* (Heart Circ. Physiol. 28) **259** (1990):H352-H369.

[52] R.L. Rasmusson, J.W. Clark, W.R. Giles, K. Robinson, R.B. Clark and D.L. Campbell, 'A mathematical model of a bullfrog cardiac pacemaker cell,' *Am. J. Physiol.* (Heart Circ. Physiol. 28) **259** (1990):H352-H369.

[53] C.S. Henriquez, 'Simulating the electrical behavior of cardiac tissue using the bidomain model,' *Critical Rev. in Biomed. Eng.* **21**, 1 (1993), pp. 1-77.

[54] L.A. Geddes, 'Electrodes and the measurement of bioelectric events,' John Wiley and Sons Inc., New York 1972.

[55] M.A. Franz, 'Atrial fibrillation and atrial flutter seen through the "eye" of monophasic action potential recording,' from Atria flutter and fibrillation from basic to clinical applications, chap 11, N. Suondi, W. schels, and N. El-Sherif eds., Futura Publishing Co. Inc., New York (1998).

[56] T.J. Ebner and G. Chen, 'Use of voltage-sensitive dyes and optical recordings in the central nervous system,' *Prog. in Neurobio.* **46** (1995), pp 463-506.

[57] F.X. Witkowski, L.J. Penkoske, P.A. Giles, W.R. Spano, M.L. Ditto, and A.T. Winfree, 'Spatiotemporal evolution of ventricular fibrillation,' *Nature* (London) **392**, 78 (1998).

[58] R.A. Gray, A.M. Pertsov, and J. Jalife, 'Spatial and temporal organization during cardiac fibrillation,' *Nature* (London) **392**, 75 (1998).

[59] P. Berge, Y. Pomeau, C. Vidal, *Order within chaos: towards a deterministic approach to turbulence* (J. Wiley and Sons, New York, 1984), pp. 40-42.

[60] M. Marden, 'The geometry of the zeros of a polynomial in a complex variable,' Amer. Math. Society, (1949).....

[61] A. Karma, 'Electrical alternans and spiral wave breakup in cardiac tissue,' *Chaos* **4**, 461 (1994).

[62] A. Karma, *Nature* **379**, 118 (1996).

[63] M. Guevara, G. Ward, A. Shrier, L. Glass, 'Electrical alternans and period-doubling bifurcations,' in *Computers in Cardiology*, IEEE Comp. Soc., (1984) p. 167

[64] '*BME 101 & 102 Lab Manual*,' Spring 1994, Department of Biomedical Engineering, Duke University, Durham, N.C.

[65] R. A. Oliver, G. M. Hall, S. Bahar, W. Krassowska, P. D. Wolf, E.G. Dixon-Tulloch and D.J. Gauthier, 'Existence of bistability and correlation with arrhythmogenesis in paced sheep atria,' Manuscript in preparation.

[66] R. Oliver, in Math 139.

[67] R. L. Verrier, B. D. Nearing, in *Cardiac Electrophysiology: from Cell to Bedside, 2nd edition,* ed. D. P. Zipes and J. Jalife (W. B. Saunders Company, Philadelphia, 1995), chap. 45; B. Surawicz, C. Fisch, J. *Am. Coll. Cardiol.* **20**, 483 (1992); M. A. Murda'h, W. J. McKenna, A. J. Camm. *PACE* **20**, 2641 (1997).

[68] M. Landau, P. Lorente, J. Henry, S. Canu. *J. Math. Biol.* **25**, 491 (1987); P. Lorente, J. Davidenko. *Ann. NY. Acad. Sci.* **591**, 109 (1990).

[69] RF Burton, *Ringer Solutions and Physiological Salines.* Bristol: Wright Scientechnica; 1975.

[70] M Guevara, A Shrier, L Glass: Chaotic and Complex Rhythms, in Zipes DP, Jalife J (eds): *Cardiac Electrophysiology, From Cell to Bedside.* Philadelphia, PA, WB Saunders Co., 1990, ch. 23

[71] J. B. Nolasco and R. W. Dahlen, 'A graphic method for the study of alternation in cardiac action potentials,' *J. Appl. Physiol.* **25**, 191 (1968).

[72] D.J. Christini and J.J. Collins 'Using chaos control and tracking to suppress a pathological nonchaotic rhythm in a cardiac model' Phys. Rev. E (Rapid Communition) **53**, R49 (1996).

[73] L. Glass. *Phys. Today* **49**, 40 (1996).

[74] Myerburg RJ, Kessler KM, Interian A, Fernandez P, Kimura S, Kozlovskis PL, Furukawa P, Bassett AL, Castellanos A: Life-threatening ventricular arrhythmias: the link between epidemiology and pathophysiology, in Zipes DP, Jalife J (eds): *Cardiac Electrophysiology, From Cell to Bedside.* Philadelphia, PA, WB Saunders Co., 1990, ch. 72

[75] F. Fenton and A. Karma, "Vortex dynamics in three-dimension continuous myocardium with fiber rotation: Filament instability and fibrillation," *Chaos*, **8**, pp 20-47 (1998)

[76] A.V. Panfilov, "spiral breakup as a model of ventricular fibrillation," *Chaos*, **8**, pp 57-64 (1998).

[77] J.E.S. Socolar and D.J. Gauthier, 'Analysis and comparison of multiple-delay schemes for controlling unstable fixed points of discrete maps,' Phys. Rev. E **75**, 6589 (1998).

[78] A. Chang, J.C. Bienfang, G.M. Hall, J.R. Gardner, and D.J. Gauthier, 'Stabilizing unstable steady states using extended time-delay autosynchronization,' Chaos **8**, 782 (1998).

[79] G.M. Hall, S. Bahar, D.J. Gauthier, 'Prevalence of rate-dependent behaviors in cardiac muscle,' *Phys. Rev. Lett.*, **82**, pp 2995-2998 (1999).

[80] G.M. Hall, S. Bahar, and D.J. Gauthier, 'Inducing transitions between bistable states in cardiac muscle using small electrical stimuli,' submitted for publication (1999).

[81] G.M. Hall, S. Bahar, and D.J. Gauthier, 'Controlling alternans in small pieces of rapidly-paced cardiac muscle,' in preparation.

[82] G. M. Hall, S. Bahar and D. J. Gauthier, unpublished.

[83] D.W. Sukow, M.E. Bleich, D.J. Gauthier, and J.E.S. Socolar, 'Controlling chaos in fast dynamical systems: Experimental results and theoretical analysis,' an Invited article in Chaos **7**, 560 (1997).

[84] Waldo AL, 'Atrial flutter: mechanisms, clinical features, and management' in *Cardiac Electrophysiology: from Cell to Bedside*, 2nd. edition, ed. D. P. Zipes and J. Jalife. (W. B. Saunders Company, Philadelphia, 1995), chap. 62.

[85] D. R. Chialvo, J. Jalife, *Nature* **330**, 749 (1987); M. Watanabe, N. F. Otani, R. F. Gilmour, *Circ. Res.* **76**, 915 (1995).

[86] D. R. Chialvo, 'Toward very simple generic models of excitable cells. Order and chaos in cardiac tissues. Facts and conjectures,' in *Mathematical Approaches to Cardiac Arrhythmias, Ann. N. Y. Acad. Sci., Vol. 591*, J. Jalife, Ed. (The New York Academy of Sciences, New York, 1990), pp. 351.

[87] K. Pyragas, ',' *Phys. Rev. Lett. A* **170**, 421 (1992).

[88] S. Bielawski, D. Derozier, and P. Glorieux, ',' *Phys. Rev. E* **50**, 262 (1994).

[89] M.L. Riccio, M.L. Koller, and R.F. Gilmour Jr, 'Electrical Restitution and Spatiotemporal Organization During Ventricular Fibrillation,' *Circ. Res.* **84**, 8 (1999), pp 955-963.

[90] K.R. Laurita, S.D. Girouard, Yrudy, and D.S. Rosenbaum, 'Role of passive electrical properties during action potential restitution in intact heart,' *Am. J. Physiol.* 273 (*Heart Circ. Physiol.* 42): H1205-H1214 (1997).

[91] D.H. Bennett, 'Cardiac Arrhythmias, Pratical Notes on Interpretation and Treatment,' John Wright & Sons Ltd. in Bristol UK (1981).

[92] C.J. Wiggers, 'The mechanism and nature of ventricular defibrillation,' Am. Heart J. **20**, 399 (1940); D.P. Zipes, J. Fischer, R.M. King, A. Nicoll, and W.W. Jolly, 'Termination of ventricular fibrillation in dogs by depolarizing a critical amount of myocardium,' Am. J. Cardiol. **36**, 37 (1975); and R.E. Ideker, P-S. Chen, N. Shibata, P.G. Colavita, and J.M. Wharton, 'Current concepts of the mechanism of ventricular defibrillation,' in *Non-Pharmacological Therapy of Tachyarrhythmias*, G. Breithardt, M. Borggrefe, and D. Zipes, Eds. (Futura, Mount Kisco, 1987), pp. 449-464.

[93] For a recent review, see A.T. Winfree, Chaos **8**, 1 (1998) and the accompanying articles on the special Focus Issue on *Fibrillation in Normal Ventricular Mycoardium.*

[94] R.L. Rasmusson

[95] M.E. Bleich and J.E.S. Socolar, 'Delayed feedback control of a paced excitable oscillator,' *Int. J. Bifur. and Chaos*, in press.

[96] C. Johnson, private communication.

[97] P.D. Wolf, D.L. Rollins, T.F. Blitchington, R.E.Ideker and W.M. Smith, 'Design for a 512 channel cardiac mapping system,' in *Biomedical Engineering: Opening New Doors, Proc. of the Fall '90 Annual Meeting of the Biomedical Eng. Soc.*, D.C. Mikulecky and A.M. Clarke, Eds., New York: New York Univ. Press, pp-5-13 (1990)

[98] Mr. Pavan Cheruvu and Dr. Joshua Socolar, Private communication.

[99] D. Pierson and F. Moss, 'Detecting periodic unstable points in noisy chaotic and limit cycle attractors with applications to biology,' Phys. Rev. Lett. **75**, 2124 (1995).

[100] J. R. Clay, R. M. Brochu, and A. Shrier, 'Phase resetting of embryonic chick atrial heart cell aggregates: Experiment and theory,' Biophys. J. **58**, 609 (1990).

[101] V. C. Kowtha, A. Kunysz, J. R. Clay, L. Glass, and A. Shrier, 'Ionic mechanisms and nonlinear dynamics of embryonic chick heart cell aggregates,' Prog. Biophys. Molec. Biol. **61**, 255 (1994).

[102] M. Delmar, L. Glass, D. C. Michaels, and J. Jalife, 'Ionic basis and analytical solution of the Wenckebach phenomenon in guinea pig ventricular myocytes,' Circ. Res. **65**, 775 (1989).

[103] B. J. Roth, 'Nonsustained reentry following successive stimulation of cardiac tissue through a unipolar electrode,' J. Cardiovasc. Electrophysiol. **8**, 768 (1997).

[104] S.-F. Lin, B. J. Roth, D. S. Echt, and J. P. Wikswo, Jr, 'Complex dynamics following unipolar stimulation during the vulnerable phase,' Circulation **94**, I-714 (1996).

[105] B. J. Roth and W. Krassowska, 'The induction of reentry in cardiac tissue. The missing link: How electric fields alter transmembrane potential,' Chaos **8**, 204 (1998).

[106] P. Holmes, 'How attractive is chaos? Nonlinear models in neurobiology,' in *Mathematical Approaches to Cardiac Arrhythmias, Ann. N. Y. Acad. Sci., Vol. 591*, J. Jalife, Ed. (The New York Academy of Sciences, New York, 1990), pp. 301.

[107] D. R. Chialvo, D. C. Michaels, J. Jalife, 'Supernormal excitability as a mechanism of chaotic dynamics of activation in cardiac Purkinje fibers,' Circ. Res. **66**, 525 (1990).

[108] D. G. Schaeffer, 'Memoirs from a small-scale course on industrial math,' Notices AMS **43,** 550, (1996).

[109] R. L. Vick, 'Action potential duration in canine Purkinje Tissue: Effects of prededing excitation,' *J. Electrocardiology* **4**, 105 (1971).

[110] V. Elharrar and B. Surawicz, 'Cycle length effect on restitution of action potential duration in dog cardiac fibers,' *Am. J. Physiol.* (*Heart Circ. Physiol.* 13) **244**, H782 (1983)

[111] R. F. Gilmour, Jr., N. F. Otani, and M. A. Wantanabe, 'Memory and complex dynamics in cardiac Purkinje fibers,' *Am. J. Physiol.* (*Heart Circ. Physiol.* 41) **272**, H1826 (1997).

[112] M. R. Boyett and B. R. Jewell, 'A study of the factors responsible for rate-dependent shortening of the action potential in mammalian ventricular muscle,' J. Physiol. **285**, 359 (1978).

[113] D. Schaeffer, 'Dynamical systems problems in modelling the heart,' Math 139 (a graduate level course given at Duke University in Spring 1999).

[114] L. Howle, D. G. Schaeffer, M. Shearer, and P. Zhong, 'Lithotripsy: The treatment of kidney stones with shock waves,' SIAM Review **40**, 356 (1998).

[115] C. S. Henriquez, 'Simulating the electrical behavior of cardiac tissue using the bidomain model,' Critical Revs. in Biomed. Engineering **21**, 1 (1993).

[116] J. Rinzel and J. B. Keller, 'Travelling wave solutions of a nerve conduction equation,' Biophys. J. **13**, 1313 (1973).

[117] D. Oldson, in Math 139.

[118] J. Guckenheimer and B. Meloon, 'Computing periodic orbits and their bifurcations with automatic differentiation,' preprint.

[119] Kalman J, Olgin J, Karch M, Lesh M: Regional entrainment of atrial fibrillation in man. *J Cardiovasc Electrophysiol* 1996; 7:867-876

[120] J. Hescheler, R. Speicher. *Eur. Biophys. J.* **17**,273 (1989).

[121] D. R. Chialvo, D. C. Michaels, J. Jalife, *Circ. Res.* **66**, 525 (1990); D. R. Chialvo, J. Jalife in *Cardiac Electrophysiology: from Cell to Bedside, 1st edition,* ed. D. P. Zipes and J. Jalife (W. B. Saunders Company, Philadelphia, 1990), chap. 24.

[122] D. Powell,D. Burstein and E.T. Fossel, 'Nuclear magnetic resonance studies of sodium/calcium exchange in frog perfused, beating hearts,' *Euro. Journal of Biochem.*, **193**, pp 887-889 (1990).

[123] M. Goto and E. Tsujiski, 'A further study on the membrane currents related to Ba-Induced pacemaker in the bullfrog atrium,' *Japanese Journal of Physiology*, **40**, pp 411-416 (1990).

[124] M. Goto, M. Urata and T. Hyodo, 'Instantaneous and delayed outward currents of the bullfrog atrial muscle in Ca-free or Na-deficient conditions,' *Japanese Journal of Physiology*, **32**, pp 573-587 (1982).

[125] H. Kawata and K. Kawagoe, 'Effects of tonicity on the resting tension in bullfrog ventricle,' *Japanese Journal of Physiology*, **25**, pp 65-78 (1975).

[126] R. Volkmann, S. Winell, and A.-S. Pettersson, 'Slow sodium-free contractures in the frog heart mediated by the sodium-calcium exchange,' *Comp. Biochem. Physio.*, **89C**, 1, pp 71-75, (1988).

[127] R. Volkmann, A Carlsten. and S. Winell, 'Sodium-free contractures in frog myocardium damaged by catecholamines,' *Comp. Biochem. Physio.*, **89C**, 1, pp 77-81, (1988).

[128] R. Volkmann, S. Winell, and L.E. Ericson, 'Effects of cyanide and verapamil on sodium-free contractures in the frog heart,' *Comp. Biochem. Physio.*, **84C**, 2, pp 247-255, (1986).

[129] F. Witkowski, private communication.

[130] Naccarelli, GV, Zipes DP, Rahilly GJ. Influence of tachycardia cycle length and antiarrhythmic drugs on pacing termination and acceleration of ventricular tachycardia. *Am. Heart. J.* **105**, 1 (1983).

[131] Roy D, Waxman HL, Buxton AE. Termination of ventricular tachycardia: role of tachycardia cycle length. *Am. J. Cardiol.* **50**, 1346 (1982).

[132] A.L. Ritzenburg, D.R. Adam, and R.J. Cohen, 'Period multupling-evidence for nonlinear behavior of the canine heart,' Nature 307, 12 (1984).

Biography

George Martin Hall was born in Decatur, Ga. on May 28, 1971. He grew up in Marietta, Georgia. He attended the Walker School, which is a private school in Marietta. After graduating high school, he enrolled at Georgia Institute of Technology as a President's Scholar. In August 1992 he recieved a B.S. in Physics. Continuing on at Ga. Tech. Martin received a M.S. in Applied Mathematics in June 1994. Then He received the Townes Perkin-Elmer fellowship to attend Duke University in Physics. In May 1997, he recieved a M.A. in Physics. Finally, in November 1999 he earned his Ph.D. in Physics with a dissertation entitled 'Controlling complex behavior in cardiac muscle.' For the next little while he can be found at The Corporate Executive Board, Washington, DC.

LIST OF PUBLICATIONS

G.M. Hall and D.J. Gauthier, 'Controlling alternans in small pieces of rapidly-paced cardiac muscle,' Manuscript in preparation (1999).

G.M. Hall, S. Bahar, and D.J. Gauthier, 'Inducing transitions between bistable states in cardiac muscle using small electrical stimuli,' Manuscript in Preparation (1999).

R.A. Oliver, G.M. Hall, S. Bahar, W. Krassowska, P.D. Wolf, E.G. Dixon-Tulloch, D.J. Gauthier, 'Existence of bistability and correlation with arrhythmogenesis in paced sheep atria,' Manuscript in preparation (1999).

G.M. Hall, S. Bahar, D.J. Gauthier, 'Prevalence of rate-dependent behaviors in cardiac muscle,' *Phys. Rev. Lett.*, **82**, pp 2995-2998 (1999).

G.M. Hall, S. Bahar, D.J. Gauthier, 'Experimental control of a chaotic point process using interspike intervals,' *Phys. Rev. E*, **58** 2:1685-1689 (1998).

A. Chang, J.C. Bienfang, G.M. Hall, J.R. Gardner, D.J. Gauthier, 'Stabilizing unstable steady states using extended time-delay autosynchronization,' *Chaos*, **8** 4:782-790 (1998).

LIST OF PRESENTATIONS

G.M. Hall, S. Bahar, D.J. Gauthier, 'Control of alternans in cardiac muscle using time-delay autosynchronization,' American Physical Society Centennial Meeting 1999, Atlanta, GA.

G.M. Hall, S. Bahar, D.J. Gauthier, 'Control of Alternans in Bullfrog Myocardium,' Dynamics Days 1999, Atlanta, GA.

G.M. Hall, S. Bahar, D.J. Gauthier, 'A Test Bed for Control of Cardaic Tissue,' Dynamics Days 1998 Chapel Hill, NC.

G.M. Hall, S. Bahar, D.J. Gauthier, 'Complex dynamical behavior of small pieces of cardiac tissue,' Dynamics Days 1997, Scottsdale, AZ.

G.M. Hall and D.J. Gauthier, 'Experimental control of a chaotic system using interspike intervals,' 4th Experimental Chaos Conference 1997, Boca Raton, FL.